

CHAPTER - 4

RESULTS AND DISCUSSION

4.1 *Clerodendrum phlomidis*

4.1.1 Development of quality control parameters

Based on literatures and preliminary hypoglycemic reports, leaf was selected as the morphological part of study.

Plant materials are used throughout developing and also in developed countries as home remedies, over-the-counter drug products, raw materials for the pharmaceutical industry, and represent a substantial proportion of the global drug market. It is therefore essential to assess their quality by using modern quality control techniques.

4.1.2 Plant profile

Clerodendrum phlomidis Linn. f. (Lamiaceae) (Figure 4.1.1)

Synonyms: *Clerodendrum multiflorum* (Burm.f) O. Kuntze;

Volkameria multiflorum Burm. f.



Figure 4.1.1: *Clerodendrum phlomidis*

4.1.3 Determination of foreign matter

Foreign matter is material consisting of any or all of the following;

- ❖ Parts of the medicinal plant material or materials other than those named with the limits specified for the plant material concerned;
- ❖ Any organism, part or product of an organism, other than that named in the specification and description of the plant material concerned;
- ❖ Mineral admixtures not adhering to the medicinal plant materials, such as soil, stones, sand, and dust.

Table 4.1.1: Foreign matter in *C. phlomidis* leaves

Mineral admixture	Other plant materials	Other organic matter	Total foreign matter
1.2 %w/w	4.32 %w/w	1.128 %w/w	6.728 %w/w

As the presence of foreign matter in medicinal plant materials may interfere throughout the study, it is crucial to quantify them. Macroscopic examination can conveniently be employed for determining the presence of foreign matter in whole or cut plant materials. However, microscopy is indispensable for powdered materials. The leaf material showed 6.728 %w/w of total foreign matter (Table 4.1.1), which is relatively high. It is seldom possible to obtain plant materials that are entirely free from some form of foreign matter. 1.2 %w/w of mineral admixture indicates the presence of appreciable quantity of soil, stones, sand and dust. 4.32 %w/w of other plant materials indicates the presence of other morphological parts of *C. phlomidis* mostly stem. 1.128 %w/w of other organic matter includes moulds or insects, and other animal contamination, including animal excreta.

4.1.4 Morphology, anatomy, histology and powder microscopy

The leaves are deltoid ovate, chartaceous, glabrescent, margins coarsely serrate, panicle axillary and terminal (Figure 4.1.2). The morphological features matched with details available in the literature.



Figure 4.1.2: Leaves of *C. phlomidis*

Toluidine blue is a polychromatic stain, hence the staining results were remarkably good; and some cytochemical reactions were also obtained. The dye rendered pink colour to the cellulose walls, blue to the lignified cells, dark green to suberin, violet to the mucilage and blue to the protein bodies. Since crystals, starch grains, and lignified cells have birefringent property, under polarized light they appeared bright against dark background.

The leaf is dorsiventral, amphistomatic, smooth and with prominent midrib (Figure 4.1.3). The midrib is planoconvex in cross sectional view with hemispherical abaxial part and flat adaxial side. The ground tissue of the midrib consists of compact, thin walled, angular parenchyma cells both on the adaxial and abaxial parts.

The vascular bundles of the midrib may be a single strand (Figure 4.1.4) or a group of 3 strands (Figure 4.1.5). In the single strand vascular bundle there is a mass of xylem elements with abaxial phloem; the 3-stranded vascular bundle are 3 discrete xylem masses each with phloem strands. The strand is 800 μm in vertical plane and 600 μm in horizontal plane.

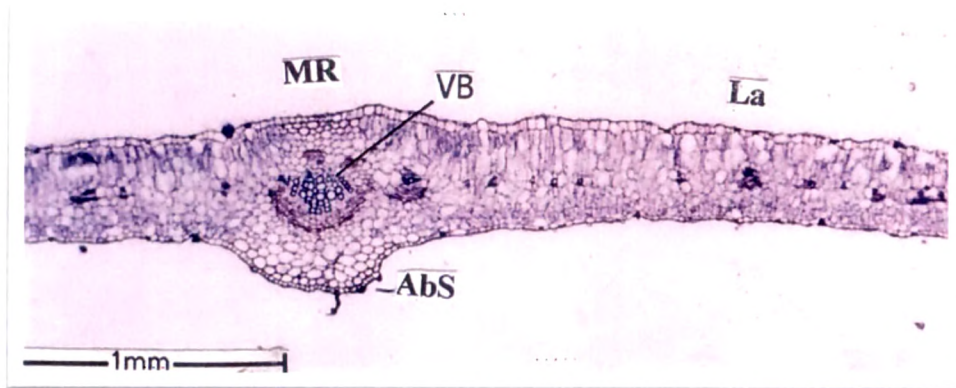


Figure 4.1.3: TS of *C. phlomis* showing prominent midrib

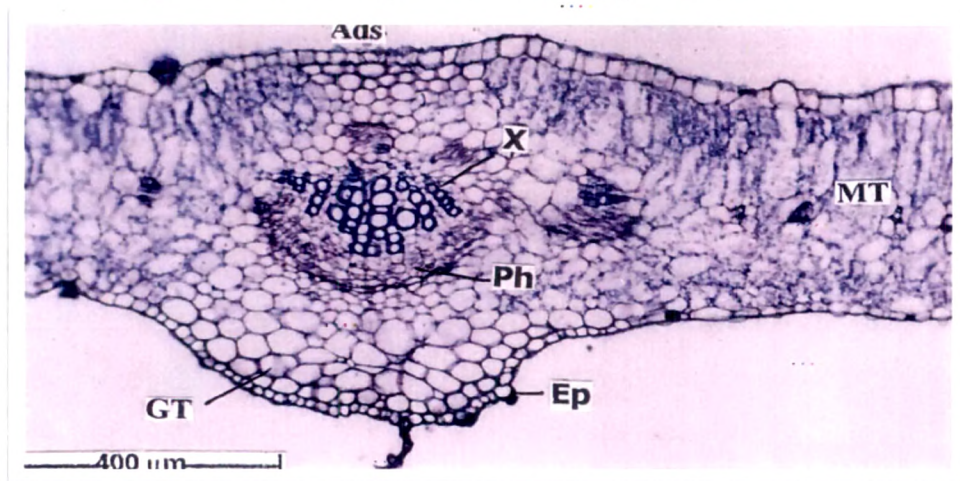


Figure 4.1.4: TS of *C. phlomis* showing single strand vascular bundles

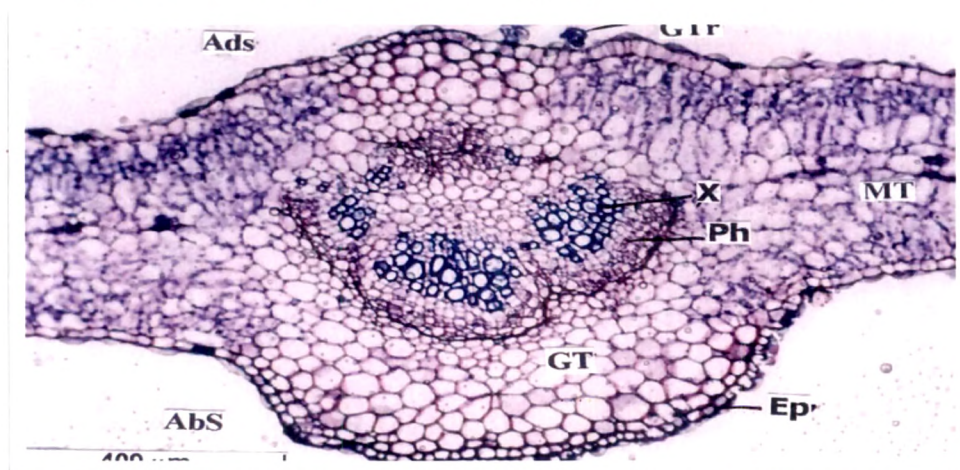


Figure 4.1.5: TS of *C. phlomis* showing three strands of vascular bundles

Legend for figures: AbS-Abaxial side; AdS-Adaxial side; Ep-Epidermis; GT-Ground tissue; GTr-Glandular trichome; La-Lamina; MT-Mesophyll tissue; Mr-Midrib; Ph-Phloem; VB-Vascular bundle; X-Xylem.

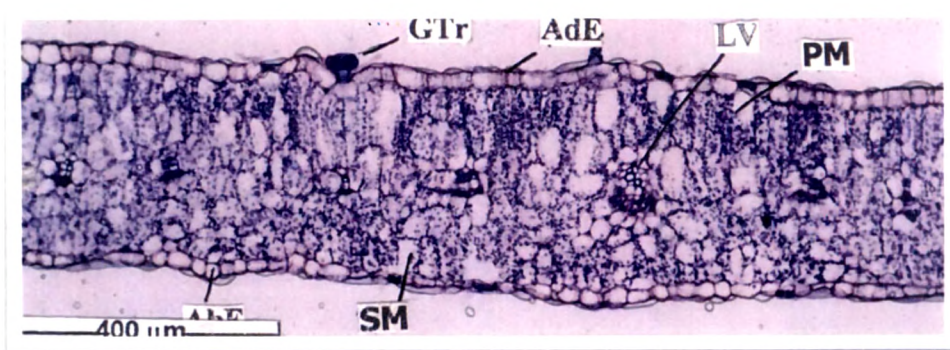


Figure 4.1.6: TS of *C. phlomidis* showing the lamina region

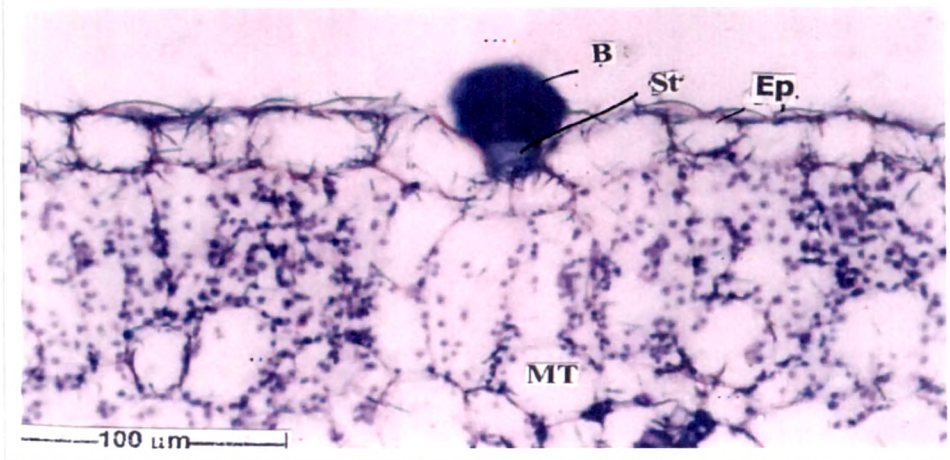


Figure 4.1.7: TS of *C. phlomidis* showing glandular trichomes

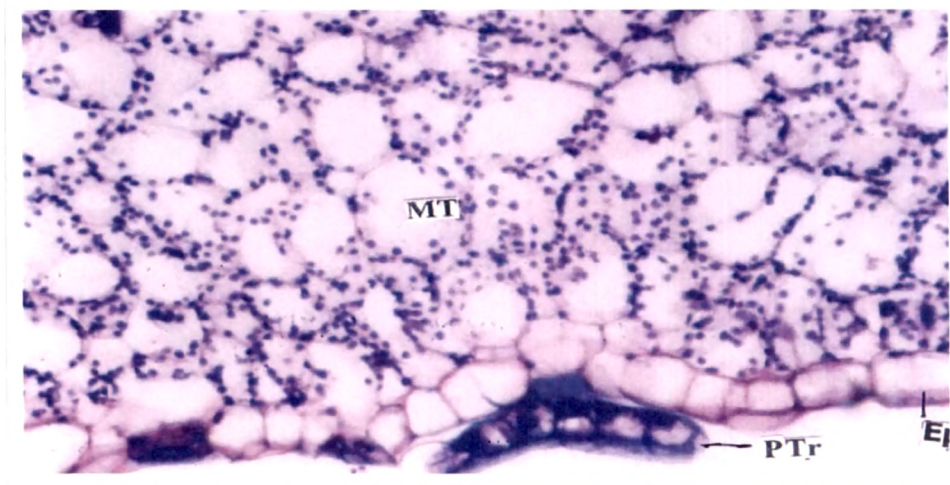


Figure 4.1.8: TS of *C. phlomidis* showing peltate trichomes

Legend for figures: AbE-Abaxial epidermis; AdE-Adaxial epidermis; B-Body cells; Ep-Epidermis; GTr-Glandular trichomes; LV-Lateral vein; MT-Mesophyll tissue; PM-Palisade mesophyll; PTr-Peltate trichomes; SM-Spongy mesophyll; St-Stalk cells.

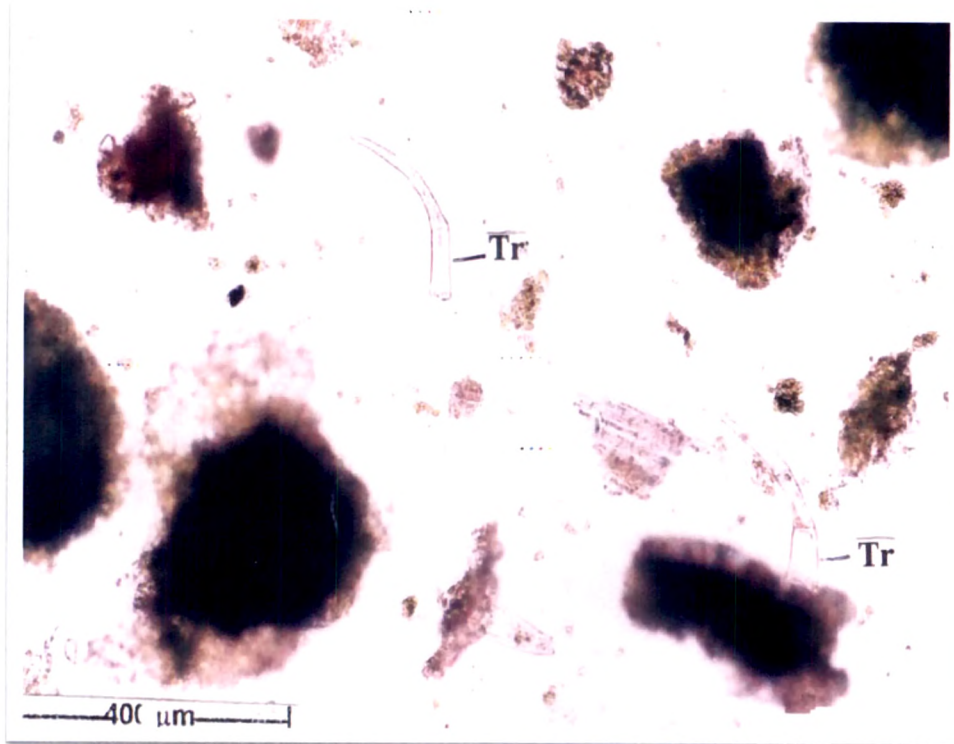


Figure 4.1.9: Powder analysis of *C. phlomidis* showing trichomes

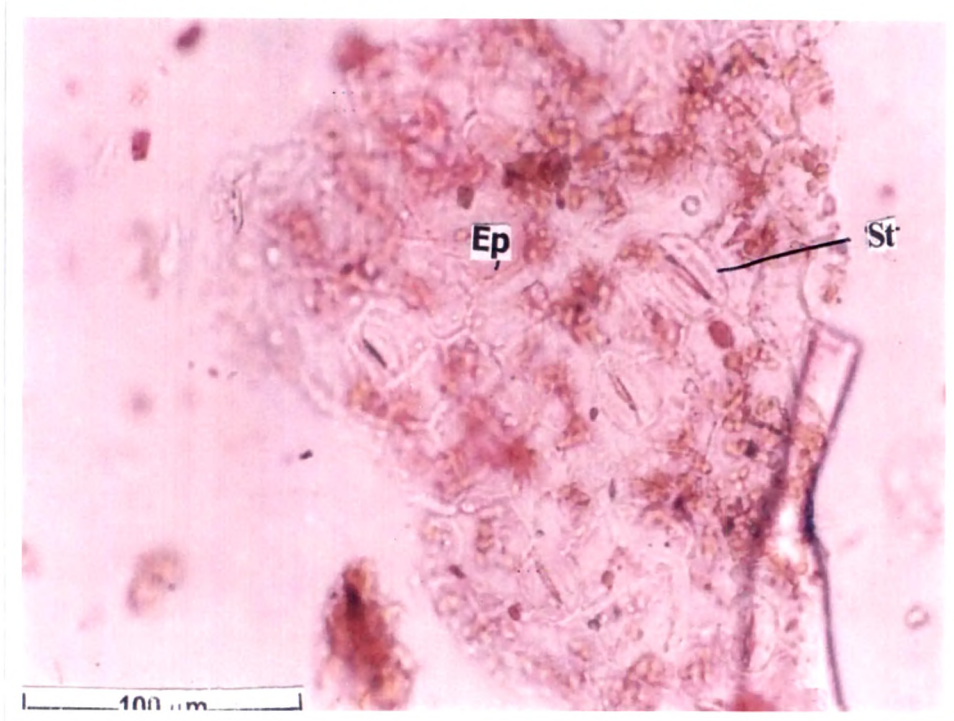


Figure 4.1.10: Powder analysis of *C. phlomidis* showing stomata

Legend for figures: Ep-Epidermis; St-Stomata; Tr-Trichomes.

The lamina is 300 μm thick; the epidermis layers are even and fairly thick. The adaxial epidermal layer has rectangular or squarish cells with thin cuticle; the abaxial epidermis is slightly thinner and consists of spindle shaped or oblong cells. The adaxial epidermis is 25 μm thick while the abaxial layer has 20 μm thick cells. The mesophyll tissue is thin walled and chlorenchymatous, it is differentiated in to adaxial zone of palisade cells and abaxial zone of spongy mesophyll tissue (Figure 4.1.6; Figure 4.1.7). The palisade consists of 2 layers of vertically elongated cylindrical cells (Figure 4.1.8). The spongy mesophyll consists of 3 or 4 layers of spherical cells which are less compact.

Glandular trichomes are frequently seen apart from the normal non glandular trichomes. The glandular trichomes have a short stalk cell which is attached to the epidermis. The body of the trichomes may be unicellular and spherical or it may be a part of 6 or more cells (Figure 4.1.9). The cells have dense cytoplasm and prominent nuclei.

The powder analysis of leaf shows numerous glandular trichomes. These trichomes are multicellular, unbranched and uniseriate. The walls are thick and the terminal cell is tapering in to a pointed tip. There are also small fragments showing stomata (Figure 4.1.10). The epidermal cells are thin walled and straight. The stomata are anomocytic type; the guard cells have no distinct subsidiary cells.

4.1.5 Proximate analysis

Ash values of *C. phlomidis* leaves show relatively high total ash of 9.66 %w/w and sulphated ash (6.24 %w/w), indicating high quantity of carbonates and oxides (Table 4.1.2). Low acid insoluble ash indicates less silicious materials like earth or sand. Ash values are helpful in determining the quality and purity of crude drugs in powdered form. The total ash usually consists of inorganic radicals like carbonates, phosphates, silicates and silica of sodium, potassium, magnesium and calcium. Sometimes, inorganic variables like calcium oxalate, silica, carbonate

content of crude drug affects “total ash” values, such variables are then removed by treating with acid (as they are soluble in hydrochloric acid) and then acid-insoluble ash value is determined. The values vary within fairly wide limits and are therefore an important parameter for the purpose of evaluation of crude drugs. A high ash value is indicative of contamination, substitution or adulteration. Ash insoluble in hydrochloric acid is the residue obtained after extracting the sulfated or total ash with hydrochloric acid. This acid-insoluble ash value particularly indicates contamination with silicious materials like earth or sand. Water soluble ash is that part of the total ash content which is soluble in water. It is a good indicator of either previous extraction of water soluble salts in the drug or incorrect preparation. While determining the total ash, very high temperature (> 600° C) may result in the conversion of carbonates to oxides. The treatment with sulphuric acid results in sulphated ash where the oxides are converted to sulphates.

Table 4.1.2: Proximate analysis of *C. phlomidis* leaves

Parameters	Values
Total ash	9.66 %w/w
Acid-insoluble ash	3.28 %w/w
Water-soluble ash	4.65 %w/w
Sulphated ash	6.24 %w/w
Water-soluble extractive	37.6 %w/w
Ethanol-soluble extractive	11.2 %w/w
Ether-soluble extractive	3.2 %w/w
Loss on drying (LOD)	7.33 %w/w
Bitterness value	220

Extractive values of *C. phlomidis* leaves show very high quantity of polar constituents than non-polar constituents (Table 4.1.2). Extractive values determine the amount of active constituents extracted with solvents from a given amount of

Results and Discussion

medicinal plant material. It is employed for materials for which as yet no suitable chemical or biological assay exists. Extractive values are useful for evaluation of crude drugs and give an idea about the nature of chemical constituents present in them. The amount of extractive drug yield to a given solvent is often an approximate measure of a certain constituent or group of related constituents the drug contains. In some cases the amount of drug soluble in a given solvent is an index of its purity. The solvent used for extraction should be in a position to dissolve appreciable quantities of substances desired.

The LOD of *C. phlomidis* leaves is 7.33 %w/w (Table 4.1.2). Loss on drying determines both water and volatile matter. Excess of water in medicinal plant materials will encourage microbial growth, the presence of fungi or insects, and deterioration following hydrolysis. This is especially important for materials that absorb moisture easily or deteriorate quickly in the presence of water.

The bitterness value is expressed in units equivalent to the bitterness of a solution containing 1 g of quinine hydrochloride in 2000 ml. The bitterness value of *C. phlomidis* leaves is 220 (Table 4.1.2). The value is comparatively very less than quinine. Bitterness test should not be carried out until the identity of the plant material has been confirmed. Medicinal plant materials that have a strong bitter taste ("bitters") are employed therapeutically. Their bitterness stimulates secretions in the gastrointestinal tract, especially of gastric juice. However, since they are mostly composed of two or more constituents with various degrees of bitterness, it is first necessary to measure total bitterness by taste.

The bitter properties of plant material are determined by comparing the threshold bitter concentration of an extract of the materials with that of a dilute solution of quinine hydrochloride. Safe drinking-water should be used as a vehicle for the extraction of plant materials and for the mouth-wash after each tasting. Taste buds dull quickly if distilled water is used. Sensitivity to bitterness varies from person to

person, and even for the same person it may be different at different times (because of fatigue, smoking, or after eating strongly flavoured food). Therefore, the same person should taste both the material to be tested and the quinine hydrochloride solution within a short space of time. The bitter sensation is not felt by the whole surface of the tongue, but is limited to the middle section of the upper surface of the tongue. A certain amount of training is required to perform this test. A person who does not appreciate a bitter sensation when tasting a solution of 0.058 mg of quinine hydrochloride in 10 ml of water is not suitable to undertake this determination.

4.1.6 Determination of arsenic and heavy metals

High sodium, iron and potassium levels (Table 4.1.3) suggest the presence of higher quantity of salts. The official limits for arsenic and mercury in herbal medicines are 2 and 0.2 ppm respectively, the quantity of arsenic and mercury detected in *C. phlomidis* leaves are within limits. Negligible quantity of arsenic, mercury, lead and cadmium indicates lesser use of pesticides and the healthy habitat of *C. phlomidis*.

Table 4.1.3: Quantity of arsenic and heavy metals in *C. phlomidis* leaves

Metals	Quantity present
Arsenic	0.13008 ppm
Mercury	0.01122 ppm
Lead	Below detection level
Cadmium	Below detection level
Manganese	64.97 ppm
Zinc	66.11 ppm
Copper	22.48 ppm
Sodium	2490 ppm
Iron	781 ppm
Potassium	120.18 ppm

4.1.7 Determination of microbial content

C. phlomidis shows high fungal contamination than bacterial. *Escherichia coli*, *Pseudomonas aeruginosa*, *Stapylococcus aureus* and *Salmonella* sp. were detected as the major bacterial species (Table 4.1.4).

Table 4.1.4: Microbial content of *C. phlomidis* leaves

Microorganisms	Colony forming units per gram (cfu/g)
Total viable count	6000
Total bacterial count	2800 <i>E. coli</i> , <i>Pseudomonas aeruginosa</i> , <i>Stapylococcus aureus</i> , <i>Salmonella</i> sp.
Total fungal count	3200

Medicinal plant materials normally carry a great number of bacteria and fungus, often originating in soil. While a large range of bacteria and fungi form the naturally occurring microflora of herbs, aerobic spore-forming bacteria frequently predominate. The practices of harvesting, handling and production may cause additional contamination and microbial growth. The determination of *Escherichia coli* and fungus may indicate the quality of production and harvesting practices.

4.1.8 Preliminary qualitative phytochemical screening

Wide arrays of natural compounds like, alkaloids, glycosides, saponins, phytosterols, phenolics, terpenoids, flavonoids, coumarins and tannins which exert physiological activity are synthesized in the plant, in addition to carbohydrates, proteins and lipids utilized by man as food. A systematic and complete study of crude drugs by different qualitative chemical tests will provide detailed information regarding the presence and absence of both primary and secondary metabolites derived as a result of plant metabolism. Establishing phyto-chemical profile of the extracts reveals the nature of chemical constituents and their composition.

Table 4.1.5: Preliminary qualitative phytochemical screening of *C. phlomidis* extracts

Successive extract	Yield % w/w	Appearance	Odour	Secondary metabolites
Petroleum ether	2.72	Yellowish brown sticky mass	No characteristic odour	Steroids, steroidal glycosides
Unaponified matter of petroleum ether extract	0.685	Bright yellow sticky paste	Very faint odour	Steroids, steroidal glycosides
Benzene	2.17	Blackish green sticky mass	Faint odour	Steroids, steroidal glycosides, phenolics
Diethyl ether	0.17	Greenish black sticky mass	Faint odour	Steroids, saponins
Chloroform	1.08	Blackish green resinous mass	Slightly pungent	Steroids, steroidal glycosides
Ethyl acetate	0.57	Green sticky mass	Characteristic odour	Phenols, saponins, coumarins
Acetone	0.72	Blackish green mass	Characteristic odour	Alkaloids, steroids, flavonoids, phenolics
Methanol	8.73	Reddish brown sticky mass	Characteristic odour	Alkaloids, steroids, coumarins, flavonoids
Water	27.24	Brown shiny powder	Pleasant, tea like odour	Steroids, coumarins, flavonoids, phenolics

Like any Cleodendrum member *C. phlomidis* leaf shows steroids as major secondary metabolites. Phenolics and flavonoids were detected in acetone, methanol and water extract. Alkaloids were detected in acetone and methanol extract. Quantitatively water soluble constituents are higher than non-polar constituents. The % yield, appearance and nature of different extracts are shown in Table 4.1.5.

4.1.9 Thin layer chromatographic study

TLC is a very effective technique for the separation of chemical constituents of extracts and for their identification. Components are separated by the differential migration of solute between two phases - a stationary phase and a mobile phase. Depending on the particular type of stationary phase and using different solvents, separation can be achieved on the basis of partition or a combination of partition and adsorption. Selection of mobile phase is based on the increasing order of polarity and the chemical tests. Moreover, TLC is often used as an alternative to other chromatographic techniques for quantification of plant products because of its simplicity, accuracy, cost effectiveness and rapidity.

In India, *Ayurvedic*, *Siddha* and other herbal derived products, which are used either as active ingredients or as adjuvants, hold paramount importance as alternative medicines but their quality evaluation poses a great challenge to practitioners and consumers. Correct identification of these drugs is often problematic in entire form as well as in powder form, since these medicinal plants are known by a variety of vernacular names and frequently many medicinal plants are known by one vernacular name.

Comparative-TLC (Co-TLC) with marker compounds can be used to standardize the herbal raw materials. The clinical efficacy and pharmacological effects of a plant material depends strongly on the quantity of biological active constituents

present and these constituents must be quantified if a plant material is to be characterized.

4.1.9.1 Identification and quantification of adrenaline

Preliminary TLC finger printing and co-TLC studies (with marker compounds) of *C. phlomidis* leaves revealed the presence of adrenaline. Further, it was confirmed by R_f comparison, multi-wavelength scanning and spectral overlay.

Chemical substances that play essential role in peripheral and central neurotransmission of animals, such as acetylcholine and biogenic monoamines have been demonstrated in the plant kingdom (Tretyn and Kendrick, 1991; Kuklin and Conger, 1995). Adrenaline (Figure 4.1.11) is 4-(1-hydroxy-2-methylamino-ethyl) benzene-1,2-diol, a biogenic monoamine belonging to the catecholamine group. Adrenaline, noradrenaline, dopamine and their derivatives have been detected in 44 plant families (Smith, 1997). In contrast to the vast amount of knowledge concerning the role and action of adrenaline in mammals, very little is known of adrenaline role in plants. Several reports suggest that adrenaline is precursor for alkaloids (Lundstrom, 1983) while others suggest that it may interact with plant hormones (Protacio et al., 1992; Dai et al., 1993). At present, high performance liquid chromatography (HPLC) methods are typically used for identification and quantification using fluorescence or electrochemical detection (Grossi et al., 1991; Sarzanini et al., 1994; Hansen et al., 1999). Considering the wide physiological significance and also as one of the marker constituent to ensure identity and quality of the plant material, a simple, sensitive and accurate TLC method was developed for the quantification of adrenaline in *C. phlomidis* leaves.

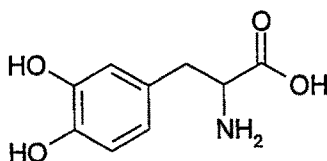


Figure 4.1.11: Chemical structure of adrenaline

Table 4.1.6: Method validation parameters for quantification of adrenaline in *C. phlomidis* leaves

S. No.	Parameter	Results
1	R _f	0.45
2	Dynamic range (ng spot ⁻¹)	100-500
3	Equation	y = 311.081+7.411x
4	Slope	7.411
5	Intercept	311.081
6	Limit of detection	18.33 ng
7	Limit of quantification	61.11 ng
8	Linearity (correlation coefficient)	0.99846

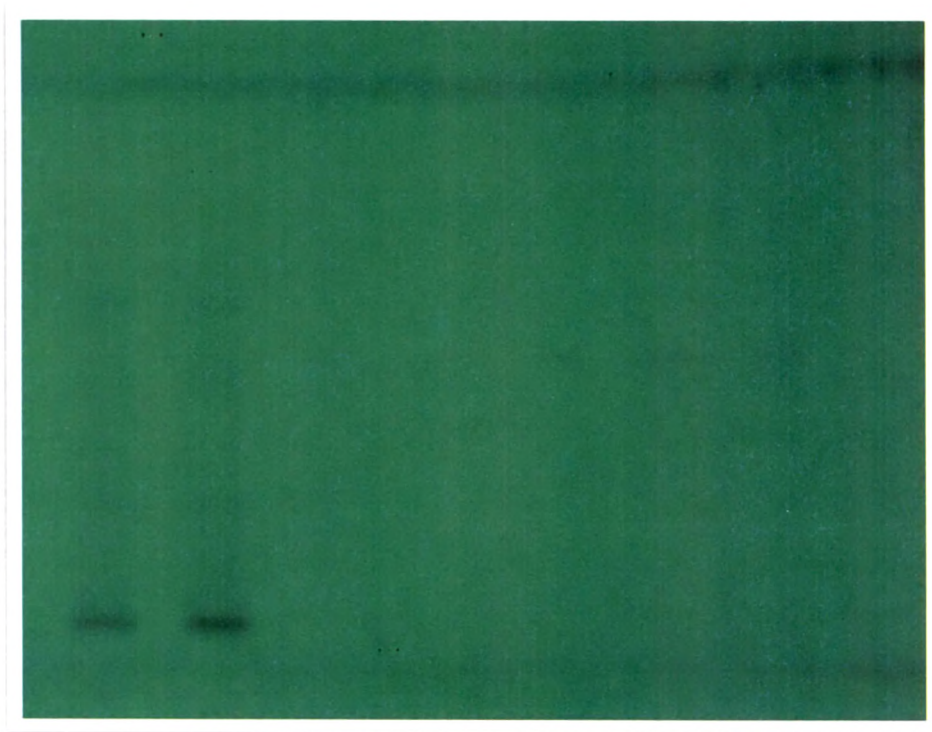


Figure 4.1.12: Standard adrenaline band and *C. phlomidis* extract

Table 4.1.7: Precision and recovery studies data for quantification of adrenaline in *C. phlomidis* leaves

Precision studies			
Concentration (ng spot ⁻¹)	Instrumental precision (% RSD)	Method precision (% RSD)	
		Intra-day	Inter-day
100	0.94	0.96	1.28
500	0.80	0.78	0.87

Recovery studies			
Amount of adrenaline in the sample (µg)	Amount of adrenaline added (µg)	Amount of adrenaline found (µg)	Recovery (%)
13.3	10.6	23.41	97.95
13.3	13.3	25.52	95.94
13.3	16.0	28.37	96.83

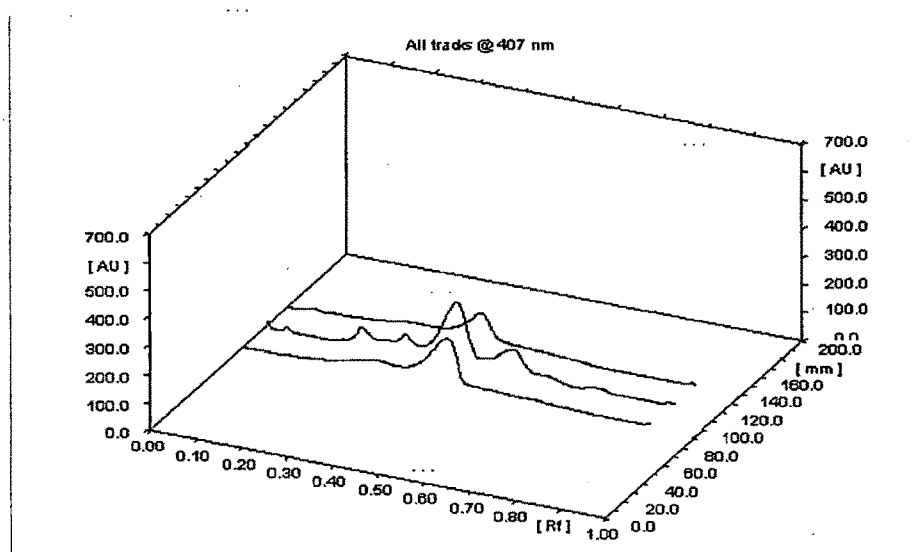


Figure 4.1.13: *C. phlomidis* leaf extract showing identical peak with standard adrenaline

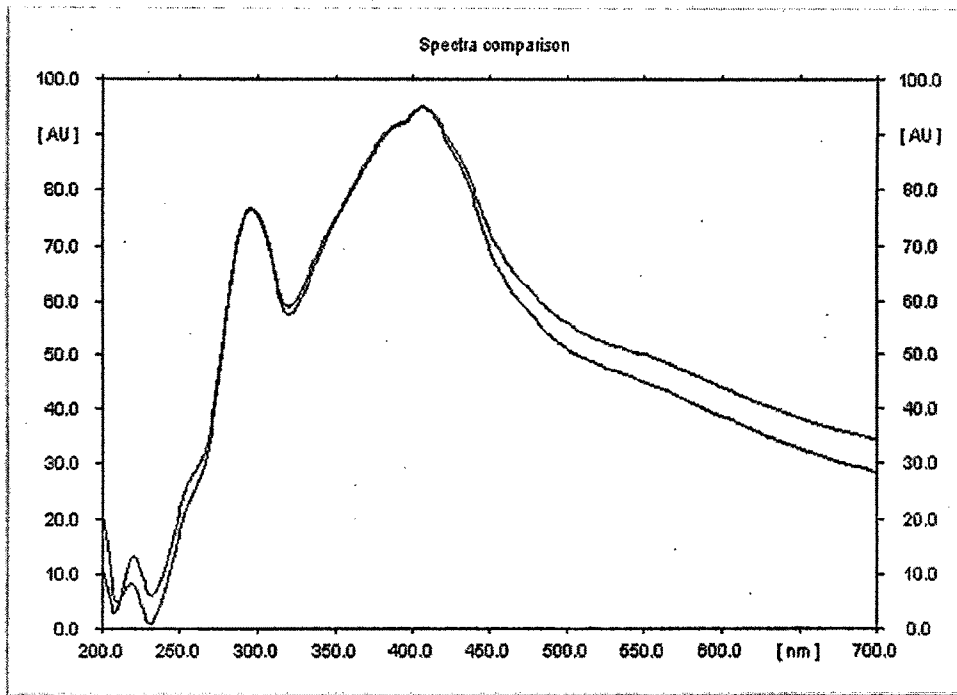


Figure 4.1.14: Spectral comparison for the peaks of standard adrenaline and *C. phlomidis* leaf extract

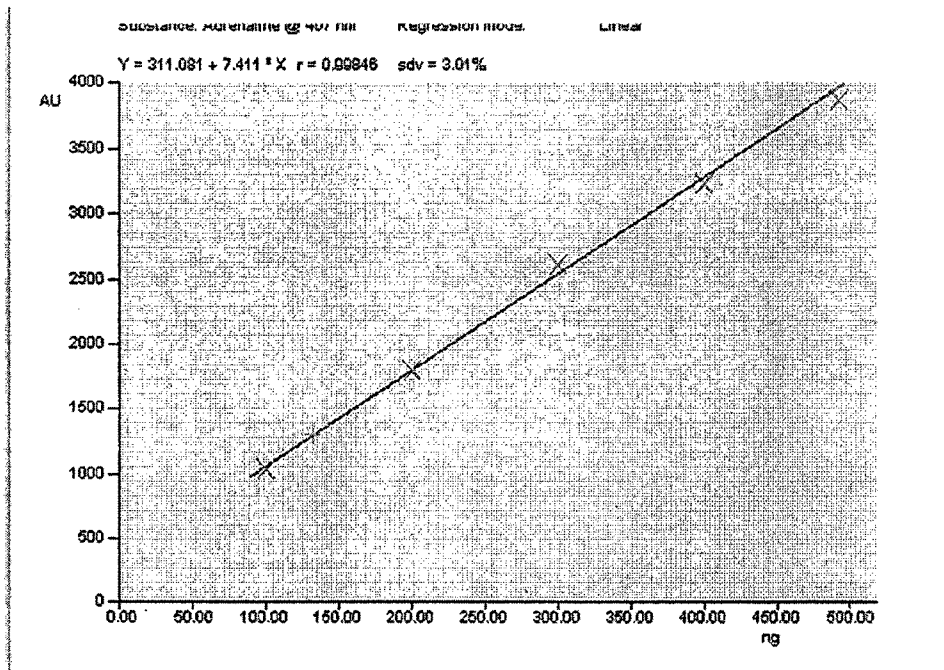


Figure 4.1.15: Calibration curve of peak area versus concentration for adrenaline

Table 4.1.8: Calibration curve parameters for quantification of adrenaline in *C. phlomidis* extract

R _f	Amount/Fraction	Area	X(calc)
0.44	100 ng	1026.30	-
0.44	200 ng	1795.49	-
0.45	300 ng	2607.59	-
0.45	400 ng	3225.93	-
0.45	500 ng	3834.18	-
0.45	-	1294.24	132.66 ng

TLC Separation Optimization: Different compositions of mobile phase were tested and the desired resolution of adrenaline with symmetrical and reproducible peak was achieved by using the mobile phase, acetone: chloroform: n-butanol: glacial acetic acid: water (60:40:40:40:35, v/v/v/v/v) with 20 min of chamber saturation. The post chromatographic derivatization was carried out with potassium hexacyanoferrate (III) - ethylenediamine reagent followed by heating at 80 °C for 15 min (Geissler and Mutschler, 1971). Densitometric scanning was performed in the absorption-reflection mode at 407 nm. The peak for adrenaline was seen at R_f 0.45. The leaf extract of *C. phlomidis*, when subjected to TLC as per the methodology described above showed the presence of adrenaline peak (Figure 4.1.12, 4.1.13). A good separation was achieved by the conditions described above. Peak purity of adrenaline was assessed by comparing its uv-visible spectra in standard and sample track. Comparison of the spectral characteristics of the peak for standard adrenaline and that of the sample peak confirmed the presence of adrenaline (Figure 4.1.14).

Linearity and Detection Limit: Linearity was checked by applying standard solutions of adrenaline at five different concentration levels. A calibration curve (Figure 4.1.15) was drawn in the concentration range of 100-500 ng spot⁻¹. The

equation for the calibration curve of adrenaline is $y = 311.081 + 7.411x$ and the correlation coefficient of the calibration curve is 0.99846, indicating good linearity. Results of regression analysis on calibration curve and detection limits are presented in Table 4.1.6.

Precision Studies: Instrumental precision was checked by repeated scanning of the same spots (100 and 500 ng spot⁻¹) of standard adrenaline three times and the % RSD values were 0.94 and 0.80 respectively. To determine the precision of the developed assay method 100 and 500 ng spot⁻¹ of adrenaline standard was analyzed three times within the same day to determine the intra-day variability.

The % RSD values were 0.96 and 0.78 for 100 and 500 ng spot⁻¹ respectively. Similarly, the inter-day precision was tested on the same concentration levels in two consecutive days and the % RSD values were 1.28 and 0.87 respectively (Table 4.1.7).

Recovery studies and sample analysis: For the examination of recovery rates, 80, 100 and 120 % of pure adrenaline was added to preanalyzed sample and quantitative analysis was performed. The recoveries were between 95.94 and 97.95 % (Table 4.1.7). This developed TLC method was subsequently applied for the analysis of adrenaline in the leaf extract of *C. phlomidis*. The adrenaline content of the leaves calculated from the area calibration curve (Table 4.1.8) by this method was found to be 0.01327 %w/w.

This TLC method developed for the quantification of adrenaline in *Clerodendrum phlomidis* leaves is simple, specific, sensitive, rapid, accurate, cost-effective and easily adaptable, should prove to be a useful alternative under circumstances where the other slower and more costly chromatographic methods are not appropriate. This TLC procedure may also be used effectively for identity, quality evaluation as well as quantitative determination for this plant or its derived products.

4.1.9.2 Identification and quantification of l-dopa

Preliminary TLC finger printing and co-TLC studies (with marker compounds) of *C. phlomidis* leaves revealed the presence of l-dopa. Further, it was confirmed by R_f comparison, multi-wavelength scanning and spectral overlay.

L-dopa (Figure 4.1.16) is used in the treatment of Parkinson's disease (Dietrichson et al., 1975) and it is considered by many clinicians as the drug of choice in the management of idiopathic parkinsonian syndrome. Considering the wide therapeutic application of this chemical constituent and to ensure identity, quality of the plant material, the study was planned to quantify l-dopa by TLC method.

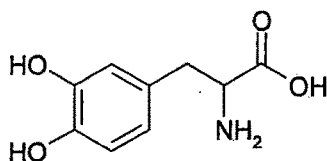


Figure 4.1.16: Chemical structure of l-dopa

Table 4.1.9: Method validation parameters for quantification of l-dopa in *C. phlomidis* leaves

S. No.	Parameter	Results
1	R_f	0.37
2	Dynamic range (ng spot ⁻¹)	100-500
3	Equation	$y=2503.286+25.433x$
4	Slope	25.433
5	Intercept	2503.286
6	Limit of detection	2.88 ng
7	Limit of quantification	8.73 ng
8	Linearity (correlation coefficient)	0.99775

Figure 4.1.17: Standard l-dopa band and *C. phlomidis* extractTable 4.1.10: Precision and recovery studies data for quantification of l-dopa in *C. phlomidis* leaves

Precision studies			
Concentration (ng spot ⁻¹)	Instrumental precision (% RSD)	Method precision (% RSD)	
		Intra-day	Inter-day
100	0.32	0.51	1.23
500	0.42	0.49	0.66
Recovery studies			
Amount of l-dopa in the sample (µg)	Amount of l-dopa added (µg)	Amount of l-dopa found (µg)	Recovery (%)
68	54.4	119.5	97.63
68	68	130.2	95.74
68	81.6	142.8	95.45

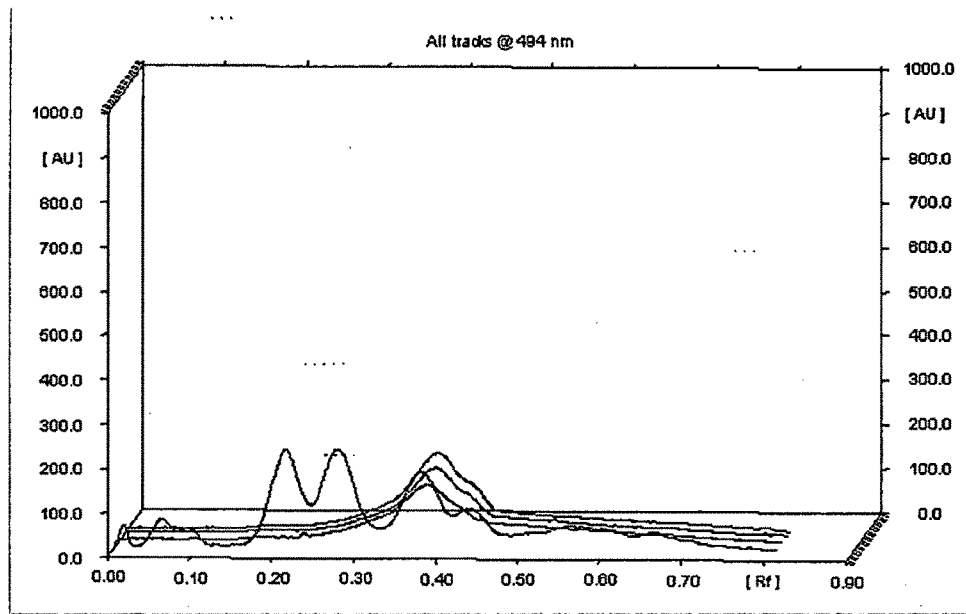


Figure 4.1.18: *C. phlomidis* leaf extract showing identical peak with standard l-dopa

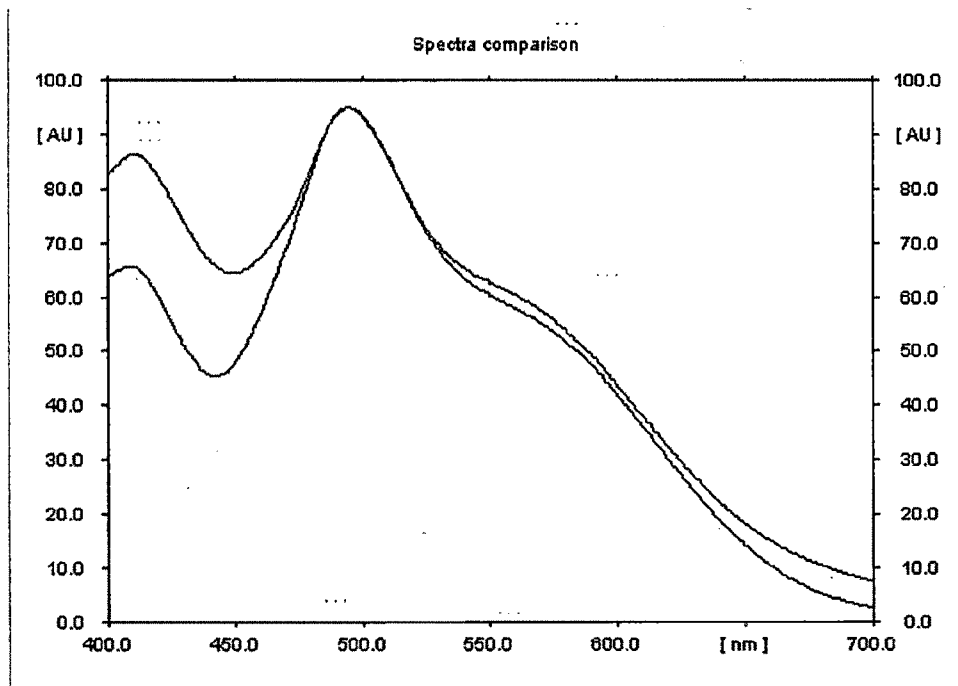


Figure 4.1.19: Spectral comparison for the peaks of standard l-dopa and *C. phlomidis* leaf extract

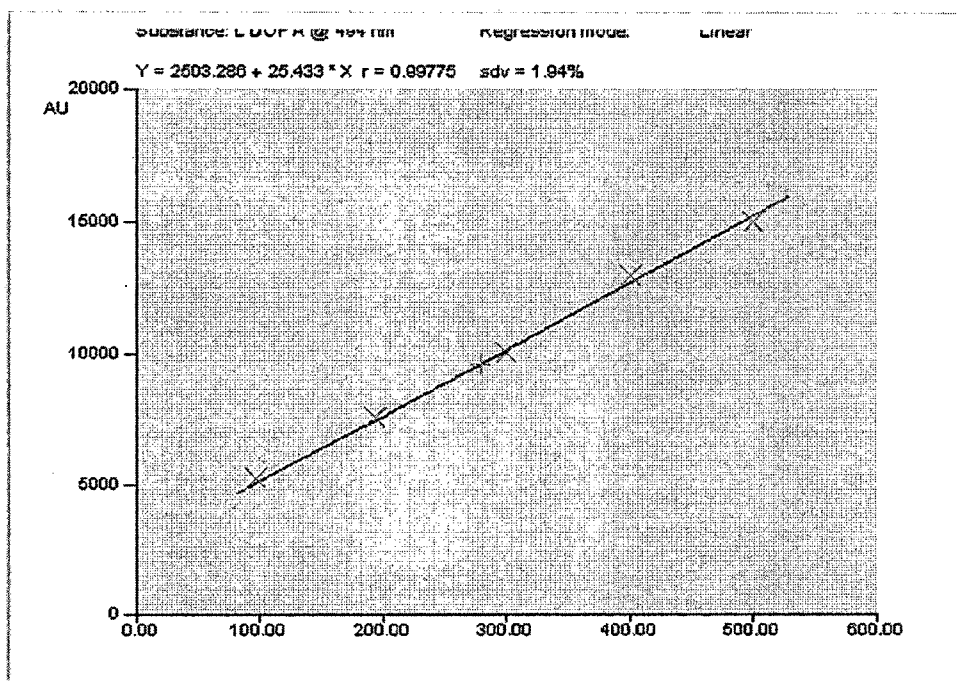


Figure 4.1.20: Calibration curve of peak area versus concentration for l-dopa

Table 4.1.11: Calibration curve parameters for quantification of l-dopa in *C. phlomidis* extract

R_f	Amount/Fraction	Area	X(calc)
0.38	100 ng	5245.72	-
0.37	200 ng	7559.78	-
0.37	300 ng	10033.01	-
0.37	400 ng	12947.07	-
0.38	500 ng	14979.47	-
0.37	-	9595.23	278.85 ng

TLC Separation Optimization: The leaves of *Clerodendrum phlomidis*, when subjected to TLC showed the presence of l-dopa peak (Figure 4.1.17, 4.1.18). A comparison of the spectral characteristics of the peaks for standard compounds and that of the sample further confirmed the identity of l-dopa present in the leaves (Figure 4.1.19).

Linearity and detection limit: The peak area versus concentration plots was found to be linear in the range of 100-500 ng spot⁻¹ for l-dopa (Figure 4.1.20). The regression equation and correlation coefficient for l-dopa indicated good linearity. The limit of detection for l-dopa was 2.88 ng. The limit of quantification was 8.73 ng for l-dopa (Table 4.1.9).

Precision studies: Instrumental precision was checked by repeated scanning of the same spots of standards three times and % RSD values were calculated. To determine the precision of the methods, standard was analyzed three times inter-day and intra-day (Table 4.1.10).

Recovery studies and sample analysis: For the examination of recovery rates 80, 100 and 120% of pure standard was added to preanalysed samples and quantitative analysis was performed (Table 4.1.10). The l-dopa content of the leaves calculated from the area calibration curve (Table 4.1.11) by this method was found to be 0.06806 %w/w (plant dry weight basis).

4.1.9.3 Identification and quantification of lupeol

Preliminary TLC finger printing and co-TLC studies (with marker compound) of *C. phlomidis* leaves revealed the presence of lupeol. Further, it was confirmed by R_f comparison, multi-wavelength scanning and spectral overlay. Good resolution with symmetrical and reproducible peaks was obtained. Lupeol (Figure 4.1.21) is reported for anti-inflammatory (Geetha and Varalakshmi, 2001), antioxidant (Shirwaikar et al., 2004), antiarthritic (Agarwal and Rangari, 2003) and antiplasmodial activity (Ziegler et al., 2002).

Considering the wide therapeutic application of this chemical constituent and to ensure identity, quality of the plant material, the study was planned to quantify this marker constituent by TLC method.

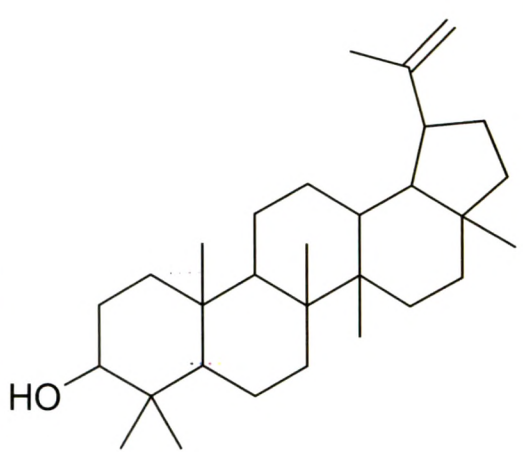
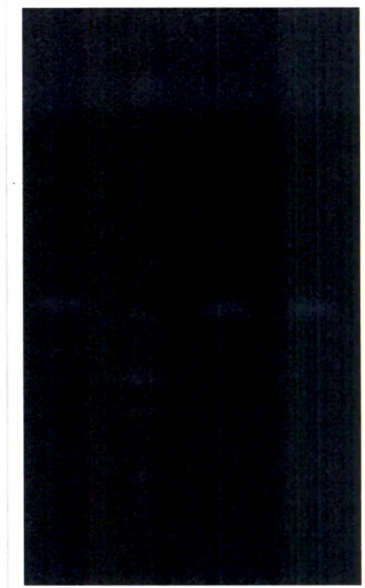
	
<p>Figure 4.1.21: Chemical structure of lupeol</p>	<p>Figure 4.1.22: Standard lupeol band and <i>C. phlomidis</i> extract</p>

Table 4.1.12: Method validation parameters for quantification of lupeol in *C. phlomidis* leaves

S. No.	Parameter	Results
1	R _f	0.40
2	Dynamic range (ng spot ⁻¹)	50 - 250
3	Equation	y=675.100+26.008x
4	Slope	26.008
5	Intercept	675.100
6	Limit of detection	5.31 ng
7	Limit of quantification	16.08 ng
8	Linearity (correlation coefficient)	0.99959

Table 4.1.13: Precision and recovery studies data for quantification of lupeol in *C. phlomidis* leaves

Precision studies			
Concentration (ng spot ⁻¹)	Instrumental precision (% RSD)	Method precision (% RSD)	
		Intra-day	Inter-day
50	0.72	1.18	1.31
250	0.41	0.65	0.71

Recovery studies			
Amount of lupeol in the sample (µg)	Amount of lupeol added (µg)	Amount of lupeol found (µg)	Recovery (%)
17.3	13.8	30.6	98.39
17.3	17.3	35.2	101.73
17.3	20.8	39.1	102.62

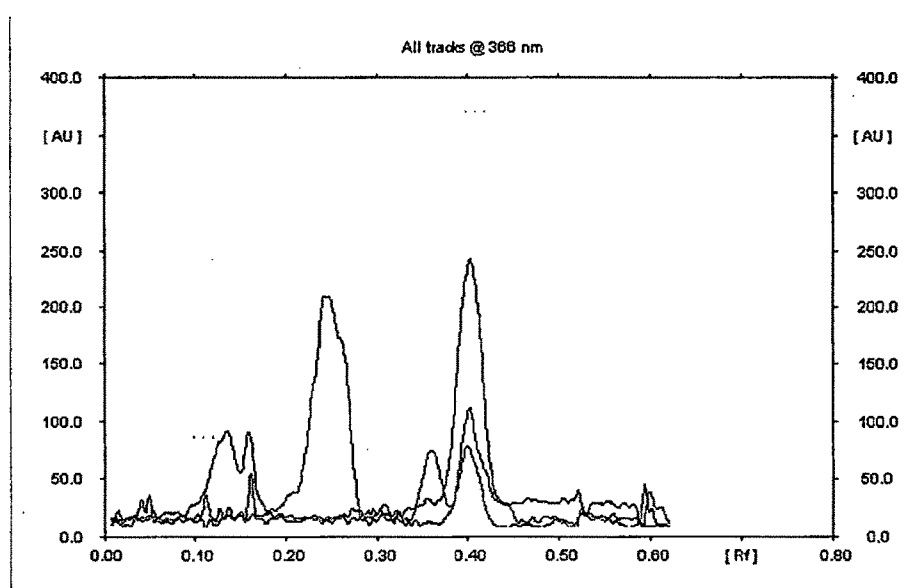


Figure 4.1.23: *C. phlomidis* leaf extract showing identical peak with standard lupeol

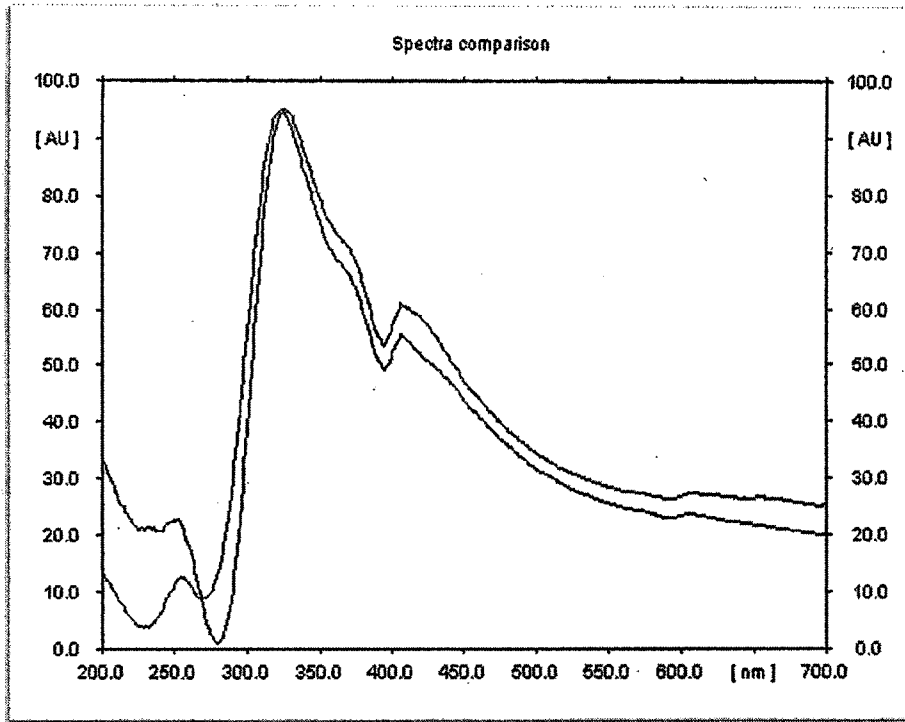


Figure 4.1.24: Spectral comparison for the peaks of standard lupeol and *C. phlomidis* leaf extract

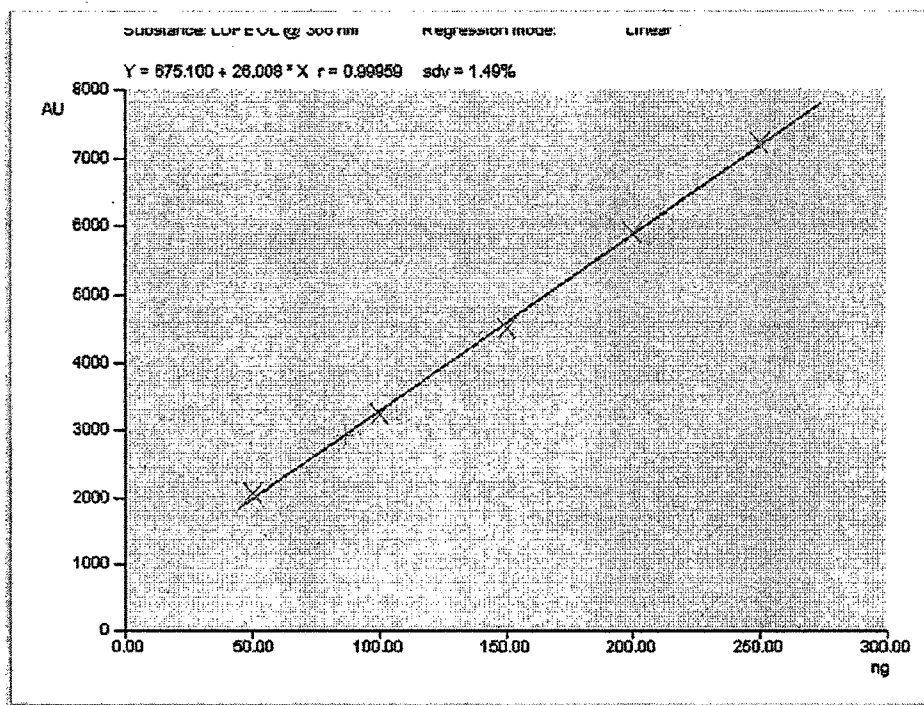


Figure 4.1.25: Calibration curve of peak area versus concentration for lupeol

Table 4.1.14: Calibration curve parameters for quantification of lupeol in *C. phlomidis* extract

R _f	Amount/Fraction	Area	X(calc)
0.39	50 ng	2045.13	-
0.40	100 ng	3228.05	-
0.39	150 ng	4506.18	-
0.39	200 ng	5881.65	-
0.41	250 ng	7220.25	-
0.41	-	2928.09	86.63 ng

TLC Separation Optimization: The leaves of *Clerodendrum phlomidis*, when subjected to TLC showed the presence of lupeol peak (Figure 4.1.22, 4.1.23). A comparison of the spectral characteristics of the peaks for standard compound and that of the sample further confirmed the identity of lupeol present in the sample (Figure 4.1.24). Good resolution with symmetrical and reproducible peaks was obtained.

Linearity and detection limit: The peak area versus concentration plots was found to be linear in the range of 50-250 ng spot⁻¹ for lupeol (Figure 4.1.25). The regression equation and correlation coefficient for lupeol indicated good linearity. The limit of detection for lupeol was 5.31 ng. The limit of quantification was 16.08 ng for lupeol (Table 4.1.12).

Precision studies: Instrumental precision was checked by repeated scanning of the same spots of standard three times and % RSD values were calculated. To determine the precision of the methods, standard was analyzed three times inter-day and intra-day (Table 4.1.13).

Recovery studies and sample analysis: For the examination of recovery rates 80, 100 and 120 % of pure standard was added to preanalysed sample and quantitative

analysis was performed (Table 4.1.13). The lupeol content of the leaves calculated from the area calibration curve (Table 4.1.14) by this method was found to be 0.01733 %w/w (plant dry weight basis).

4.1.9.4 Identification and quantification of β -sitosterol

β -sitosterol (Figure 4.1.26) has been reported previously from *C. phlomidis* leaves (Bhakuni et al., 1962). Although β -sitosterol has shown an amazing array of scientifically acknowledged benefits for key areas of health in immune dysfunctions, inflammatory disorders, rheumatoid arthritis (Bouic et al., 1996; Bouic, 2001), hypercholesterolemia (Law, 2000), colon cancer (Awad et al., 1997), breast cancer (Awad et al., 2001) and prostate cancer (Awad et al., 2000), there is no report on quantification of β -sitosterol.

Considering the wide therapeutic application of this chemical constituent and to ensure identity, quality of the plant material, the study was planned to quantify this marker constituent by TLC method. Preliminary TLC finger printing and co-TLC studies (with marker compound) of *C. phlomidis* leaves revealed the presence of β -sitosterol. Further, it was confirmed by R_f comparison, multi-wavelength scanning and spectral overlay.

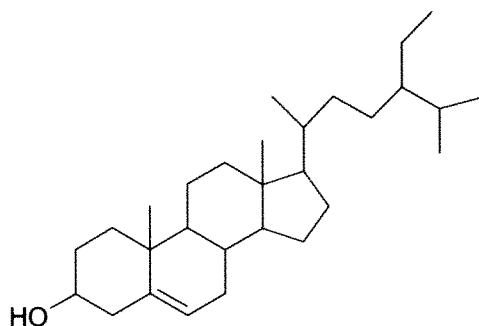


Figure 4.1.26: Chemical structure of β -sitosterol

Table 4.1.15: Method validation parameters for quantification of β -sitosterol in *C. phlomidis* leaves

S. No.	Parameter	Results
1	R _f	0.55
2	Dynamic range (ng spot ⁻¹)	100-600
3	Equation	$y=324.473+9.729x$
4	Slope	9.729
5	Intercept	324.473
6	Limit of detection	6.16 ng
7	Limit of quantification	18.66 ng
8	Linearity (correlation coefficient)	0.99788

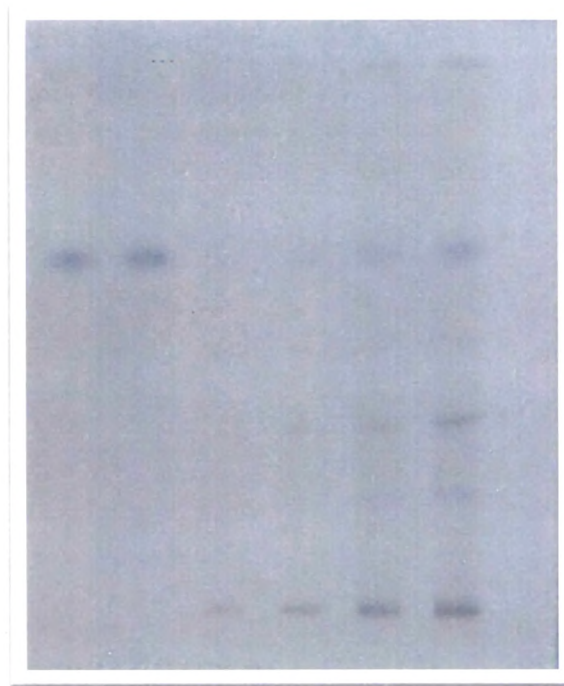


Figure 4.1.27: Standard β -sitosterol band and *C. phlomidis* extract

Table 4.1.16: Precision and recovery studies data for quantification of β -sitosterol in *C. phlomidis* leaves

Precision studies			
Concentration (ng spot ⁻¹)	Instrumental precision (% RSD)	Method precision (% RSD)	
		Intra-day	Inter-day
100	0.47	0.74	0.94
600	0.57	0.58	0.75

Recovery studies			
Amount of β -sitosterol in the sample (μ g)	Amount of β -sitosterol added (μ g)	Amount of β -sitosterol found (μ g)	Recovery (%)
63.2	50.6	110.6	97.18
63.2	63.2	124.6	98.57
63.2	75.8	141.3	101.65

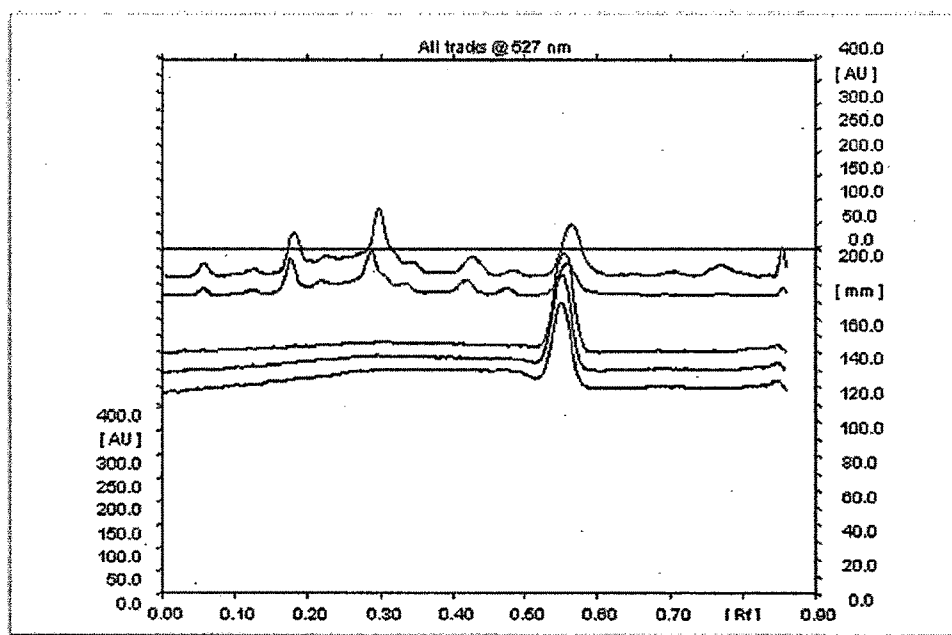


Figure 4.1.28: *C. phlomidis* leaf extract showing identical peak with standard β -sitosterol

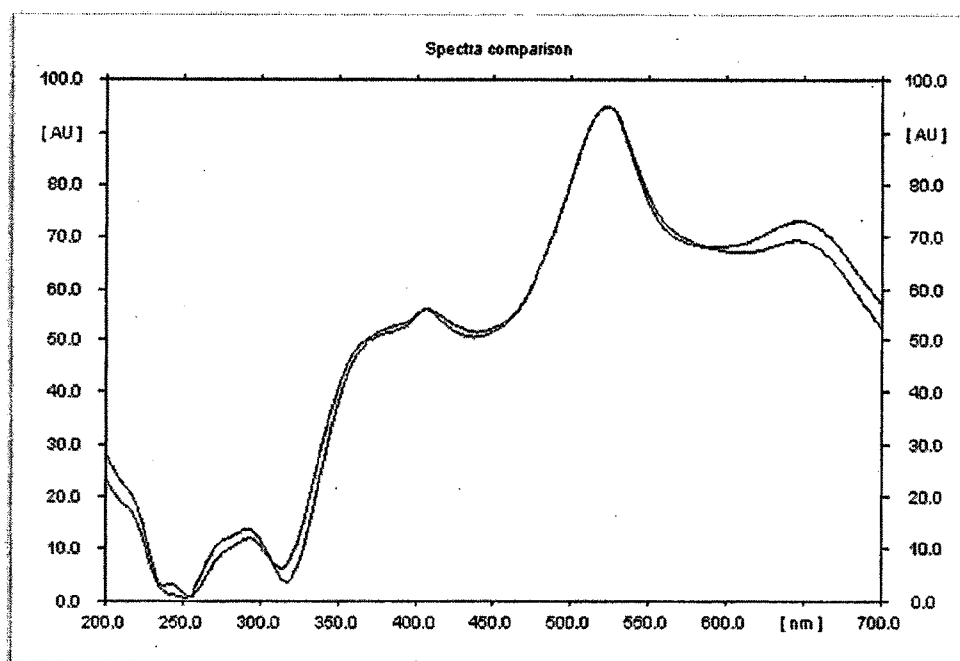


Figure 4.1.29: Spectral comparison for the peaks of standard β -sitosterol and *C. phlomidis* leaf extract

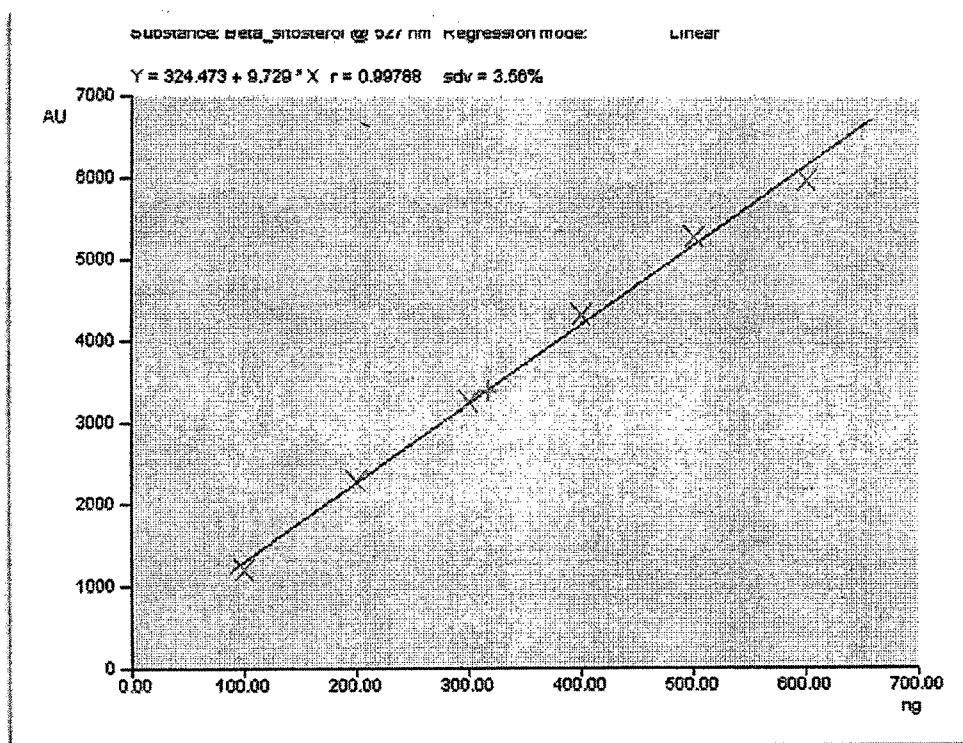


Figure 4.1.30: Calibration curve of peak area versus concentration for β -sitosterol

Table 4.1.17: Calibration curve parameters for quantification of β -sitosterol in *C. phlomidis* extract

R _f	Amount/Fraction	Area	X(calc)
0.56	100 ng	1194.08	-
0.55	200 ng	2284.29	-
0.55	300 ng	3277.62	-
0.55	400 ng	4341.24	-
0.55	500 ng	5295.75	-
0.55	600 ng	5984.79	-
0.56	-	3404.82	316.61 ng

TLC Separation Optimization: The leaves of *Clerodendrum phlomidis*, when subjected to TLC showed the presence of β -sitosterol peak (Figure 4.1.27, 4.1.28). A comparison of the spectral characteristics of the peaks for standard compounds and that of the sample further confirmed the identity of β -sitosterol present in the sample (Figure 4.1.29). Good resolutions with symmetrical and reproducible peaks were obtained.

Linearity and detection limit: The peak area versus concentration plots was found to be linear in the range of 100-600 ng spot⁻¹ for β -sitosterol (Figure 4.1.30). The regression equation and correlation coefficient for β -sitosterol indicated good linearity. The limit of detection for β -sitosterol was 6.16 ng. The limit of quantification was 18.66 ng for β -sitosterol (Table 4.1.15).

Precision studies: Instrumental precision was checked by repeated scanning of the same spots of standard three times and % RSD values were calculated. To determine the precision of the methods, standard was analyzed three times inter-day and intra-day (Table 4.1.16).

Recovery studies and sample analysis: For the examination of recovery rates 80, 100 and 120 % of pure standard was added to preanalysed samples and quantitative analysis was performed (Table 4.1.16). The β -sitosterol content of the leaves calculated from the area calibration curve (Table 4.1.17) by this method was found to be 0.06324 %w/w (plant dry weight basis).

4.1.9.5 Identification and quantification of β -carotene

β -carotene (Figure 4.1.31) is a carotenoid, with beta-rings at both ends, it is the most common form of carotenoid. It is a precursor to vitamin A via the action of beta-carotene 15,15'-monooxygenase. β -carotene as an antioxidant, provides protection against cancer, heart disease, macular degeneration and ageing (Burri, 1997).

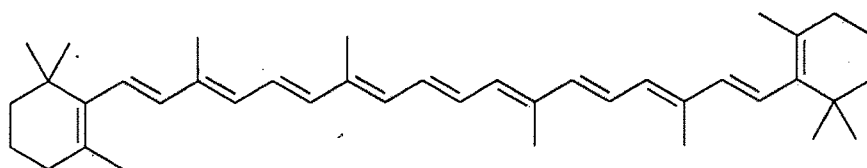


Figure 4.1.31: Chemical structure of β -carotene

Table 4.1.18: Validation parameters for quantification of β -carotene in *C. phlomidis* leaves

S. No.	Parameter	Results
1	R_f	0.40
2	Dynamic range (ng spot ⁻¹)	100-500
3	Equation	$y=42.383+3.762x$
4	Slope	3.762
5	Intercept	42.383
6	Linearity (correlation coefficient)	0.99692

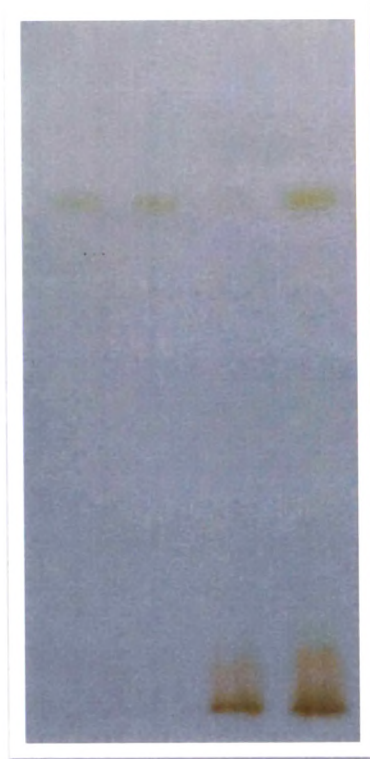


Figure 4.1.32: Standard β -carotene band and *C. phlomidis* extract

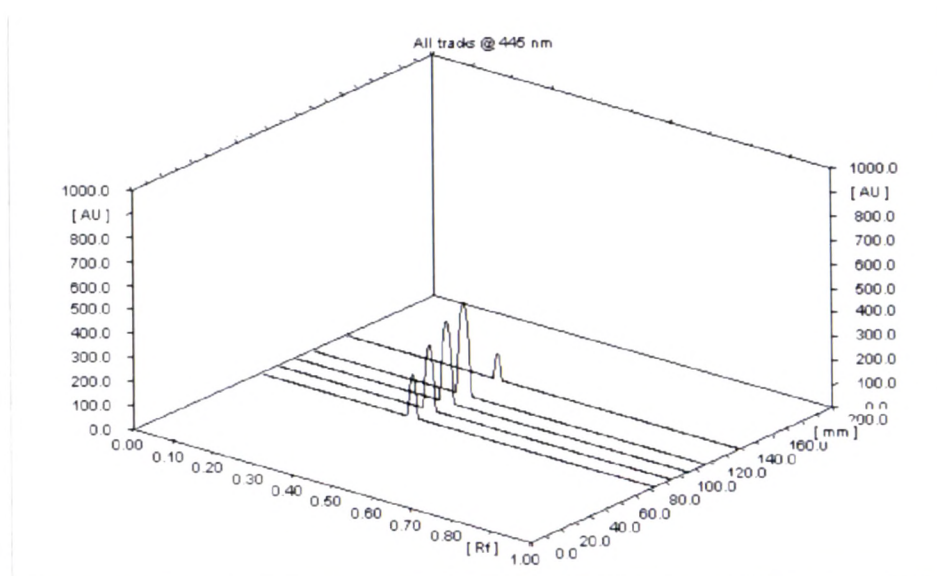


Figure 4.1.33: *C. phlomidis* leaf extract showing identical peak with standard β -carotene

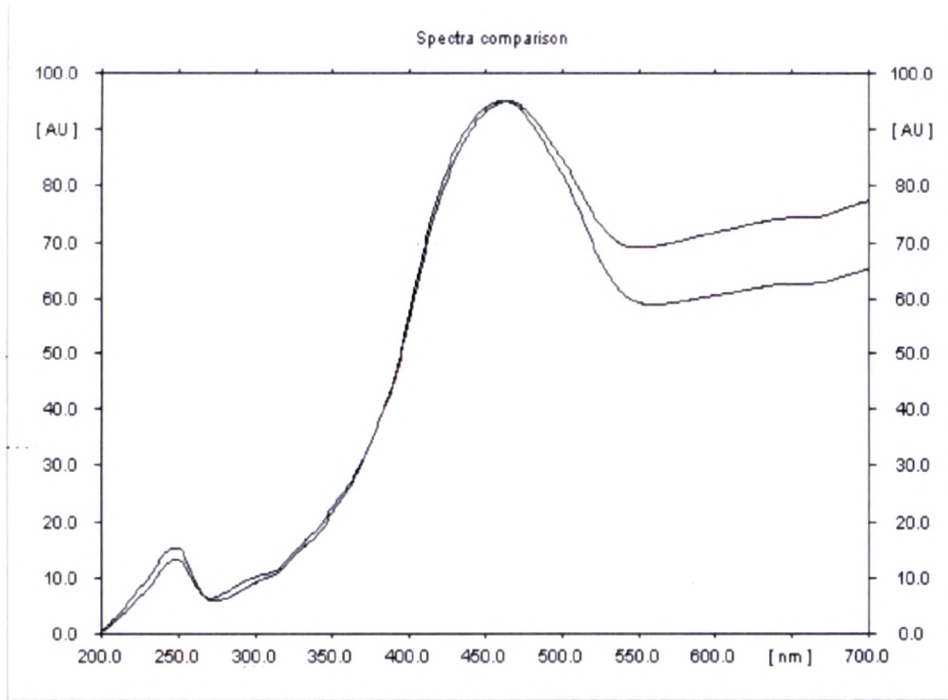


Figure 4.1.34: Spectral comparison for the peaks of standard β -carotene and *C. phlomidis* leaf extract

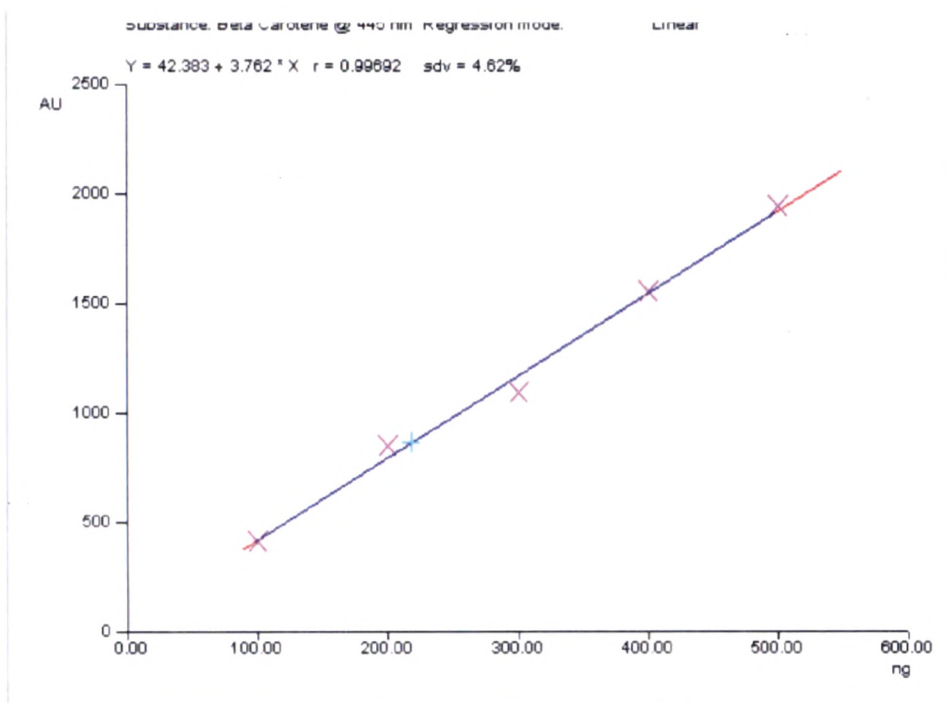


Figure 4.1.35: Calibration curve of peak area versus concentration for β -carotene

Table 4.1.19: Calibration curve parameters for quantification of β -carotene in *C. phlomidis* extract

R _f	Amount/Fraction	Area	X(calc)
0.39	100 ng	413.33	-
0.39	200 ng	848.60	-
0.39	300 ng	1097.02	-
0.39	400 ng	1554.82	-
0.40	500 ng	1941.25	-
0.39	-	862.20	217.92 ng

TLC Separation Optimization: The leaves of *Clerodendrum phlomidis*, when subjected to TLC showed the presence of β -carotene peak (Figure 4.1.32, 4.1.33). A comparison of the spectral characteristics of the peaks for standard compounds and that of the sample further confirmed the identity of β -carotene present in the sample (Figure 4.1.34). Good resolutions with symmetrical and reproducible peaks were obtained.

Linearity and detection limit: The peak area versus concentration plots was found to be linear in the range of 100-500 ng spot⁻¹ for β -carotene (Figure 4.1.35). The regression equation and correlation coefficient for β -carotene indicated good linearity (Table 4.1.18).

Sample analysis: The β -carotene content of the leaves calculated from the area calibration curve (Table 4.1.19) by this method was found to be 0.021792 %w/w (plant dry weight basis).

4.1.9.6 Amino acid identification

The plant amino acids are conveniently divided into two groups, the 'protein' and 'non-protein' acids, although the division between the two groups is not entirely sharp and methods of identifying and separating both groups are essentially the

same. The 'protein' amino acids are generally recognized to be twenty in number and are those found in acid hydrolysates of plant proteins (Glycine, alanine, serine, cysteine, threonine, valine, leucine, isoleucine, methionine, aspartic acid, asparagine, glutamic acid, glutamine, arginine, lysine, proline, phenylalanine, tyrosine, tryptophan and histidine).

The preliminary chemical tests showed high quantitative presence of amino acids and also positive reaction for alkaloids, hence the identification of amino acids was studied (Figure 4.1.36) particularly the aromatic amino acids. The co-TLC study showed the presence of tyrosine, phenylalanine, alanine, valine, leucine, isoleucine, glutamic acid and threonine (Figure 4.1.37).

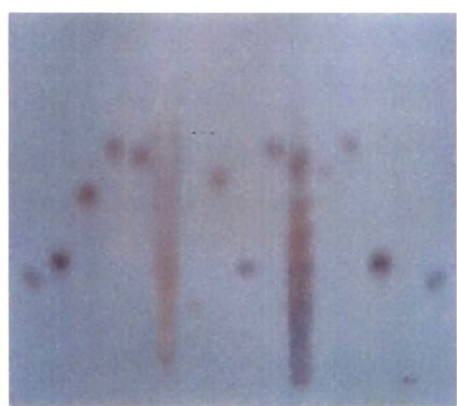


Figure 5.1.36: Amino acid identification in *C. phlomidis* extract (a)

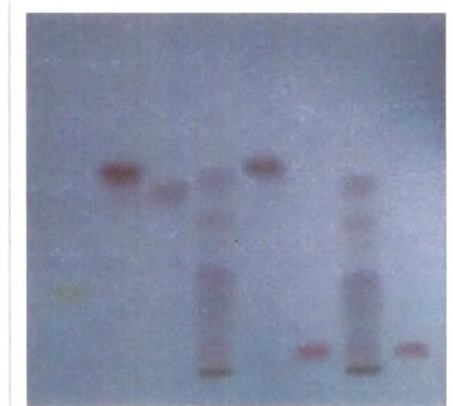


Figure 5.1.37: Amino acid identification in *C. phlomidis* extract (b)

The amino acids also occur together in the free amino acid pool of plant tissues at varying concentrations, they also considerably vary quantitatively from tissue to tissue depending on the metabolic status of the plant. Two aromatic amino acids tyrosine and phenylalanine were detected; on the other hand the third aromatic amino acid, tryptophan is generally present in such low amounts in plant tissues that they cannot be readily detected. In general glutamic acid tends to be present in larger amount than others, since they represent a storage form of nitrogen.

4.1.9.7 Crude polyamine extract (CPECP)

Polyamines are widely distributed in plants, microorganisms, and animal tissues (Tabor et al., 1961). In contrast to monoamines, polyamines are less volatile, although they still possess offensive odours.

Wide spread polyamines include putresine ($\text{NH}_2(\text{CH}_2)_4\text{NH}_2$), spermidine ($\text{NH}_2(\text{CH}_2)_3\text{NH}(\text{CH}_2)_4\text{NH}_2$), agmatine ($\text{NH}_2(\text{CH}_2)_4\text{NHC(=NH)NH}_2$) and spermine ($\text{NH}_2(\text{CH}_2)_3\text{NH}(\text{CH}_2)_4\text{NH}(\text{CH}_2)_3\text{NH}_2$). Their distribution in microorganisms, conjugation with glutathione, nucleic acids, lipids and viruses, function as a growth factor and abilities to stabilize cells, protoplast and mitochondria have been studied and reviewed (Tabor and Tabor, 1964). Since then, increasing attention has been given to their effects on metabolism and biological functions in animal tissues (Herbst and Bachrach, 1970; Janne, 1967.) and particularly of their growth-stimulating activity in relation to their effect on ribosomal RNA. The co-TLC of crude polyamine extract showed the presence of numerous polyamine bands (Figure 4.1.38), but absence of spermidine.

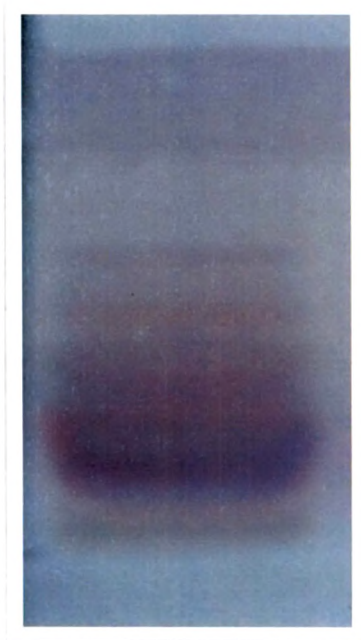


Figure 4.1.38: TLC of crude polyamine extract of *C. phlomidis*

4.1.9.8 Identification of alkaloids

The crude alkaloidal fraction (CAFCP) yielded 320 mg of brown residue. The preliminary phytochemical test showed positive for the presence of alkaloids. When CAFCP separated in TLC showed no clear individual spots for alkaloids with dragendorffs reagent. The alkaloid/s may be individually insufficient for a quantitative reaction with dragendorffs reagent.

4.1.10 DNA sequence for internal transcribed spacer (ITS) of *C. phlomidis*

The recent advances in molecular biology have offered an additional tool for the quality control of medicinal plants. DNA is the basic component of a living organism whereas chemical and phenotypic expression is controlled by the arrangement and expression of genes in the DNA. Polymerase chain reaction (PCR) technology-based DNA profiling as a novel approach has several significant advantages over morphological and chemical methods;

- since the nucleotides are the basic units of genetic information encoded in organism, the genotype rather than the phenotype is assayed,
- one or more characters such as genomic fingerprint or DNA sequence, appropriated in solving the particular problem can be selected, and
- it can be applied to dried commercial samples from any part of organs because DNA can be prepared from a small amount of tissues (Hui et al., 2000).

Currently, DNA sequencing is applied to distinguish species and study phylogenetic relationship, population genetics, systematics and evolution (Wang et al., 2005). There are many reports concerning the application of DNA sequence-based markers to differentiate medicinal plants from its substitutes or adulterants. Most of them involves the sequencing of internal transcribed spacer (ITS) ribosomal DNA (rDNA) (Liu et al., 2001; Chen 2004; Wang et al., 2005). The ITS rDNA region has become an important locus for the molecular systematic

investigation of angiosperms at the interspecific and intraspecific levels. Specific PCR primers are positioned on the conserved rDNA genes (18S, 5.8S, 26S) to amplify the entire ITS spacer region (Figure 4.1.39). The ITS region of rDNA, defined as the unit containing the ITS1 spacer, 5.8S rDNA gene and ITS2 spacer, has been proven to be a useful gene for screening different medicinal plants.

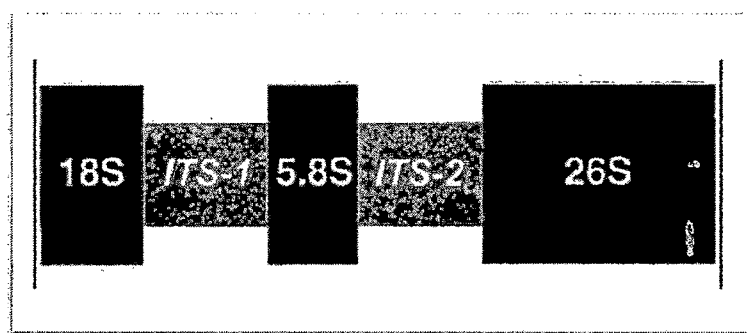


Figure 4.1.39: Schematic diagram of the nuclear rDNA internal transcribed spacer region. The three rDNA subunits: 18S, 5.8S and 26S are separated by ITS1 and ITS2

The DNA sequences for ITS of two samples of *C. phlomidis* A and B (Figure 4.1.40) differed by one base pair, may be one of the samples is polymorphic/heterozygous for that position in the sequence. Figure 4.1.41 illustrates the position of *C. phlomidis* relative to other species of *Clerodendrum* and related genera. The cladistic analysis shows that *C. phlomidis* belongs to clade II – the African clade. In a phenetic study by Stenzel et al. (1988) *C. phlomidis* was placed in a group with other Asian species (clade I) which is contradicting. Moreover the cladistic study has shown that *C. phlomidis* is very closely related to *Clerodendrum hildebrandtii* var. *puberula* Verdc., a Tanzanian species.

```
>C._phlomidis_A  
TGGGAGGATAAAAAACGTAACAAGGTTTCCGTAGGTGAACCTGCGGAAGG  
ATCATTGTCGAAACCTGCATAGCAGACCGCGAACACGTGTTTAAACAAAT  
CGGGGCTGCGGTCTTCTGCGGTCCCCTCATCGCCGGCGTGCGCCAACGCG  
TCGCTGTGCGGTCTAACAAAATCGGGCGCGGAATGCGCCAAGGAATACAC  
AAAAGAGTGTTCCCCTCCCCAGGGCCCATGTGCGGAGATCGTGGGGAGGT  
TGGGATGCCCCGTCGTATACAAAAACGACTCTCGGCAACGGATATCTCGGC  
TCTCGCATCGATGAAGAACGTAGCGAAATGCGATACTTGGTGTGAATTGC  
AGAATCCCGTGAACCATCGAGTCTTTGAACGCAAGTTGCGCCCGAAGCCA  
TTAGCCCCGAGGGCACGTCTGCCTGGGCGTCACGCATCACGTGCGCTCCCT  
CCACACACAGTGCTGTTGATGGGGGCGGATATTGGCCTCCCGTGCATCAT  
TCATGCGCGGCCGGTCCAAATGCAATCCCTCGGTGGCGAAAGTCACGACC  
AGTGTGGTTGAAGTATCAACTCGCGTGCTGTCGTGACACAAGACGTCGT  
CCGATCGGGAGTCACTACAGACCCAGTGGCGCATTACGCATTGCGCCTC  
CGACCGCGACCCCAGGTCAGGCGG
```

```
>C._phlomidis_B  
AACCAAGGTTTCCGTAGGTGAACCTGCGGAAGGATCATTGTCGAAACCTGC  
ATAGCAGACCGCGAACACGTGTTTAAACAAATCGGGGCTGCGGTCTTCTG  
CGGTCCCCTCATCGCCGGCGTGCGCCAACGCGTCGCTGTGCGGTCTAACA  
AAATCGGGCGCGGAATGCGCCAAGGAATACACAAAAGAGTGTTCCCCTCC  
CCAGGGCCCCATGTGCGGAGATCGTGGGGAGGTTGGGATGCCCCGTCGTATA  
CAAAAACGACTCTCGGCAACGGATATCTCGGCTCTCGCATCGATGAAGAA  
CGTAGCGAAATGCGATACTTGGTGTGAATTGCAGAATCCCGTGAACCATC  
GAGTCTTTGAACGCAAGTTGCGCCCGAAGCCATTAGGCCGAGGGCACGTC  
TGCCTGGGCGTCACGCATCACGTGCGCTCCCTCCACACACAGTGCTGTTG  
ATGGGGGCGGATATTGGCCTCCCGTGCATCATTATGCGCGGCCGGTCCA  
AATGCAATCCCTCGGTGGCGAAAGTCACGACCAGTGTTGGTTGAAGTATC  
AACTCGCGTGCTGTCGTGACACAAGACGTCGTCCGATCGGGAGTCACTAC  
AGACCCAGTGGCGCATTACGCATTGCGCCTCCGTCCGCGACCCCAGGTC  
AGGCGGGATTACCCGCTGAGTTAAGCATATC
```

Figure 4.1.40: DNA sequences for ITS of *C. phlomidis*

The sequence was also compared to all other sequences on GenBank (GenBank database accession number gb|U77743.1|CBU77743) and it is most similar to *Clerodendrum buchneri*, a species in Clade II (African), the details are as follows; *Clerodendrum buchneri* 18S ribosomal RNA gene, partial sequence, internal transcribed spacer 1, 5.8S ribosomal RNA gene and internal transcribed spacer 2, complete sequence, and 26S ribosomal RNA gene, partial sequence. Length=689; Score = 1014 bits (1124); Expect = 0.0; Identities = 621/659 (94%); Gaps = 4/659 (0%); Strand=Plus/Plus.

Although *C. phlomidis* was closely related to *Clerodendrum buchneri* from GenBank database rather than *Clerodendrum hildebrandtii* from cladistic study, it is evident that this species belongs to clade II (African) than clade I (Asian) as placed by Stenzel et al., (1988).

4.1.11 Isolation and characterization of chemical constituents

Defatted ethanol extract of leaves have been reported for antidiabetic activity (Dhanabal et al., 2008). The literature review and the preliminary qualitative phytochemical screening showed steroids as major secondary metabolite of *C. phlomidis*. Nymphayol, a sterol has been reported recently for its partial regeneration of β -cells (Subash Babu et al., 2009). Considering these facts the unsaponified petroleum ether fraction of methanol extract (UPFMCP) was chosen for phytochemical studies.

4.1.11.1 Compound CP I

The fractions obtained by elution with petroleum ether (60-80 °C) yielded 178 mg of white flakes with m.p. 49 °C. It was soluble in petroleum ether, benzene, diethyl ether and slightly soluble in chloroform. The compound showed positive reaction with anisaldehyde – sulphuric acid reaction. This compound was designated as CP I.

Results and Discussion

Characterization of CP I: The structure of the isolated compound CP I was unambiguously elucidated by analysis of IR, ^1H NMR and CHNOS data. The IR spectrum revealed the presence of hydroxyl group (O-H stretching, ν_{max} 3443.05 cm^{-1} and O-H bending, ν_{max} 1261.49 cm^{-1}) (Figure 4.1.42). The CHNOS analysis showed carbon, hydrogen and oxygen percentage as 79.803, 14.036 and 5.834 respectively (Table 4.1.20, Figure 4.1.43, Figure 4.1.44). The ^1H NMR spectra of CP I was very similar to that of fatty alcohols (Figure 4.1.45). From the ^1H NMR data compound CP I was identified as 1-hexadecanol ($\text{C}_{16}\text{H}_{34}\text{O}$; Mol. wt. 242) (Figure 4.1.46).

IR(KBr): ν_{max} : 3443.05, 2956.97, 2918.40, 2848.96, 1464.02, 1377.22, 1261.49, 1097.53, 1028.09, 802.41, 729.12 cm^{-1} (Figure 4.1.42); ^1H NMR (400MHz, C_6D_6) δ : 7.26 (1H, -OH), 2.17 (2H, -CH₂), 1.90 (2H, -CH₂), 1.30-1.25 (26H, -CH₂), 0.89-0.86 (3H, -CH₃) (Figure 4.1.45)

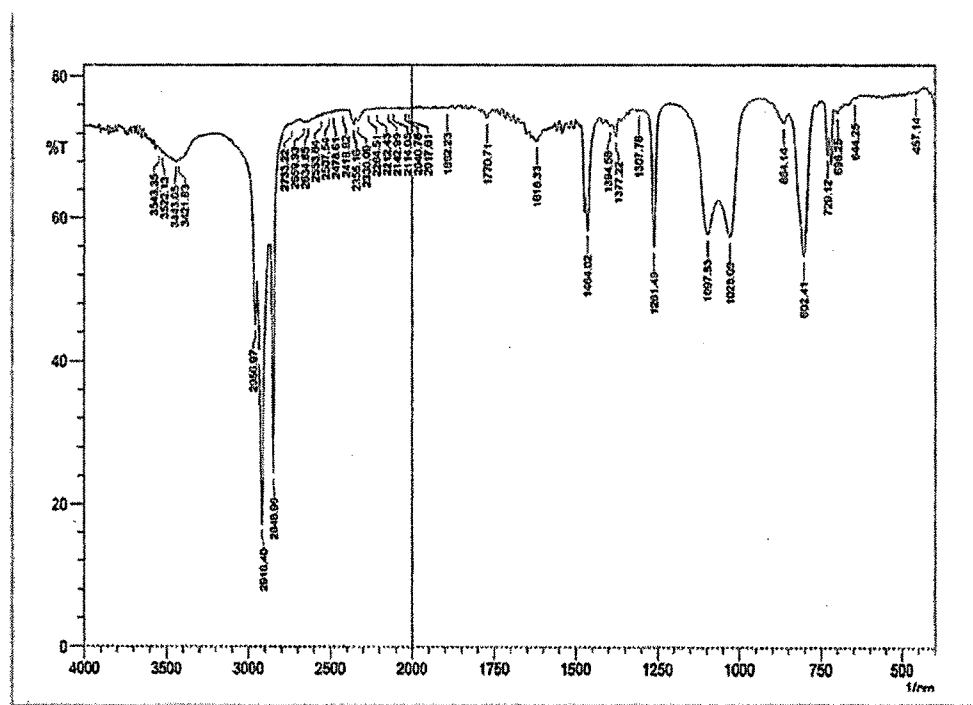


Figure 4.1.42: IR spectrum of CP I

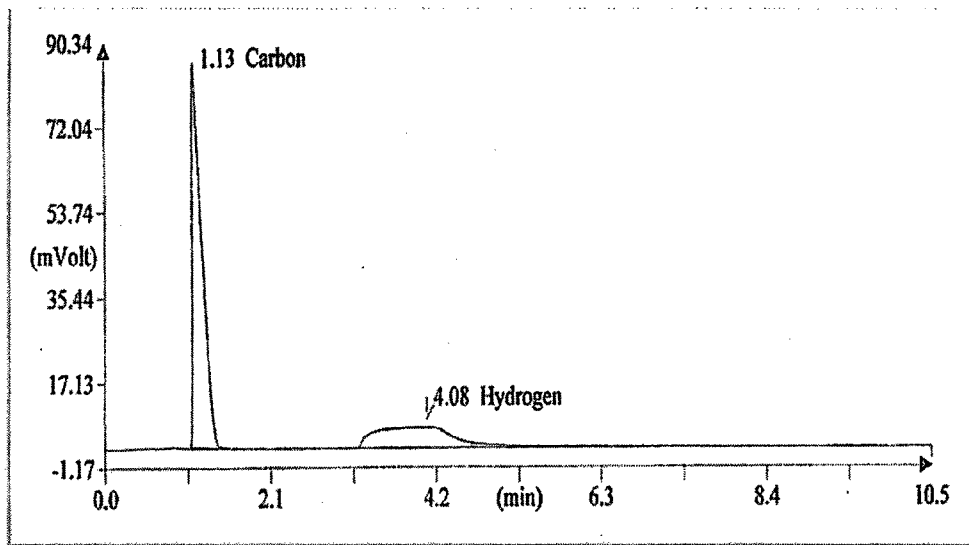


Figure 4.1.43: CHN analysis of CP I

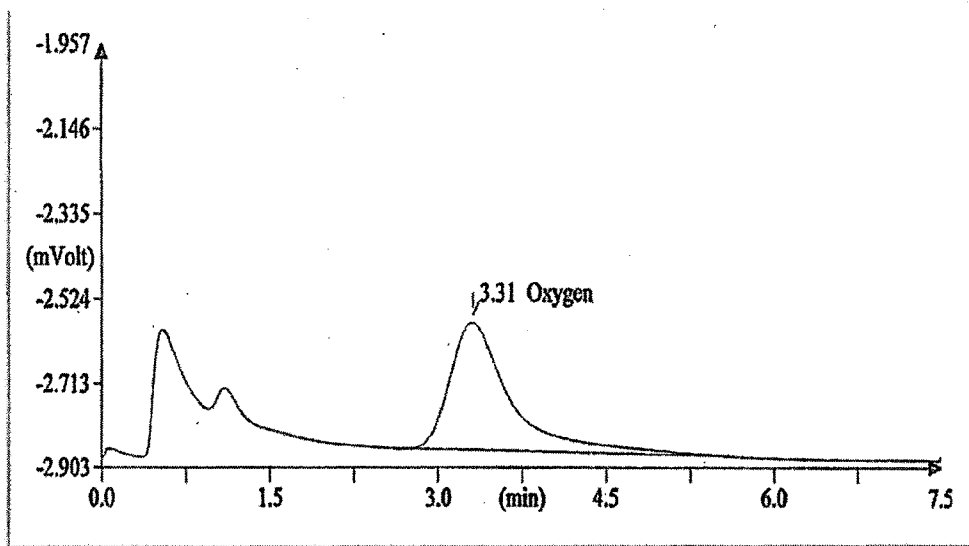


Figure 4.1.44: Oxygen analysis of CP I

Table 4.1.20: CHNOS analysis of CP I

Retention time (min)	Element percentage	Compound
1.125	79.803	Carbon
4.075	14.036	Hydrogen
3.308	5.834	Oxygen

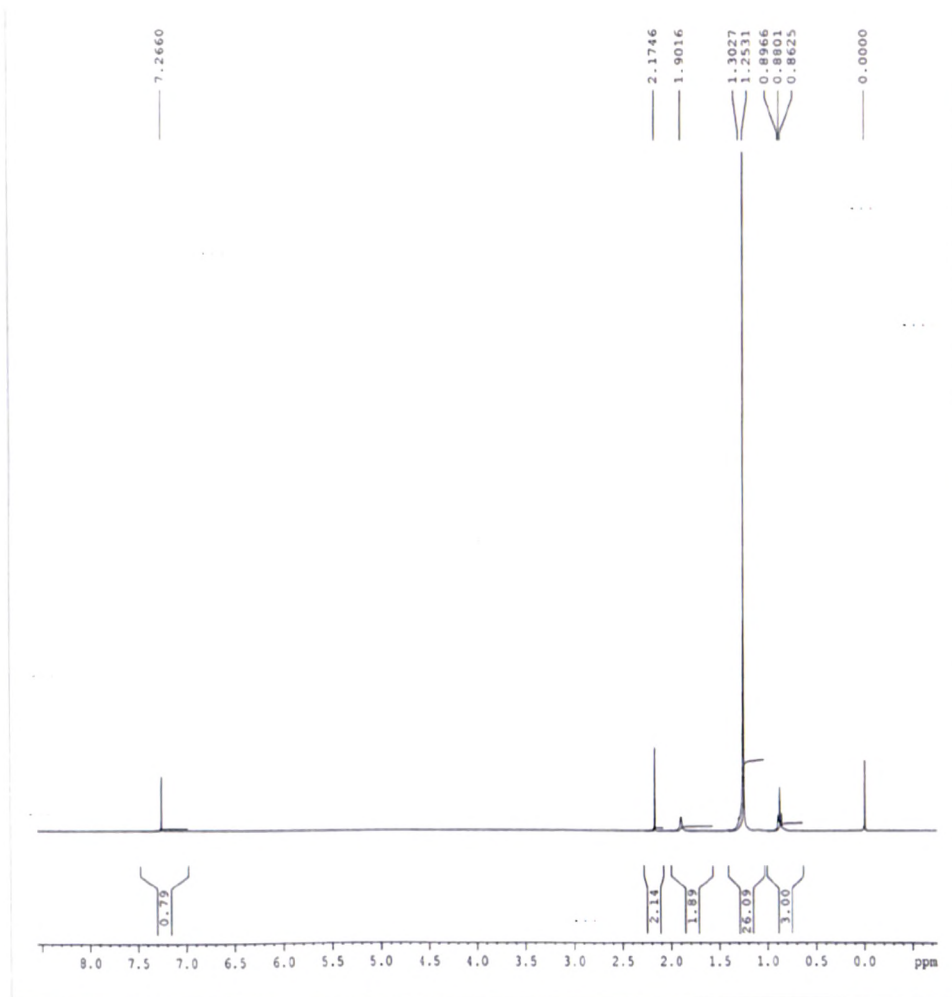


Figure 4.1.45: ¹H NMR of CP I

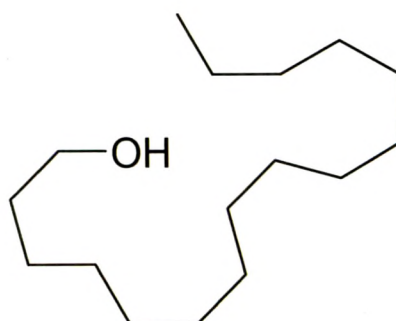


Figure 4.1.46: Chemical structure of CP I

Results and Discussion

TLC of CP I: TLC for CP I was performed with the mobile phase petroleum ether (60-80 °C) with anisaldehyde – sulphuric acid reagent as detecting agent and scanned at 540 nm to check the purity. CP I gave a single dark blue-violet spot at R_f 0.81 (Figure 4.1.47). The spectra of CP I is shown in Figure 4.1.48.

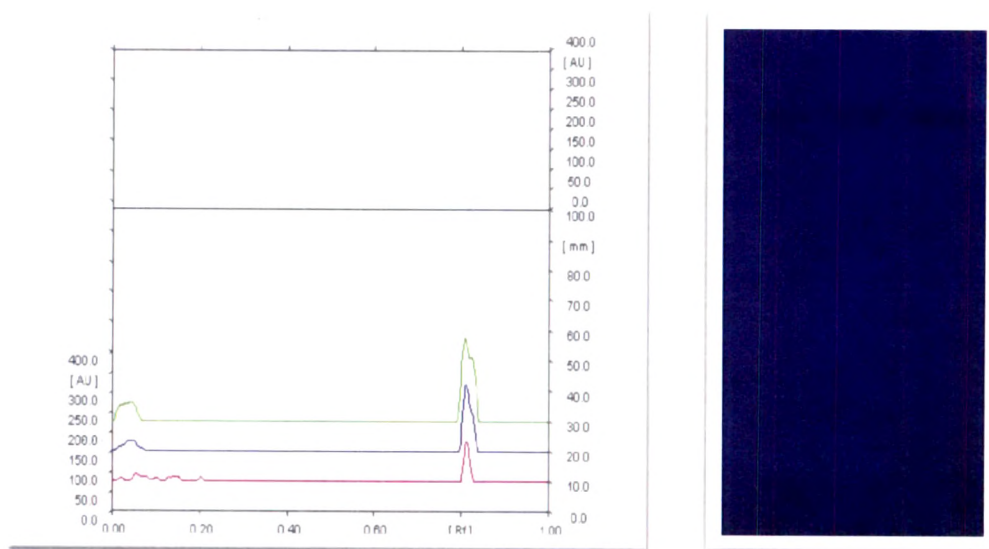


Figure 4.1.47: Densitogram and TLC photograph of CP I

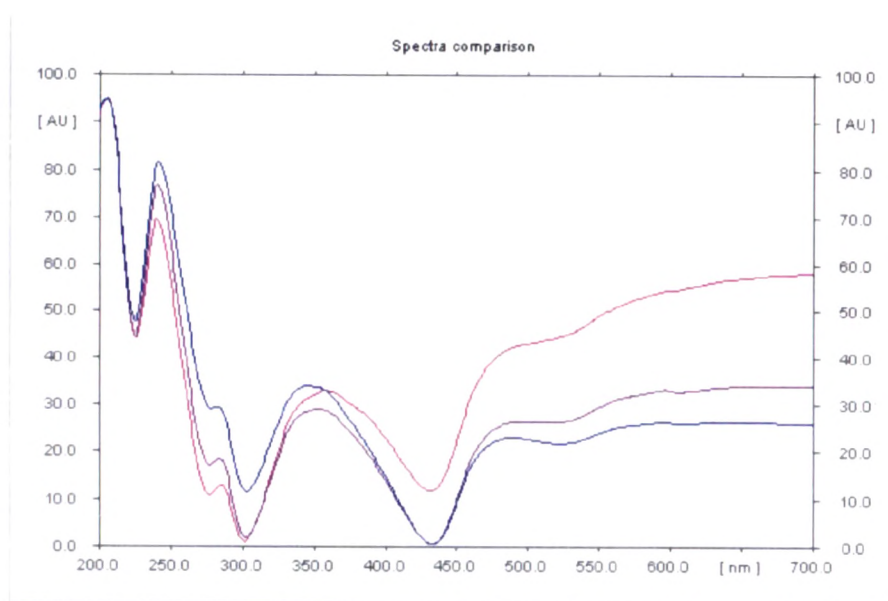


Figure 4.1.48: UV-Vis spectra of CP I

4.1.11.2 Compound CP II

The fractions obtained by elution with petroleum ether (60-80 °C): ethyl acetate (95:05) yielded 80 mg of a yellow oily substance. It was soluble in petroleum ether, benzene, diethyl ether and slightly soluble in chloroform. The compound showed positive reaction with anisaldehyde – sulphuric acid reaction. This compound was designated as CP II.

Characterization of CP II: The structure of the isolated compound CP II was unambiguously elucidated by analysis of IR, ¹H NMR, Mass, and CHNOS data. The IR spectrum revealed the presence of carbonyl group (ν_{\max} 1726.35 cm^{-1}) and C=C (ν_{\max} 1643.41 cm^{-1}) in the molecule (Figure 4.1.49). Although the molecular ion peak was not detected, the mass spectrum clearly exhibited two major fragment ion peaks at m/z 393.4 [M-palmitic acid]⁺ and 255.2 [palmitoxyl]⁺, the typical peaks that derived from the clerosterol and palmityl moieties, respectively (Yin et al., 2005) (Figure 4.1.50). Detailed analysis of the ¹H NMR data demonstrated that, apart from the clerosterol signals, the rest signals were in good agreement with those of the palmityl group (Yan, et al., 2002) (Figure 4.1.51). The CHNOS analysis also confirmed the elemental ratio carbon, hydrogen and oxygen for clerosterol palmityl ester (Table 4.1.21, Figure 4.1.52, Figure 4.1.53). From all the evidence mentioned above, the structure of compound CP II was elucidated as clerosterol palmityl ester (C₄₅H₇₈O₂; Mol. wt. 650) (Figure 4.1.54).

IR(KBr): ν_{\max} : 2933, 2851, 1726, 1643, 1460, 1379, 1190, 1132, 1058, 960, 889, 800 cm^{-1} (Figure 4.1.49); ESI-MS m/z 393.4 [M-C₁₆H₃₂O₂]⁺, 255.2 [C₁₆H₃₂O₂]⁺, 202.2 [C₁₅H₂₄]⁺, 137.2 [C₁₀H₁₆]⁺ (Figure 4.1.50); ¹H NMR (400MHz, CDCl₃) δ : 5.35 (1H, =CH), 4.69 (2H, =CH₂), 2.42-2.41 (4H, -CH₂), 2.28-2.17 (1H, -CH), 2.04-1.97 (2H, -CH), 1.85-1.83 (4H, -CH₂), 1.67-1.64 (1H, -CH), 1.56 (26H, -CH₂), 1.48-1.38 (3H, -CH), 1.25 (12H, -CH₂), 1.21-1.11 (4H, -CH₂), 1.07-1.00 (9H, -CH₃), 0.96-0.93 (6H, -CH₃), 0.89-0.85 (3H, -CH₃) (Figure 4.1.51)

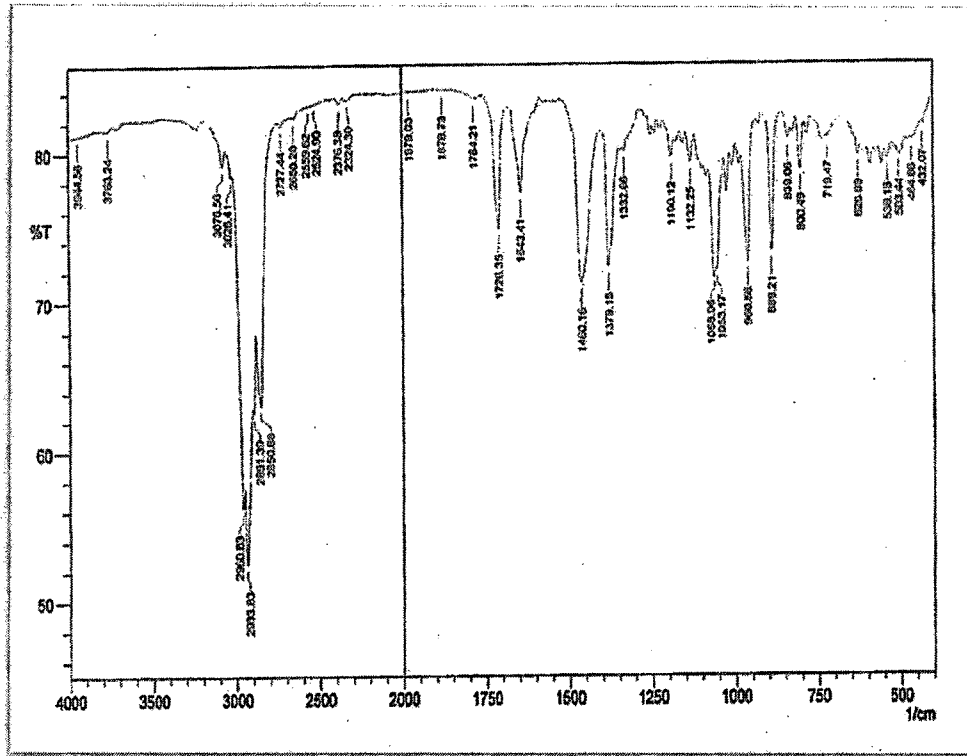


Figure 4.1.49: IR spectrum of CP II

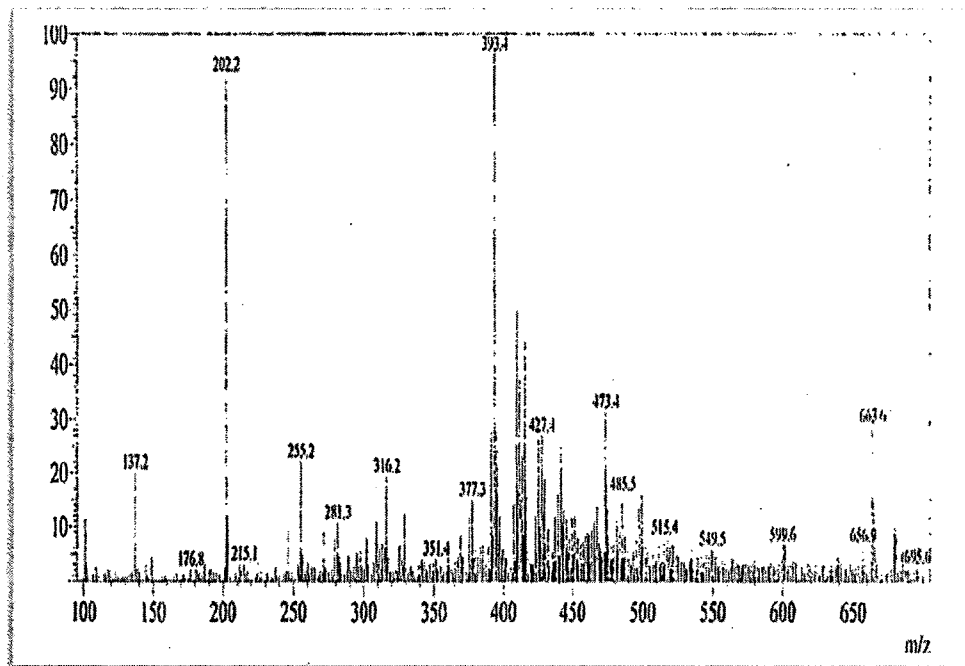


Figure 4.1.50: Mass spectrum of CP II

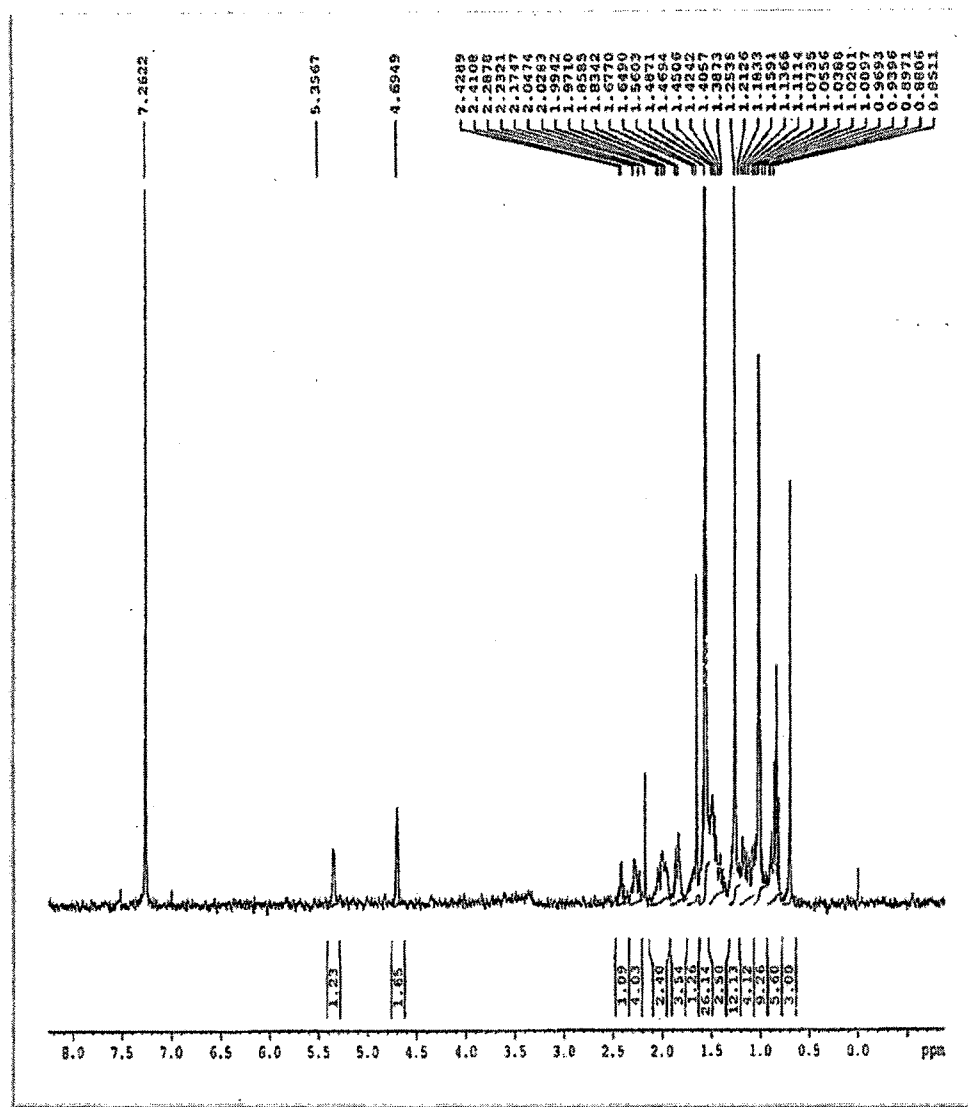


Figure 4.1.51: ¹H NMR of CP II

Table 4.1.21: CHNOS analysis of CP II

Retention time (min)	Element percentage	Compound
1.167	82.957	Carbon
3.592	11.562	Hydrogen
3.042	5.101	Oxygen

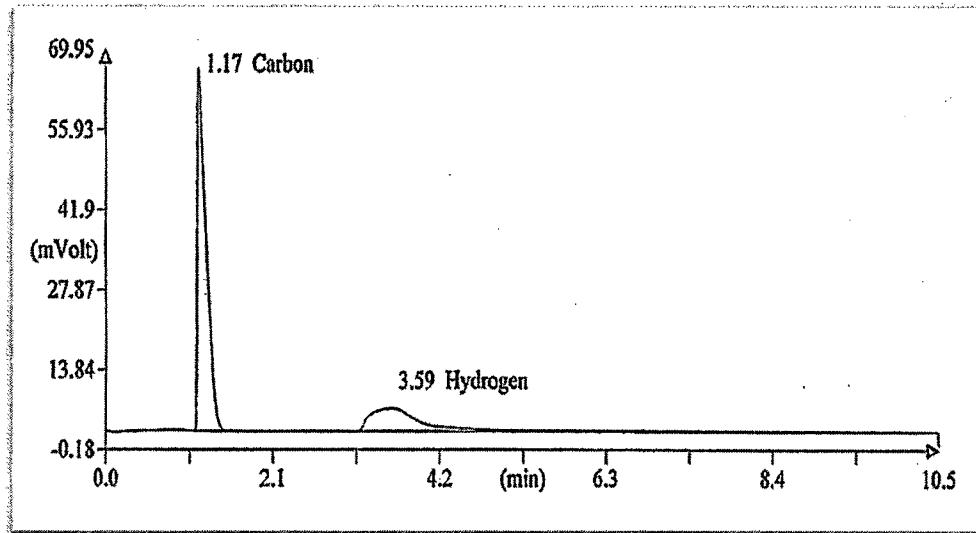


Figure 4.1.52: CHN analysis of CP II

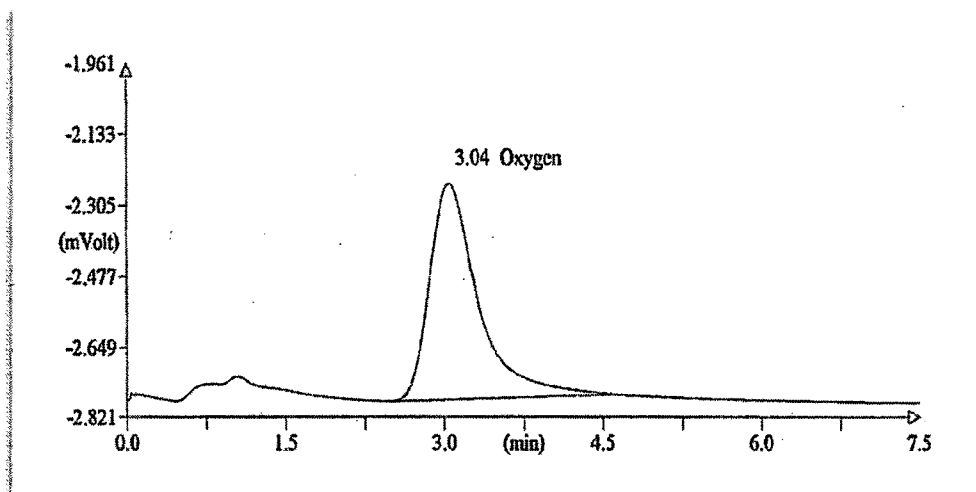


Figure 4.1.53: Oxygen analysis of CP II

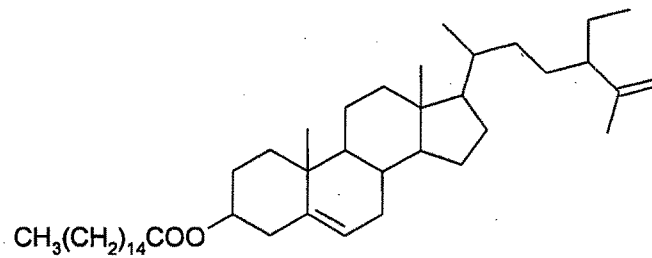


Figure 4.1.54: Chemical structure of CP II

TLC method development and quantification of CP II: TLC for CP II was performed with the mobile phase petroleum ether (60-80 °C): ethyl acetate (95:05, v/v) with anisaldehyde – sulphuric acid reagent as detecting agent and scanned at 527 nm to check the purity. CP II gave a single spot at R_f 0.64. Considering the uniqueness of this constituent a TLC method was developed.

Preparation of sample and standard solutions: Accurately weighed 7.5 g of the coarse powder of *C. phlomidis* leaves was extracted with methanol (4 X 50 mL) under reflux (30 min each time) on a water bath. The combined extracts were filtered, concentrated and transferred to a 50 ml volumetric flask and the volume was made up with methanol. A stock solution of CP II (100 µg/ml) was prepared in methanol. Working solutions were prepared by appropriate dilution of the stock solution with the same solvent.

Calibration curve for CP II: CP II stock solution in the range of 100 to 500 ng spot⁻¹ was applied on TLC plate for preparation of calibration curve of peak area versus concentration.

Quantification of CP II in test sample: Quantification was performed by external standard method, using pure CP II as standard. 10 µl of the sample solution was applied in triplicate on the TLC plate and developed with mobile phase petroleum ether (60-80 °C): ethyl acetate (95:05, v/v). The post chromatographic derivatization was carried out with anisaldehyde – sulphuric acid reagent placed in a dipping chamber (CAMAG) followed by heating in an oven at 100 °C for 5-10 min (Wagner and Bladt, 1996). Densitometric scanning was performed in absorption-reflection mode at 527 nm. Peak areas were recorded and the amount of CP II was calculated using the calibration curve.

TLC separation optimization: The leaves of *Clerodendrum phlomidis*, when subjected to TLC showed the presence of CP II peak (Figure 4.1.55). A comparison

of the spectral characteristics of the peak for isolated compound and that of the sample further confirmed the identity of CP II present in the sample (Figure 4.1.56). Good resolutions with symmetrical and reproducible peaks were obtained.

Linearity and detection limit: The peak area versus concentration plots was found to be linear in the range of 100-500 ng spot⁻¹ for CP II (Figure 4.1.57). The regression equation and correlation coefficient for CP II indicated good linearity. The limit of detection and the limit of quantification was 15.49 and 46.95 respectively (Table 4.1.22).

Precision studies: Instrumental precision was checked by repeated scanning of the same spot of standard three times and % RSD values were calculated. To determine the precision of the method, standard was analyzed three times inter-day and intra-day (Table 4.1.23).

Recovery studies and sample analysis: For the examination of recovery rates 80, 100 and 120% of pure standard was added to preanalysed samples and quantitative analysis were performed (Table 4.1.23). The CP II content of the leaves calculated from the area calibration curve (Table 4.1.24) by this method was found to be 0.012772 %w/w (plant dry weight basis).

This TLC method is rapid, simple, specific and effective in quantification of CP II, should prove to be a useful alternative under circumstances where the other slower and more costly chromatographic methods are not appropriate. This TLC procedure may be used effectively for identity, quality evaluation as well as quantitative determination for this plant or its derived products.

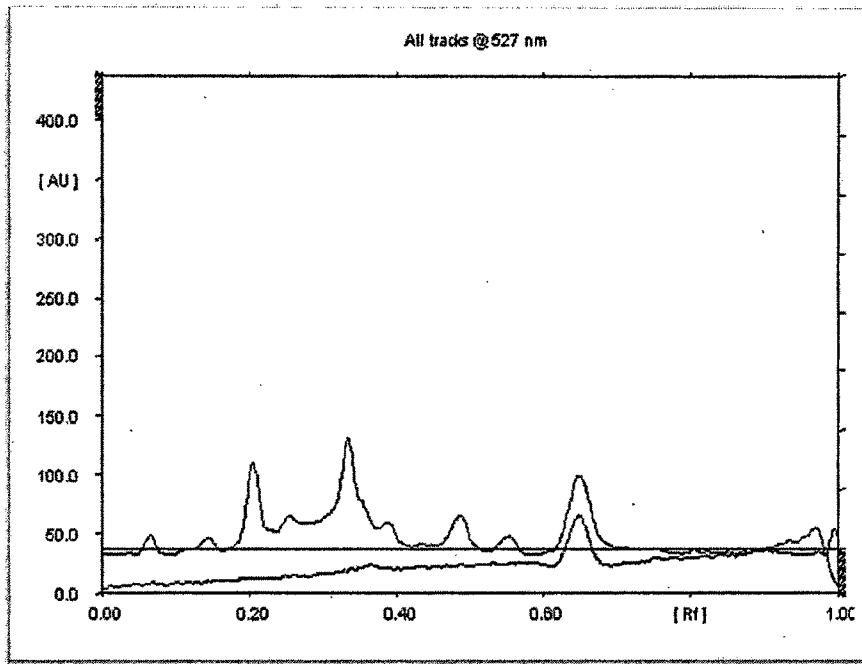


Figure 4.1.55: *C. phlomidis* leaf extract showing identical peak with isolated CP II

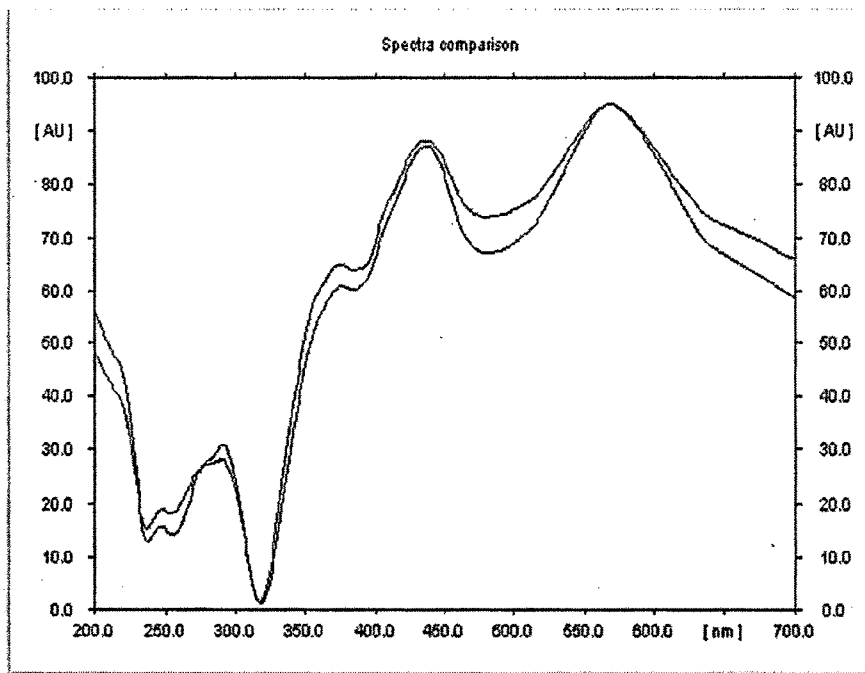


Figure 4.1.56: Spectral comparison for the peaks of isolated CP II and *C. phlomidis* leaf extract

Table 4.1.22: Method validation parameters for quantification of CP II

S. No.	Parameter	Results
1	R _f	0.64
2	Dynamic range (ng spot ⁻¹)	100-500
3	Equation	y = 480.006+10.106x
4	Slope	10.106
5	Intercept	480.006
6	Limit of detection	15.49 ng
7	Limit of quantification	46.95 ng
8	Linearity (correlation coefficient)	0.99913

Table 4.1.23: Precision and recovery studies data for quantification of CP II

Precision studies			
Concentration (ng spot ⁻¹)	Instrumental precision (% RSD)	Method precision (% RSD)	
		Intra-day	Inter-day
100	0.58	0.79	1.31
500	0.17	0.22	0.37
Recovery studies			
Amount of CP II in the sample (µg)	Amount of CP II added (µg)	Amount of CP II found (µg)	Recovery (%)
95.79	76.62	165.24	95.84
95.79	95.80	184.71	96.41
95.79	114.9	209.63	99.50

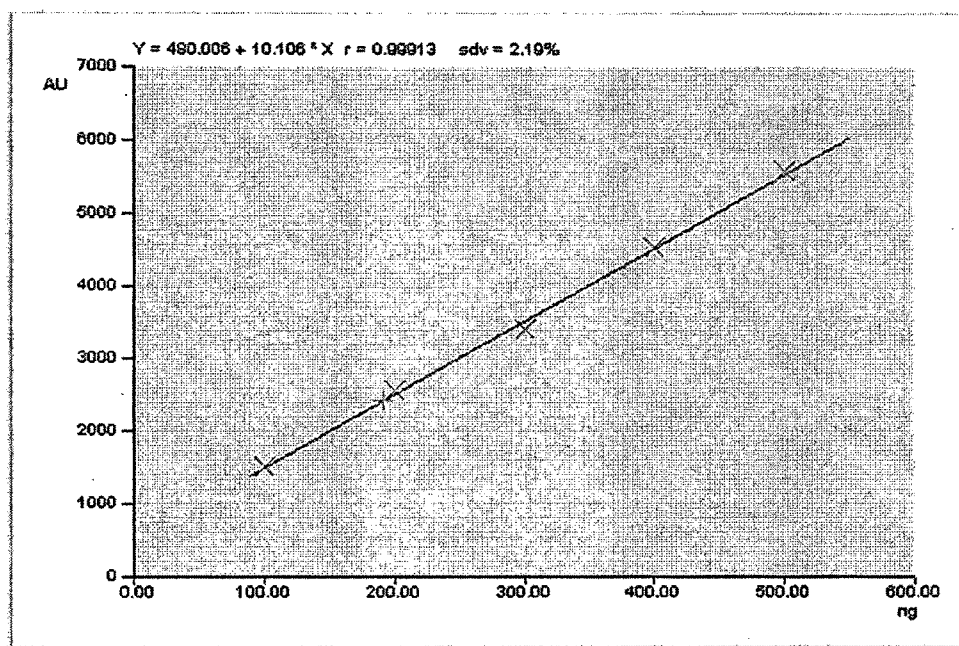


Figure 4.1.57: Calibration curve of peak area versus concentration for CP II

Table 4.1.24: Calibration curve parameters for quantification of CP II in *C. phlomidis* extract

R_f	Amount/Fraction	Area	X(calc)
0.65	100 ng	1501.70	-
0.64	200 ng	2560.24	-
0.64	300 ng	3399.49	-
0.64	400 ng	4524.86	-
0.64	500 ng	5572.22	-
0.64	-	2416.05	191.58 ng

4.1.11.3 Compound CP III

The fractions obtained by elution with chloroform: ethyl acetate (70:30) yielded 120 mg of white crystalline compound with m.p. 146 °C. It was soluble in diethyl ether, chloroform and ethyl acetate. The compound showed positive reaction for sterols with Libermann - Burchard's reaction. This compound was designated as CP III.

Characterization of CP III: The structure of the isolated compound CP III was unambiguously elucidated by analysis of IR, ^{13}C NMR and CHNOS data. The IR spectrum revealed the presence of hydroxyl group (ν_{max} 3440.32 cm^{-1}) and carbonyl group (ν_{max} 1724.37 cm^{-1}) (Figure 4.1.58). The CHNOS analysis showed carbon, hydrogen and oxygen percentage as 85.763, 9.991 and 3.884 respectively (Table 4.1.25, Figure 4.1.59, Figure 4.1.60). The ^{13}C NMR spectrum of CP III was almost very similar to that of clerosterol (Figure 4.1.61) (Rubinstein and Goad, 1974; Ahmad et al., 1993). From the ^{13}C NMR data compound CP III was identified as clerosterol ($\text{C}_{29}\text{H}_{48}\text{O}$; Mol. wt. 412) (Figure 4.1.62).

IR(KBr): ν_{max} : 3440.32, 2935.64, 1724.37, 1383.82, 1259.61, 1172.14, 1074.74, 978.12 cm^{-1} (Figure 4.1.58); ^{13}C NMR (100MHz, CDCl_3): δ 148.64 (C-25), 140.75 (C-5), 121.70 (C-6), 109.51 (C-26), 71.81 (C-3), 56.84 (C-14), 55.86 (C-17), 52.0 (C-9), 50.13 (C-24), 42.29 (C-13), 42.25 (C-12), 40.21 (C-4), 39.67 (C-1), 37.25 (C-10), 36.51 (C-20), 31.89 (C-22), 31.89 (C-2), 31.66 (C-7), 31.66 (C-8), 29.71 (C-23), 28.72 (C-16), 25.70 (C-28), 24.32 (C-15), 21.06 (C-11), 20.80 (C-19), 20.23 (C-21), 19.40 (C-27), 12.15 (C-29), 12.05 (C-18). (Figure 4.1.61)

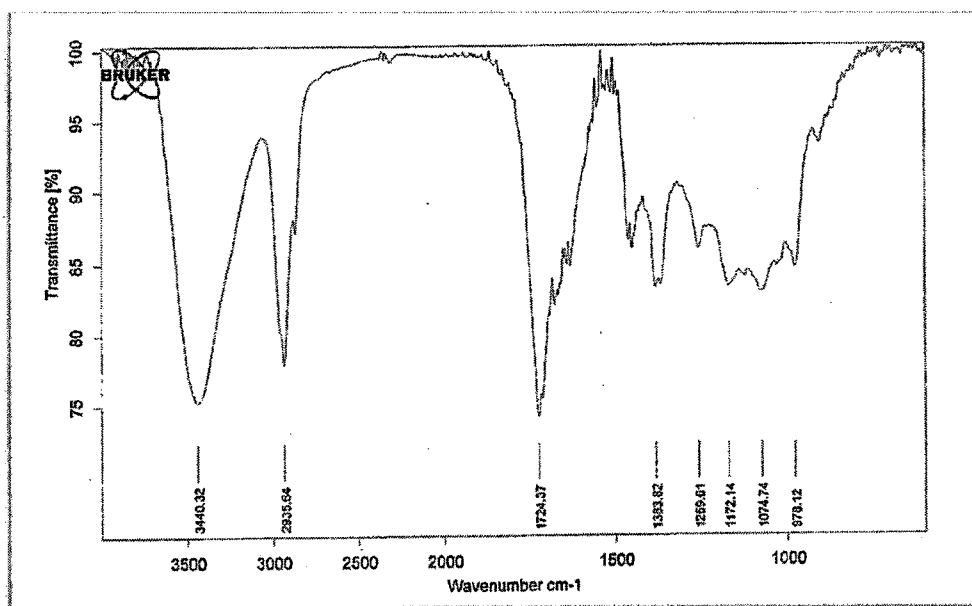


Figure 4.1.58: IR spectrum of CP III

Results and Discussion

Table 4.1.25: CHNOS analysis of CP III

Retention time (min)	Element percentage	Compound
1.23	85.763	Carbon
3.92	9.991	Hydrogen
3.0	3.884	Oxygen

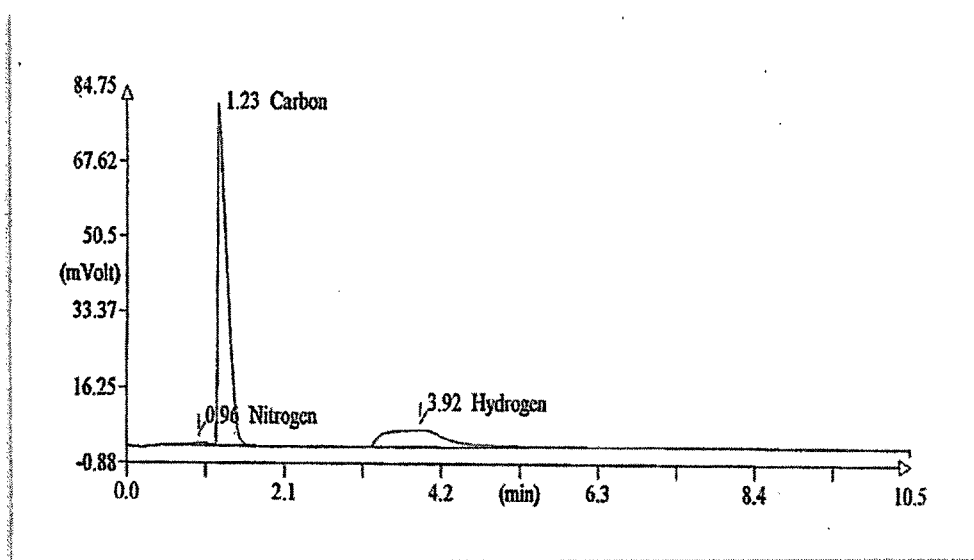


Figure 4.1.59: CHN analysis of CP III

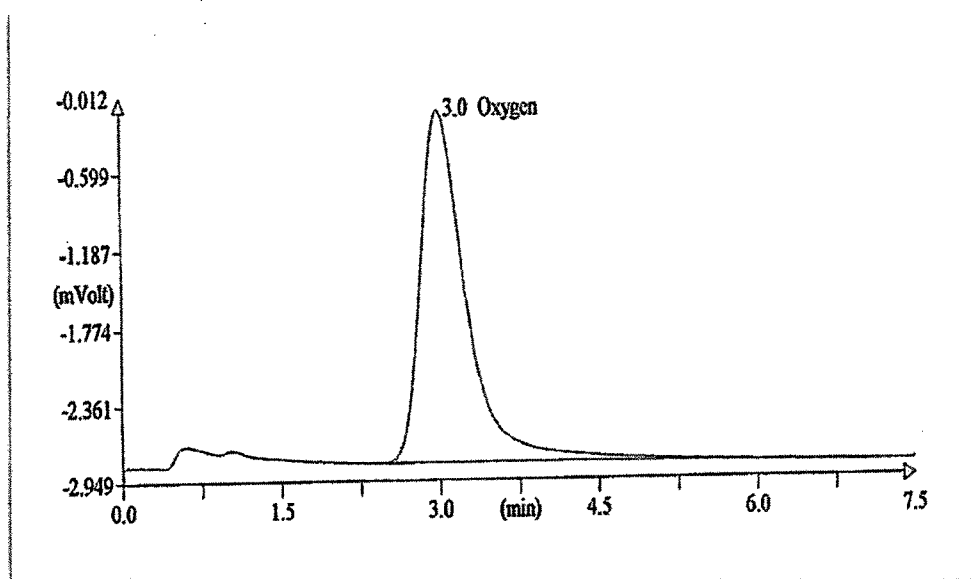


Figure 4.1.60: Oxygen analysis of CP III

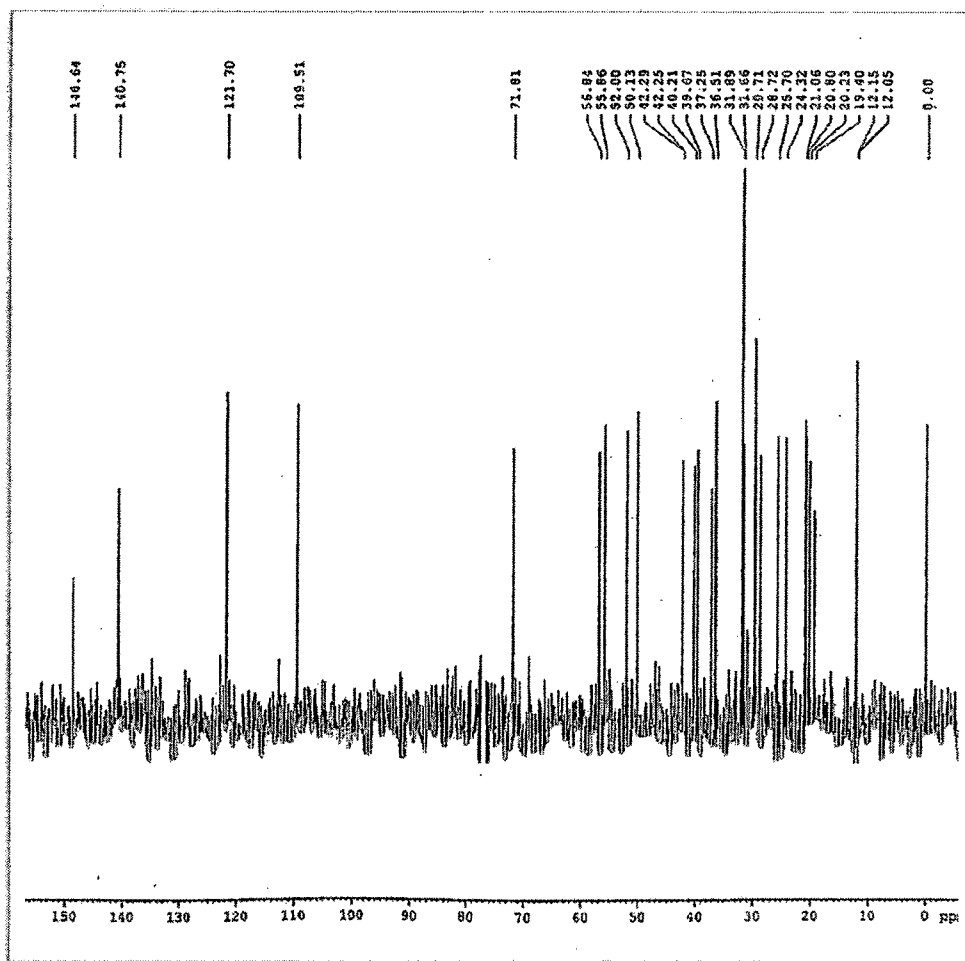


Figure 4.1.61: ¹³C NMR of CP III

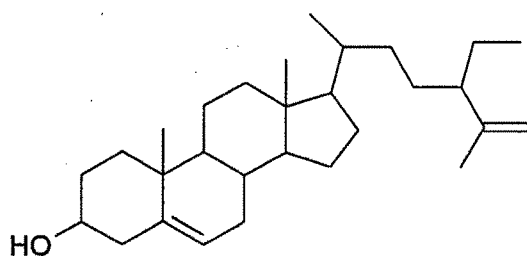


Figure 4.1.62: Chemical structure of CP III

TLC of CP III: TLC for CP III was performed with the mobile phase chloroform: ethyl acetate (70:30, v/v) with Libermann - Burchard reagent as detecting agent and scanned at 540 nm to check the purity. CP III gave a single dark green spot at

R_f 0.82 (Figure 4.1.63). The spectra showed maximum absorption at 420 nm (Figure 4.1.64).

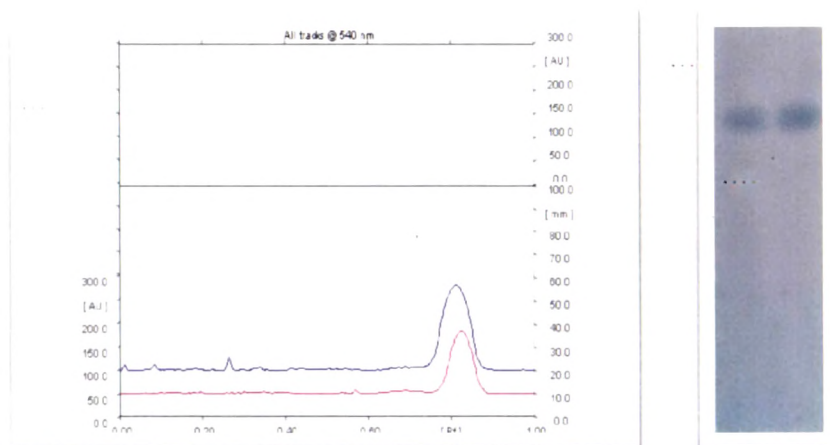


Figure 4.1.63: Densitogram and TLC photograph of CP III

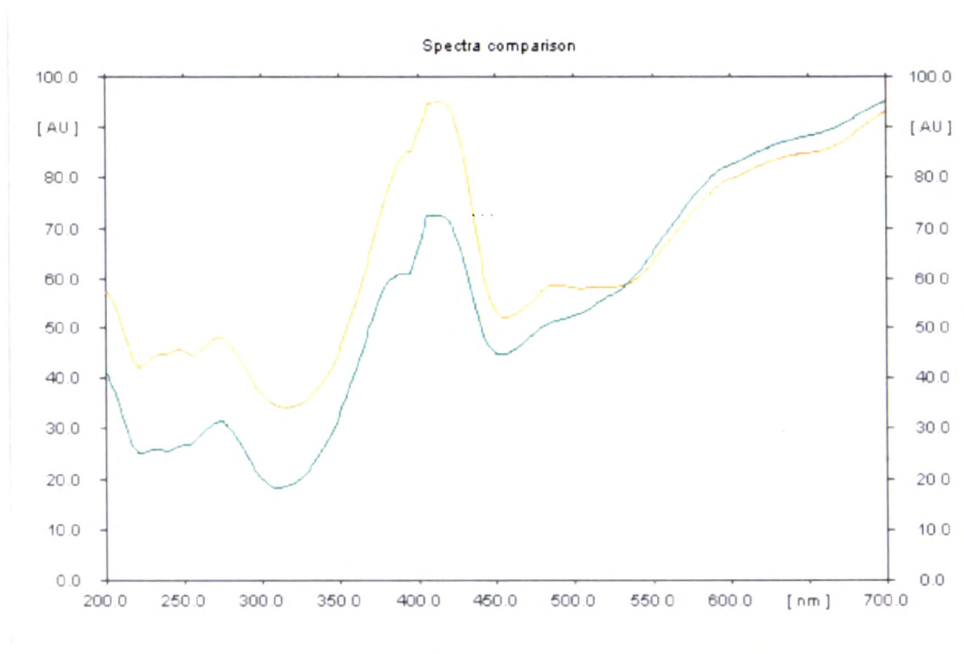


Figure 4.1.64: UV-Vis spectra of CP III

4.1.12 Acute toxicity study

The acute toxicity study was aimed for establishing the therapeutic index i.e. the ratio between the pharmacologically effective dose and the lethal dose, and also to

perform the primary screening. The extracts/fractions showed no signs of toxicity up to the dose of 2000 mg/kg. Similarly the isolated compounds also showed no signs of toxicity up to the dose of 300mg/kg. One-tenth of the maximum tested dose was considered as effective dose.

4.1.13 Antidiabetic study

Defatted ethanol extract of leaves has been reported for antidiabetic activity (Dhanabal et al., 2008). For further investigation the alcoholic extract was fractionated to petroleum ether fraction and the left out extract was considered as residual methanolic extract (RMECP). Unsaponified matter of petroleum ether fraction of methanol extract (UPFMCP) was prepared based on the earlier report of defatted ethanol extract. TLC studies have shown the presence of polyamines. Considering the fact that existing four classes of oral hypoglycemic drugs except alpha-glucosidase inhibitors other three (Sulfonylureas, Biguanides & Thiazolidinediones) are amino compounds, crude polyamine extract (CPECP) was also considered for the study. RMECP, UPFMCP, CPECP and the compounds (CP I, CP II and CP III) isolated from UPFMCP were studied for their antidiabetic activity.

Non-insulin dependent diabetes mellitus (NIDDM) condition, which is common amongst diabetic subjects, is characterized by reduced circulating concentration of insulin, poor insulin sensitivity or insulin resistant, poor glucose tolerance resulting in high sugar in plasma. STZ (N- [methylnitrocarbonyl]-D-glucosamine) is taken up by pancreatic β -cells via the glucose transporter (GLUT2) and causes alkylation or breakage of DNA strands and a consequent increase in the activity of poly-ADP-ribose synthetase, an enzyme depleting nicotinamide (NAD) in beta cells finally leading to energy deprivation and death of beta cells. These hypotheses have been confirmed by different studies in which the administrations of various chemicals such as antioxidants (superoxide dismutase; SOD), free radical scavenger (alpha-phenyl-tertbutylnitron), NAD and poly ADP-ribosyl synthase

inhibitors, concomitantly or before STZ injection have been shown to either prevent or lessen the severity of the induction of diabetes, respectively (Ozturk et al., 1996; Lukic et al., 1998; Szkudelski, 2001; Ho et al., 2008). Administration of STZ and NAD produce moderate hyperglycemia which has clinical similarities especially with respect to the insulin response to the glucose. As NAD is an antioxidant it exerts protective effect on the β -cell cytotoxic action of STZ by scavenging free radicals and causes only minor damage to pancreatic β -cell mass producing type 2 diabetes. Therefore, this model was found to be advantageous tool for investigation of antidiabetic agents in the treatment of type 2 diabetes (Masiello et al., 1998).

The diabetic control group showed a marked increase in plasma glucose and a reduction in insulin level while the metformin treated group restored the elevated glucose level to near normal level and also increased the reduced insulin level. UPFMCP 200 mg/kg, CP III 30 mg/kg, CP II 30 mg/kg and GPECP 200 mg/kg treated groups showed significant change ($p < 0.01$) in restoring the glucose and insulin levels (Table 4.1.26) when compared to the diabetic control. But UPFMCP and CP III treated groups showed restoration of both glucose and insulin levels relatively comparable to the standard drug than other treated groups (Figure 4.1.65, Figure 4.1.66). The significant decrease in the glucose levels of diabetic rats treated with UPFMCP and CP III may be by stimulation of the residual pancreatic mechanism like stimulating insulin secretion from the remnant β -cells or regenerated β -cells or probably by increasing peripheral utilization of glucose or both (Erah et al., 1996). The significant hyperglycemic effect of UPFMCP and CP III may also be due to its insulin-like effects (Akhtar and Ali, 1985; Day et al., 1990), including stimulation of glycogen synthesis and improvement of glucose homeostasis.

Table 4.1.26: Changes in plasma glucose and insulin in control and experimental groups of *C. phlomidis*

Groups	Plasma glucose (mg/dl)	Plasma insulin (μ U/ml)
Diabetic control (2 % gum acacia solution)	275.34 \pm 28.86	4.86 \pm 1.05
Standard control (Metformin, 11.3 mg/kg)	145.26 \pm 24.22 **	14.56 \pm 1.54 **
UPFMCP 100 mg/kg	238.04 \pm 14.14 **	9.35 \pm 0.56 **
UPFMCP 200 mg/kg	188.55 \pm 10.32 **	11.24 \pm 0.98 **
RMECP 100mg/kg	253.82 \pm 21.29 ^{ns}	6.29 \pm 1.95 ^{ns}
RMECP 200mg/kg	255.19 \pm 19.02 ^{ns}	6.5 \pm 1.37 ^{ns}
CPECP 100mg/kg	249.14 \pm 11.83 ^{ns}	7.01 \pm 0.67 ^{ns}
CPECP 200mg/kg	240.94 \pm 8.39 **	7.81 \pm 1.07 **
CP I 15 mg/kg	259.44 \pm 13.98 ^{ns}	6.09 \pm 1.68 ^{ns}
CP I 30 mg/kg	248.63 \pm 7.84 ^{ns}	6.95 \pm 0.84 ^{ns}
CP II 15 mg/kg	255.81 \pm 10.13 ^{ns}	7.54 \pm 2.04 **
CP II 30 mg/kg	235.92 \pm 10.22 **	9.76 \pm 1.11 **
CP III 15 mg/kg	220.38 \pm 19.66 **	7.48 \pm 1.23 *
CP III 30 mg/kg	207.10 \pm 11.78 **	10.13 \pm 1.38 **

Values are expressed as Mean \pm SD; n=6; *-p<0.05; **-p<0.01; ^{ns}-not significant

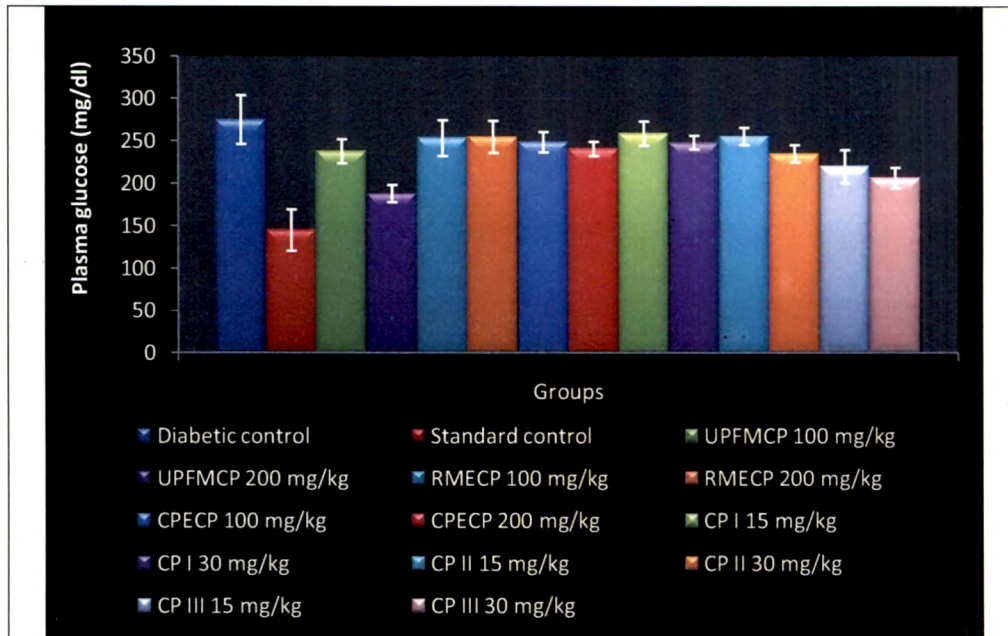


Figure 4.1.65: Comparison of changes in plasma glucose level in control and experimental groups of *C. phlomidis*

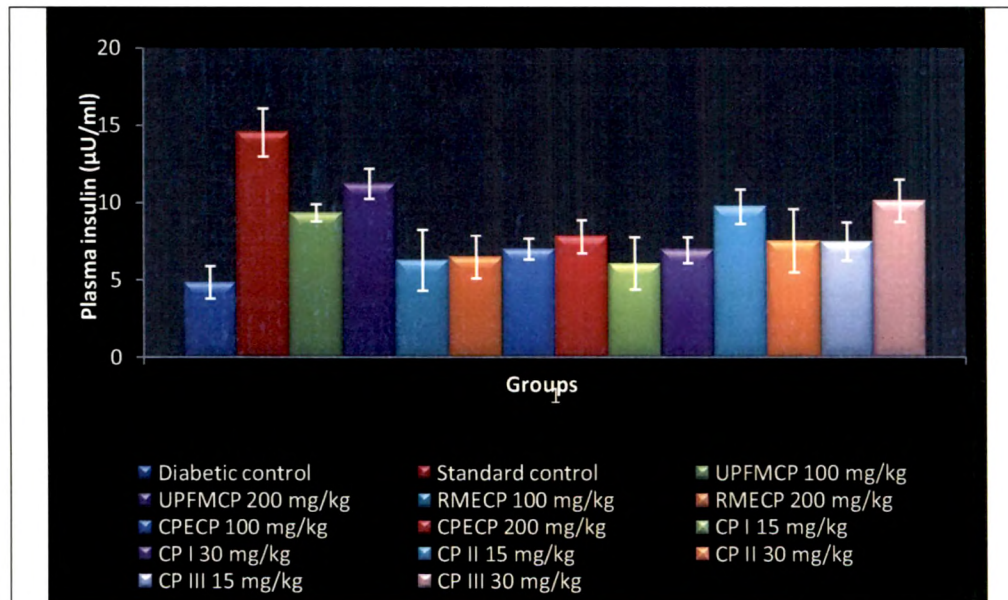


Figure 4.1.66: Comparison of changes in plasma insulin level in control and experimental groups of *C. phlomidis*

The increase in the insulin levels of treated groups also showed same pattern as in glucose levels (Table 4.1.26). Considerable increase in insulin level of UPFMCP 200 mg/kg, CP III 30 mg/kg and CP II 30 mg/kg (Figure 4.1.66) treated diabetic animals may be attributed to the stimulation of the surviving β -cells and increasing the secretion of insulin (Pari and Latha, 2002). Reports are available to show that antidiabetic plants may affect circulating insulin levels (Lamela et al., 1985). Thus, it may also be suggested that UPFMCP, CP III and CP II may induce the release of insulin from the bound form thereby potentiating its effect. It has been suggested that bioactive compounds from plants sources having antihyperglycemic activities might act by several mechanisms such as stimulating insulin secretion, increasing repair or proliferation of β -cells and enhancing the effects of insulin (Shanmugasundaram et al., 1990; Fayed et al., 1998).

Diabetes mellitus is also characterized by derangement of carbohydrate metabolism causing a decrease in enzymatic activity of hexokinase and increased glucose-6-phosphatase activity resulting in depletion of liver glycogen (Murphy and Anderson, 1974). Hence these parameters were studied for understanding the possible mechanism of action.

Hepatic hexokinase is considered an important regulator of blood glucose levels. Hexokinase is expressed predominantly in the liver and the β -cells, and hexokinase gene transcription is stimulated by insulin. Hexokinase being a key glycolytic enzyme brings about the first phosphorylation step of glucose metabolism is reduced significantly in the diabetic rats (Nehal and Baquer, 1989; Baquer et al., 1998).

Table 4.1.27: Changes in hepatic hexokinase, glucose-6-phosphatase and liver glycogen levels in control and experimental groups of *C. phlomidis*

Groups	Hexokinase (U/g/min)	Glucose-6-phosphatase (U/g/min)	Liver glycogen (μ g of glucose/mg of wet tissue)
Diabetic control (2 % gum acacia solution)	2.24 \pm 1.69	35.38 \pm 6.54	25.13 \pm 3.21
Standard control (Metformin, 11.3 mg/kg)	8.54 \pm 1.1 **	19.35 \pm 5.67 **	52.24 \pm 1.28 **
UPFMCP 100 mg/kg	5.96 \pm 1.71 **	26.38 \pm 3.98 *	30.69 \pm 4.58 **
UPFMCP 200 mg/kg	7.05 \pm 0.54 **	23.14 \pm 4.31 **	45.21 \pm 1.29 **
RMECP 100mg/kg	3.54 \pm 0.85 ^{ns}	29.94 \pm 5.41 ^{ns}	26.98 \pm 2.67 ^{ns}
RMECP 200mg/kg	3.91 \pm 0.67 ^{ns}	28.1 \pm 2.01 ^{ns}	28.34 \pm 1.68 ^{ns}
CPECP 100mg/kg	3.68 \pm 1.27 ^{ns}	31.02 \pm 8.14 ^{ns}	28.96 \pm 2.31 ^{ns}
CPECP 200mg/kg	4.18 \pm 1.67 ^{ns}	29.68 \pm 2.37 ^{ns}	30.34 \pm 1.39 *
CP I 15 mg/kg	3.71 \pm 1.62 ^{ns}	28.64 \pm 4.12 ^{ns}	27.61 \pm 2.11 ^{ns}
CP I 30 mg/kg	3.91 \pm 1.02 ^{ns}	25.12 \pm 3.68 **	28.95 \pm 3.65 ^{ns}
CP II 15 mg/kg	4.09 \pm 2.01 ^{ns}	29.27 \pm 6.98 ^{ns}	29.67 \pm 3.01 *
CP II 30 mg/kg	4.59 \pm 1.91 *	24.68 \pm 6.98 **	31.29 \pm 1.29 **
CP III 15 mg/kg	4.68 \pm 1.26 *	29.64 \pm 2.57 ^{ns}	29.68 \pm 2.67 *
CP III 30 mg/kg	5.96 \pm 1.35 **	24.08 \pm 7.12 **	39.16 \pm 3.67 **

Values are expressed as Mean \pm SD; n=6; *-p<0.05; **-p<0.01; ^{ns}-not significant

In STZ-NAD induced diabetic rats the hexokinase synthesis is decreased due to low levels of mRNA coding for the hexokinase and also may be due to the direct stimulation of glycolysis in tissues with increased glucose removal from the blood. STZ induced diabetes has been demonstrated in this study by the decrease in the activities of hexokinase as it is regulated by insulin (Barthel and Schmoll, 2003). Metformin, UPFMCP 200 mg/kg and CP III 30 mg/kg treated groups showed a significant ($p < 0.01$) increase while CP II 30 mg/kg treated groups showed less significant ($p < 0.05$) increase in hexokinase level (Table 4.1.27). The activation of glycolysis and increase the utilization of glucose for energy production may be the reason for the significant increase of hexokinase in UPFMCP and CP III treated. Conversely the mechanism played by UPFMCP and CP III in enhancing the hexokinase activity could also be due to glycogen synthesis activation or activation of mRNA coding for hexokinase in diabetic rats (Spence, 1983).

Glucose-6-phosphatase, a key enzyme in gluconeogenesis, plays an important role in glucose homeostasis in the liver and kidney (Berg et al., 2001). The increased activity of this enzyme in liver of diabetic rats may be due to the activation or increased synthesis of the enzyme contributing to the increased glucose production during diabetes by the liver (Baquer et al., 1998). Metformin, UPFMCP 200 mg/kg, CP III 30 mg/kg, CP II 30 mg/kg and CP I 30 mg/kg treated groups showed significant ($p < 0.01$) decreased activity of glucose-6-phosphatase (Table 4.1.27). The decreased levels observed in treated diabetic animals may be due to its primarily modulating and regulating the gluconeogenic enzyme activity either through the regulation by 3'5'-cyclic adenosine monophosphate (cyclic AMP) and any other metabolic activation or inhibition of glycolysis and gluconeogenesis.

Liver plays an important role in buffering the postprandial hyperglycemia and is involved in synthesis of glycogen. The conversion of glucose to glycogen in the liver cells is dependent on the extracellular glucose concentration and on the

availability of insulin which stimulates glycogen synthesis over a wide range of glucose concentration (Stalmans et al., 1997). Assessment of glycogen levels serves as a marker for studying insulinomimetic activity. The regulation of glycogen metabolism *in vivo* occurs by the multifunctional enzyme glycogen synthase and glycogen phosphate that play a major role in the glycogen metabolism (Carabaza et al., 1990). The reduced glycogen store in diabetic rats has been attributed to reduced activity of glycogen synthase (Akatsuka et al., 1983) and increased activity of glycogen phosphorylase (Roesler and Khanderwal, 1986) or insulin deficiency (Vats et al., 2004). Many studies have also demonstrated that impaired insulin sensitivity or hyperglycemic or hyperinsulinemia affects glucose storage in liver and muscle (Fery and Balasse, 1994; Pratipanawatr et al., 2002).

The hepatic glycogen content of diabetic control was reduced significantly as compared to other treated groups. Metformin, UPFMCP 200 mg/kg, CP III 200 mg/kg and CP II 200 mg/kg treated groups showed significant ($p < 0.01$) change but comparably UPFMCP 200 mg/kg and CP III 200 mg/kg treated groups restored the depleted glycogen level better than other treated groups (Table 4.1.27). Accumulation of glycogen in liver of UPFMCP and CP III treated animals is somewhat similar to that reported during insulin therapy (Spiro et al., 1958; Anderson, 1974). UPFMCP and CP III treated groups prevented the alteration in glycogen content but could not normalise it. This prevention of depletion of glycogen in liver may be possibly due to decreased activity of glycogen phosphorylase and increased activity of glycogen synthase. Conversely it may also be possible due to either stimulation of insulin release from β -cells (Lolitkar and Rao, 1966) or due to insulinomimetic activity (Broadhurst et al., 2000) or direct peripheral glucose uptake or due to a combination of the two (Lolitkar and Rao, 1966). Therefore, the mechanism of action appears to be both pancreatic (Bansal et al., 1981) and extra pancreatic effect (Achrekar et al., 1991).

Table 4.1.28: Changes in body weight in control and experimental group of *C. phlomidis*

Groups	Body weight (g)
Diabetic control (2 % gum acacia solution)	165.24±9.56
Standard control (Metformin, 11.3 mg/kg)	220.35±4.87 **
UPFMCP 100 mg/kg	171.64±4.57 ^{ns}
UPFMCP 200 mg/kg	190.65±7.13 **
RMECP 100mg/kg	171.37±5.67 ^{ns}
RMECP 200mg/kg	170.35±6.98 ^{ns}
CPECP 100mg/kg	168.25±8.51 ^{ns}
CPECP 200mg/kg	169.12±4.87 ^{ns}
CP I 15 mg/kg	166.24±8.12 ^{ns}
CP I 30 mg/kg	168.59±9.67 ^{ns}
CP II 15 mg/kg	164.24±5.49 ^{ns}
CP II 30 mg/kg	170.24±5.97 ^{ns}
CP III 15 mg/kg	168.38±9.37 ^{ns}
CP III 30 mg/kg	170.58±7.49 ^{ns}

Values are expressed as Mean ± SD; n=6; **-p<0.01; ^{ns}-not significant

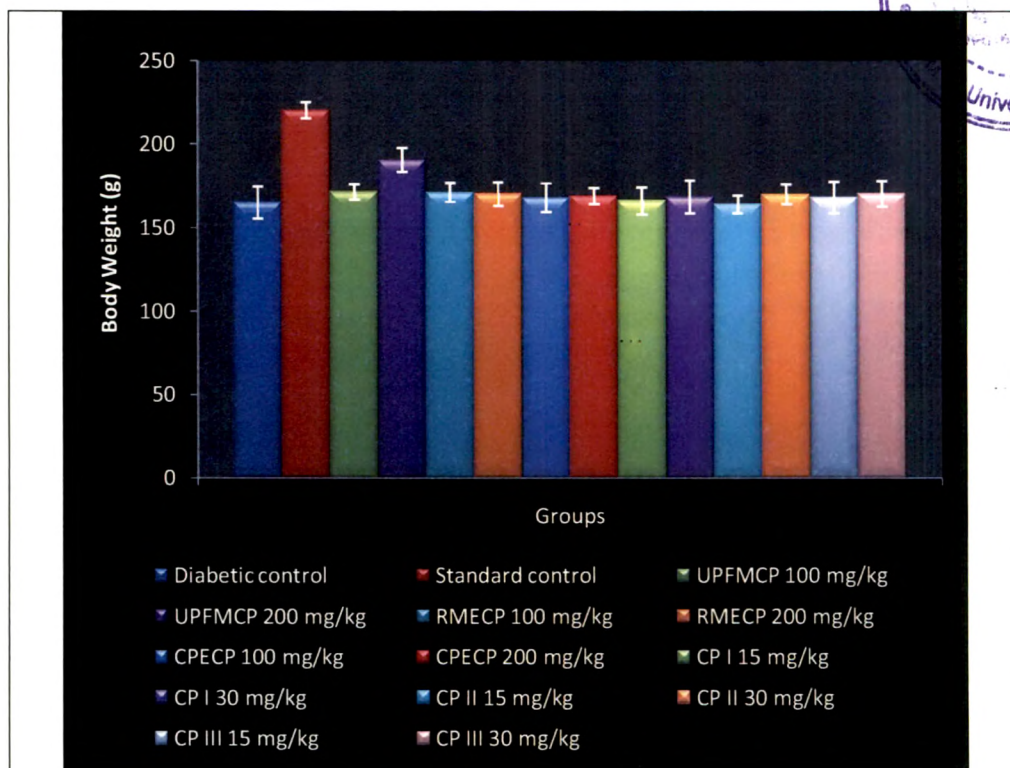


Figure 4.1.67: Comparison of changes in body weight in control and experimental groups of *C. phlomidis*

STZ-NAD induced diabetes is associated with a characteristic loss of body weight which is due to increased muscle wasting in diabetic state (Swanston-Flatt et al., 1990; Raju et al., 2001). Metformin and UPFMCP 200 mg/kg treated groups showed significant change ($p < 0.01$) in restoring the body weight (Table 4.1.28, Figure 4.1.67). The reversal of weight loss in the UPFMCP treated diabetic rats indicates the reversal of gluconeogenesis and glycogenolysis. However, it did not normalize the body weight completely. The resumption of moderate body weight also strongly suggests that sugar and lipid metabolism in these animals may be improved.

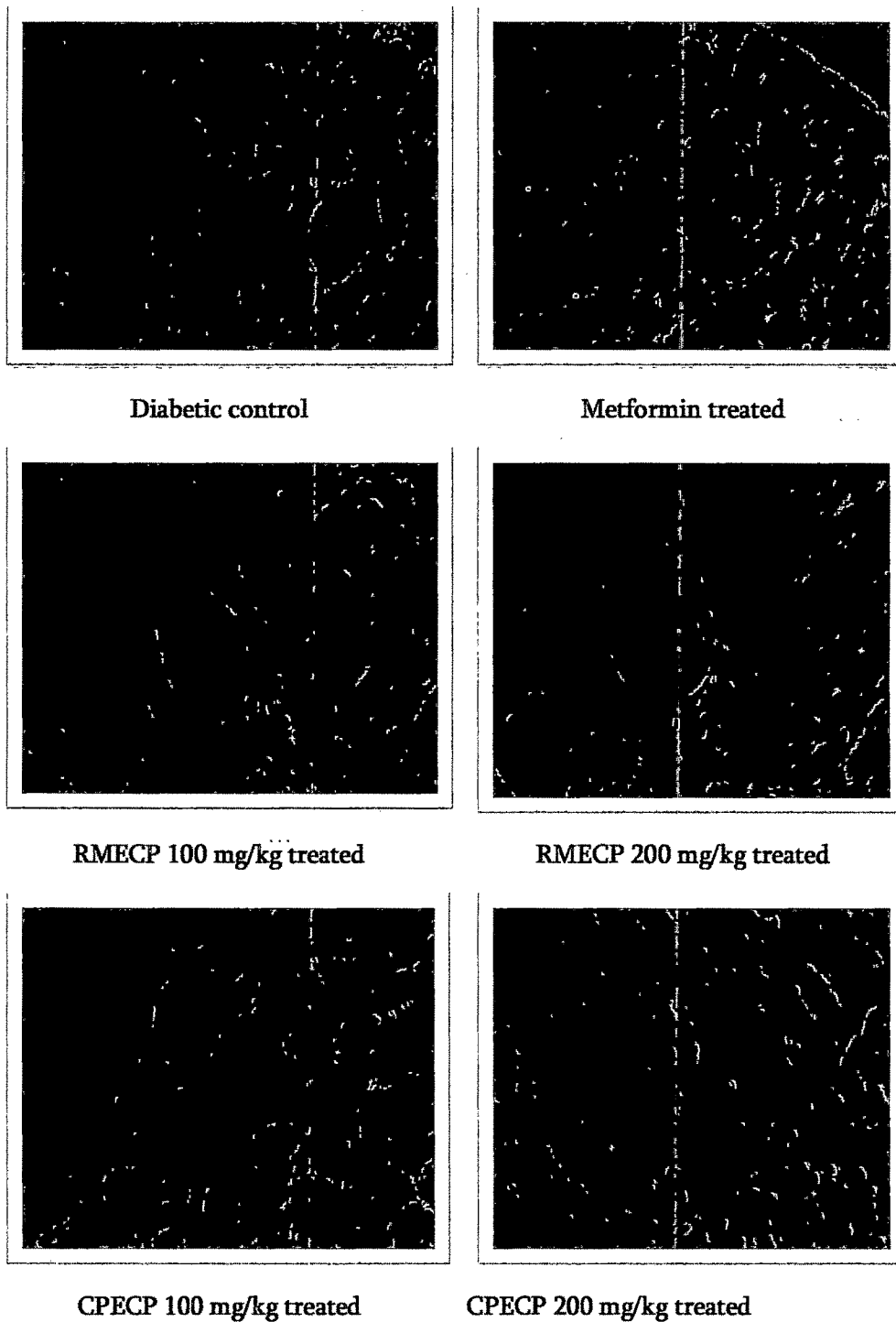


Figure 4.1.68: Histological slides showing changes in the endocrine (islets of Langerhans) and exocrine pancreas (acini) of control and experimental groups of *C. phlomidis* (Cont.)

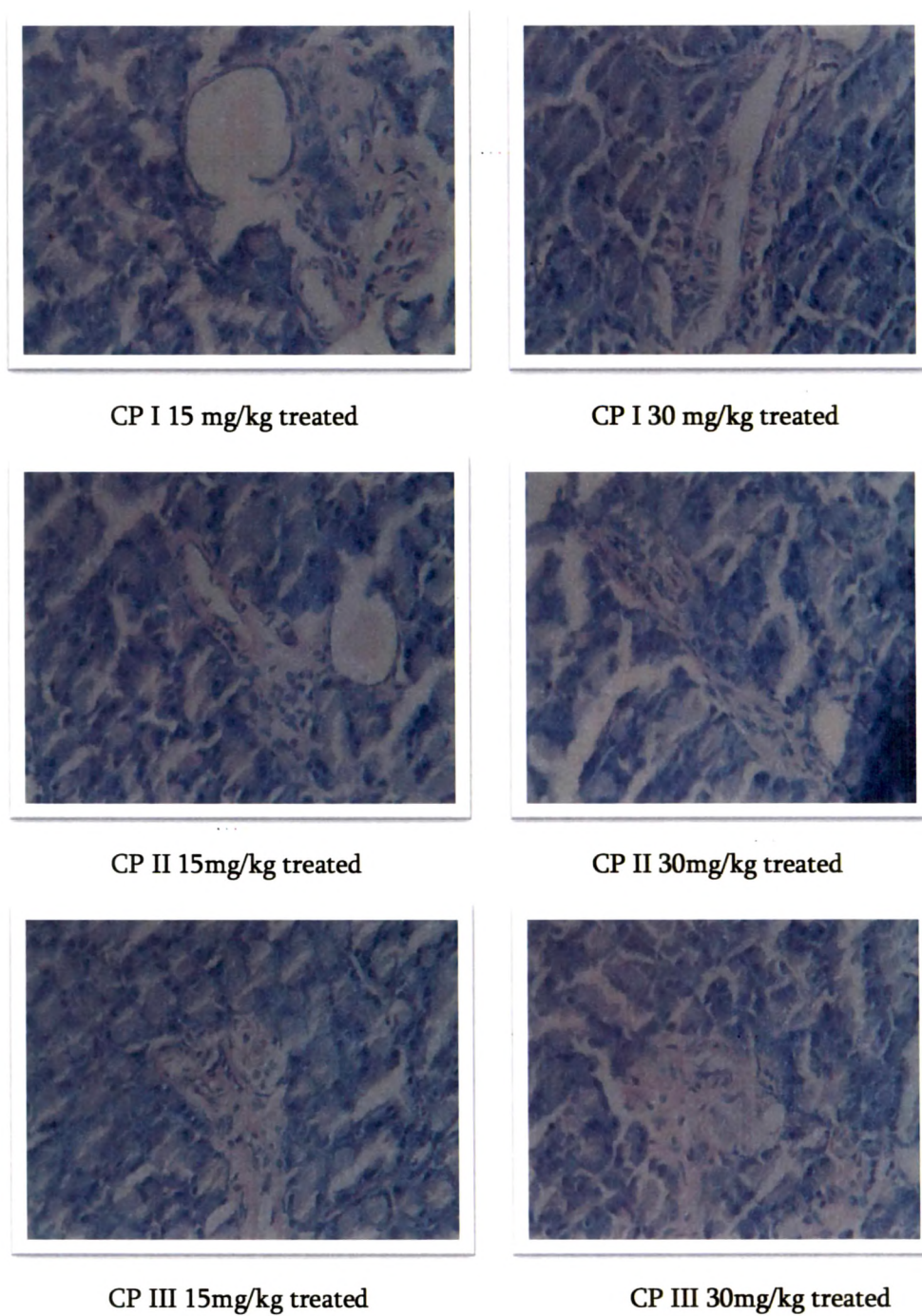


Figure 4.1.68: Histological slides showing changes in the endocrine (islets of Langerhans) and exocrine pancreas (acini) of control and experimental groups of *C. phlomidis* (Cont.)

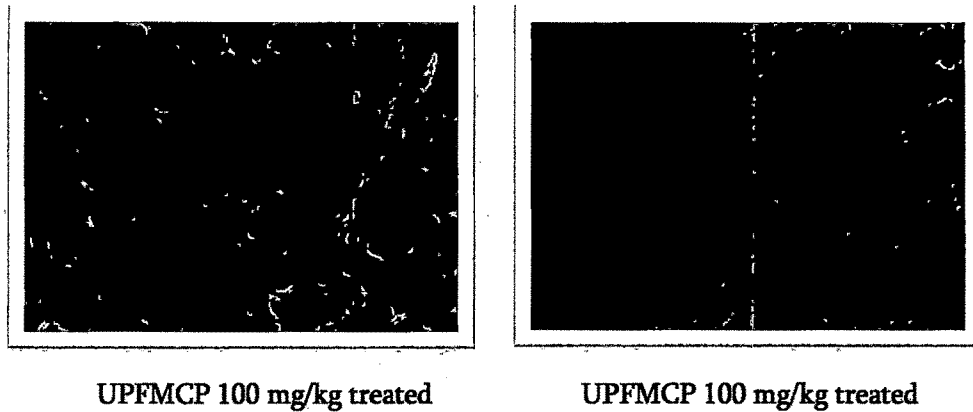


Figure 4.1.68: Histological slides showing changes in the endocrine (islets of Langerhans) and exocrine pancreas (acini) of control and experimental groups of *C. phlomidis*

Diabetic control group (Figure 4.1.68) showed shrunken islets of Langerhans displaying degenerative and necrotic changes while acinar structure appeared in disarray. Prominent disruption of the islet cellular architecture was found and acini with large clear vacuoles. Significant reduction in total number of cells per pancreatic islet with marked degranulation was also observed. This provides clear evidence that STZ-NAD treatment destroyed the pancreatic β -cells. The metformin treated group (Figure 4.1.68) showed significant higher number of cells per islet and the cellular architecture was preserved. It showed no vacuoles and degranulation. RMECP (100 and 200 mg/kg) treated (Figure 4.1.68), CPECP (100 and 200 mg/kg) treated (Figure 4.1.68), CP I (15 and 30 mg/kg) treated (Figure 4.1.68) and CP II 15 mg/kg group (Figure 4.1.68) showed similar observation as that of diabetic control with no significant change. CP II 30 mg/kg treated (Figure 4.1.68) and CP III (15 and 30 mg/kg) treated groups (Figure 4.1.68) showed shrunken islet with disrupted cellular architecture and significant reduction in total number of cells per islet, but comparatively showed less vacuoles. UPFMCP (100 and 200 mg/kg) treated groups (Figure 4.1.68) showed relatively intact, larger size islet and reduced vacuoles. It also showed significant number of cells per islet

which suggests that UPFMCP treated shows signs of regenerated pancreatic islet cells. This may be an indication of rejuvenation of β -cells leading to increase in insulin production and secretion.

The overall results show that RMECP and CP I are completely inactive. CPECP reduced glucose level and increased glycogen level, neither had it increased insulin level, hexokinase level, body weight nor did it reduce glucose-6-phosphatase level. CPECP in the histopathological studies also have shown no effect on stimulation of the residual pancreatic mechanism like stimulating insulin secretion from the remnant β -cells or regenerated β -cells. The plasma glucose lowering effect in the absence of a significant change in plasma insulin concentration suggests that the CPECP treatment may involve an insulin-independent-mechanism. CPECP might be producing its hypoglycaemic effect by an extra-pancreatic action e.g. possibly by stimulating glucose utilisation in peripheral tissues. Also, it could be the result of an increase in glycolytic and/or glycogenic enzymes activity in peripheral tissues. Although, it remains possible that the CPECP may decrease the secretion of the counter-regulatory hormones (glucagon, cortisol and growth hormones) or inhibition of intestinal glucosidase.

CP II and CP III have shown moderate effect on glucose, insulin, hexokinase, glucose-6-phosphatase and glycogen but no increase in body weight. The histopathological studies have shown very modest effect or no effect on stimulation of the residual pancreatic mechanism like stimulating insulin secretion from the remnant β -cells or regenerated β -cells. No weight gain indicates the non-reversal of gluconeogenesis and glycogenolysis. The observed hypoglycemic effect may be due to insulinomimetic effect or by increasing peripheral utilization of glucose or increased glycogen synthase or increased glycolysis. CP II being the palmityl ester of CP III explains the parallel pattern of activity but comparatively CP III has shown better hypoglycemic activity. Physiologically CP III (clerosterol)

is considered as the precursor phytosterol for some phytosteroids, such as cyasterone and isocyasterone (Fujimoto et al., 2000).

UPFMCP has shown nearly comparable effect to that of metformin on all the parameters. The moderately active CP II and CP III being constituents of UPFMCP explain the better activity of UPFMCP. In addition β -sitosterol, β -carotene and lupeol were also identified from UPFMCP. β -sitosterol has been reported for its antihyperglycemic due to insulin releasing effect (Ivorra et al., 1988; Ivorra et al., 1989; Marles and Farnsworth, 1994; Marles and Farnsworth, 1995). β -sitosterol lowers hepatic cholesterol level (Ikeda et al., 1985; Fuhrman et al., 1997) and exerts hypocholesterolemic effect (Pollak, 1985; Ling and Jones, 1995; Wang and Ng, 1999). However, it has been stated that 'the ubiquitous occurrence of β -sitosterol, plant sterols in general, and their glucosides in all vegetables makes it highly unlikely that they have any drug related properties and many reports on their medicinal properties are based on *in vitro* or unrealistically high *in vivo* doses which make a therapeutic application of these compounds highly unlikely (Marles and Farnsworth, 1994; Marles and Farnsworth, 1995). In a way this statement is correct, since sitosterol is not drug in the accepted sense, but rather slow acting essential micronutrients or adaptogens better considered as minor but nevertheless important cell membrane constituents.

Reddy et al., 2009 demonstrated lupeol's antidyslipidemic activity along with an antihyperglycemic effect (Harborne and Baxter, 1983) which revealed the lupeol's potential as a scaffold for developing drugs targeting coronary diseases and diabetes (Reddy et al., 2009).

β -carotene being an antioxidant could exhibit antidiabetic activity. Beneficial role of beta-carotene in reducing diabetic complications like glycosylation in alloxan-induced diabetic rats (Aruna et al., 1999) has been reported previously. β -carotene has been reported to significantly decrease blood glucose levels and provide more

protection to pancreatic tissues against damage caused by STZ (Attia, 2009). β -carotene is also reported for hypocholesterolemic effect (Wang and Ng, 1999). Dietary supplementation with lycopene brought about a decline in plasma LDL cholesterol level, probably by inhibiting macrophage HMG CoA reductase activity (Fuhrman et al., 1997).

The insulin releasing effect of β -sitosterol, antihyperglycemic effect of lupeol and antioxidant activity of β -carotene may have contributed to the observed synergistic antidiabetic of UPFMCP. Hypocholesterolemic and hypolipidemic of β -sitosterol, β -carotene and lupeol explains the altered lipid metabolism contributing to weight gain observed in UPFMCP. The signs of β -cell regeneration in the histopathological study may be due to pancreatic protective effect of β -carotene or due to unidentified compounds of UPFMCP.

Biguanides produce hypoglycaemia in diabetic animals by an extrapancreatic mechanism and are devoid of significant activity in normal animals (Schweizer et al., 1983). Although biguanides do not require the pancreas for effectiveness, in practice, they appear to augment rather than to create insulin. With the biguanide, metformin, insulin is a prerequisite to convert glucose to glycogen and a patient cannot survive with biguanide alone without some endogenous or exogenous insulin (Kxall, 1970). Therefore, it seemed reasonable to speculate that these extracts may possess a biguanide-like hypoglycaemic activity, despite the fact that the STZ diabetic rats used in this study are moderately diabetic and their pancreatic insulin production is not completely destroyed. From the results, it may also be postulated that at least more than one hypoglycemic principle may be present. An extract of *Ganoderma lucidum*, exerts its hypoglycemic activity by functioning as a β -blocker, inhibiting the effects of catecholamines, which are known to promote gluconeogenesis and glycogenolysis. The option of UPFMCP being a β -receptor antagonist cannot also be ruled out.

4.1.14 GC-MS analysis of unsaponified matter of petroleum ether fraction of methanol extract of *C. phlomidis* (UPFMCP)

The percentage yield of unsaponified matter from petroleum ether fraction of methanol extract was found to be 25.19 %w/w. The bioactive UPFMCP was subjected to GC-MS analysis, the Figure 4.1.69 shows the retention time and peak area of various compounds detected.

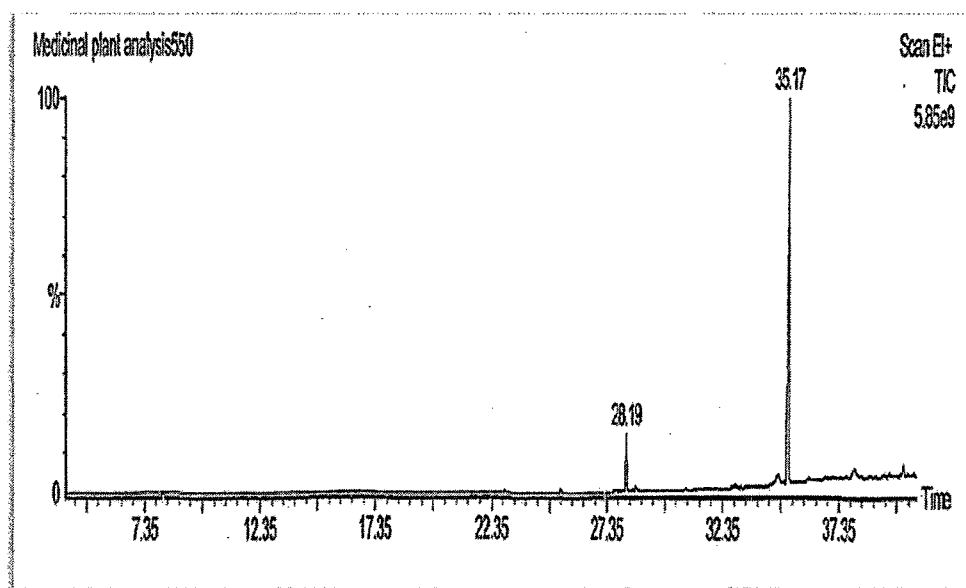


Figure 4.1.69: Gas chromatogram of UPFMCP of *C. phlomidis* leaves

Based on their retention time and molecular weight, compounds were matched from library database (NIST Ver.2.0-Year 2005). 1,2-benzenedicarboxylic acid diisooctyl ester ($C_{24}H_{38}O_4$) was found to be the compound with highest peak area of 74.80 %. Other compounds identified with significant peak percentage area were Phytol ($C_{20}H_{40}O$, 8.40 %), 1-Monolinoleoylglycerol trimethylsilyl ether ($C_{27}H_{54}O_4Si_2$, 7.65 %), vitamin E ($C_{29}H_{50}O_2$, 6.44 %) and 8,11,14-Eicosatrienoic acid ($C_{20}H_{34}O$, 1.30 %) (Table 4.1.29).

Table 4.1.29: Compounds identified by GCMS in UPFMCP of *C. phlomidis* leaves

No.	Retention time (min)	Name of the Compound	Molecular Formula	Molecular Weight	Peak Area (%)
1	3.10	1,3,5,7-Cyclooctatetraene	C ₈ H ₈	104	0.15
2	15.11	2H-cyclopropa(a) naphthalene-2-one, 1,1a,4,5,6,7,7a,7b- octahydro-1,1,7,7a- tetramethyl- (1α,7α,7α,7β) derivative	C ₁₅ H ₂₂ O	218	0.05
3	15.75	Butylated hydroxytoluene	C ₁₅ H ₂₄ O	220	0.08
4	16.17	2(4H)- benzofuranone,5,6,7,7a- tetrahydro-4,4,7a- trimethyl-derivative	C ₁₁ H ₁₆ O ₂	180	0.02
5	22.94	2-Pentadecanone,6,10,14- trimethyl-derivative	C ₁₈ H ₃₆ O	268	0.34
6	25.33	n-Hexadecanoic acid	C ₁₆ H ₃₂ O ₂	256	0.76
7	28.19	Phytol	C ₂₀ H ₄₀ O	296	8.40
8	28.61	8,11,14-Eicosatrienoic acid	C ₂₀ H ₃₄ O	306	1.30
9	34.71	Vitamin E	C ₂₉ H ₅₀ O ₂	430	6.44
10	35.17	1,2-benzenedicarboxylic acid diisooctyl ester	C ₂₄ H ₃₈ O ₄	390	74.80
11	38.03	1-Monolinoleoylglycerol trimethylsilyl ether	C ₂₇ H ₅₄ O ₄ Si ₂	498	7.65

The beneficial effect of Vitamin E in diabetic patients and its complications has been reported (Davi et al., 1999; Ceriello et al., 1991; Lonn et al., 2002). US patent 7179842 (Method of treating non-insulin dependent diabetes mellitus with phytanic acid derivatives) covers the use of phytanic acid derivatives for treatment and/or prevention of type 2 diabetes or other conditions associated with impaired glucose tolerance such as obesity. Phytanic acid and phytol are metabolites of phytol. The conversion of phytol to phytanic acid is regulated via PPAR α and phytanic acid is a natural peroxisome proliferator-activated receptor agonist, regulates glucose metabolism in rat primary hepatocytes (Heim et al., 2002; Gloerich et al., 2007). Phytol is also reported as a cholesterol lowering agent. Nearly comparable hypoglycemic effect of UPFMCP to metformin may also be due to vitamin E or phytol or both.

4.1.15 PTP1B inhibition study

The interaction of insulin with its receptor leads to autophosphorylation of certain tyrosine residues within the receptor, thus activating the receptor kinase. However, protein tyrosine phosphatases (PTPases) (Figure 4.1.70) dephosphorylate the activated insulin receptor and attenuate the tyrosine kinase activity thus reducing the metabolic action of insulin and leading to hyperglycaemia (Kenner et al., 1996; Goldstein et al., 1998; Kennedy and Ramachandran, 2000).

Among PTPases, PTP1B has been particularly demonstrated to dephosphorylate insulin receptor and act as a negative regulator of insulin signaling. A recent study on PTP1B knockout mice showed that the loss of PTP1B activity enhanced sensitivity towards insulin and resistance to obesity, indicating that potent, orally active PTP1B inhibitors could be useful for the treatment of type II diabetes and obesity (Elchebly et al., 1999; Klaman et al., 2000).

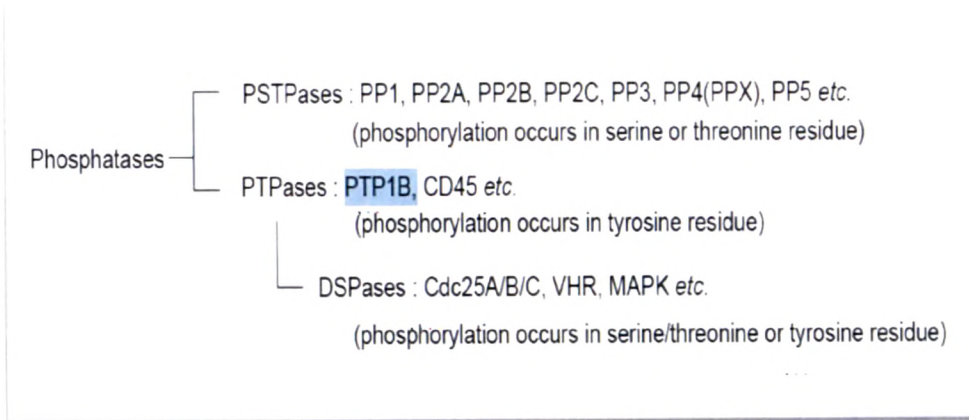


Figure 4.1.70: Different phosphatases showing the site of phosphorylation

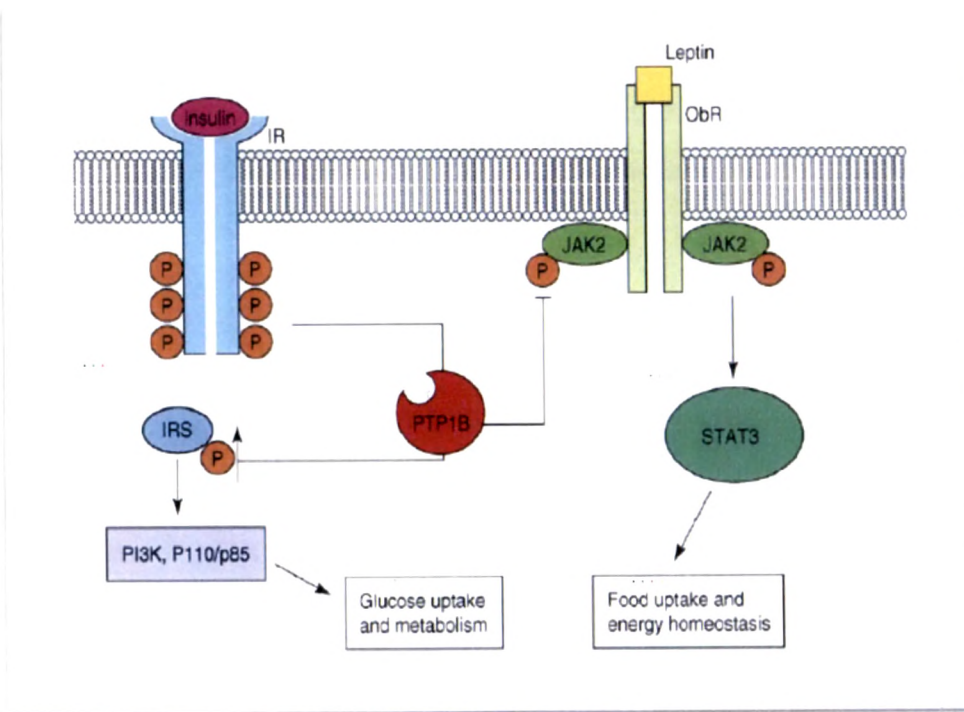


Figure 4.1.71: The role of PTP1B in insulin and leptin signaling

Leptin is a major hormone involved in obesity and its signaling pathway is negatively regulated by the tyrosine phosphatase PTP1B (Montague et al., 1997). Leptin administration reduces appetite, and leads to a decrease in body weight in leptin deficient obese animals and humans (Hallas et al., 1995).

In the insulin signalling pathway (Figure 4.1.71), PTP1B can associate with and dephosphorylate activated insulin receptor (IR) or insulin receptor substrates (IRS) (Bandyopadhyay et al., 1997; Dadke et al., 2000; Walchli et al., 2000; Goldstein et al., 2000; Calera et al., 2000). In the leptin pathway, PTP1B binds and dephosphorylates JAK2 (Janus kinase2), which is downstream of the leptin receptor, ObR (Zabolotny et al., 2002; Cheng et al., 2002). STAT3 and P110/p85 are downstream targets of JAK2 and IRS1, respectively. P110/p85 is a specific form of PI3K responsive to insulin signalling.

PTP1B inhibitors through insulin signaling could potentially ameliorate insulin resistance and normalize plasma glucose and insulin without inducing hypoglycemia. PTP1B inhibitors through leptin signaling can reduce body fat and protect from dietary induced obesity. Thus, PTP1B has emerged as an attractive therapeutic target for treatment of insulin resistance related to type 2 diabetes and obesity.

The Calbiochem® Protein Tyrosine Phosphatase 1B Assay Kit is a colorimetric, non-radioactive assay designed to measure PTP1B activity in purified preparations and for inhibitor or activator screening. The kit includes human, recombinant PTP1B (residues 1-322; M.W. 37,400), expressed in *E. coli*. The phosphopeptide substrate supplied with this kit contains sequence from the insulin receptor β subunit domain that must be autophosphorylated to achieve full receptor kinase activation. This "activation loop" is the target of several protein phosphatase regulators of insulin signaling, including, notably, PTP1B. The detection of free phosphate released is based on the classic Malachite green assay and offers the following advantages: non-radioactive; convenient 1-step detection; excellent sensitivity. The PTP1B inhibitor Suramin is supplied as a control for inhibitor detection. Suramin is a reversible and competitive inhibitor of PTP1B, with a K_i of 5.5 μ M.

Table 4.1.30: % inhibition of PTP1B by extracts/fractions/compounds of *C. phlomidis*

Extracts/fractions/isolated or identified compounds	% Inhibition of PTP1B
Suramin (10 μ M)	93.06
Aqueous extract (4000 μ g/ml)	94.44
50 % methanolic extract (4000 μ g/ml)	83.33
Methanolic extract (4000 μ g/ml)	55.56
UPFMCP (Unsaponified petroleum ether fraction of methanol extract) (4000 μ g/ml)	77.78
RMECP (Residual methanolic extract (4000 μ g/ml)	76.39
CPECP (Crude polyamine extract) (4000 μ g/ml)	86.39
CAFCP (Crude alkaloidal fraction) (4000 μ g/ml)	93.06
β -sitosterol (400 μ g/ml)	50
Lupeol (400 μ g/ml)	81.94
L-dopa (400 μ g/ml)	34.72
Adrenaline (400 μ g/ml)	30.56
β -carotene (400 μ g/ml)	29.16
CP I (400 μ g/ml)	54.17
CP II (400 μ g/ml)	75
CP III (400 μ g/ml)	81.94

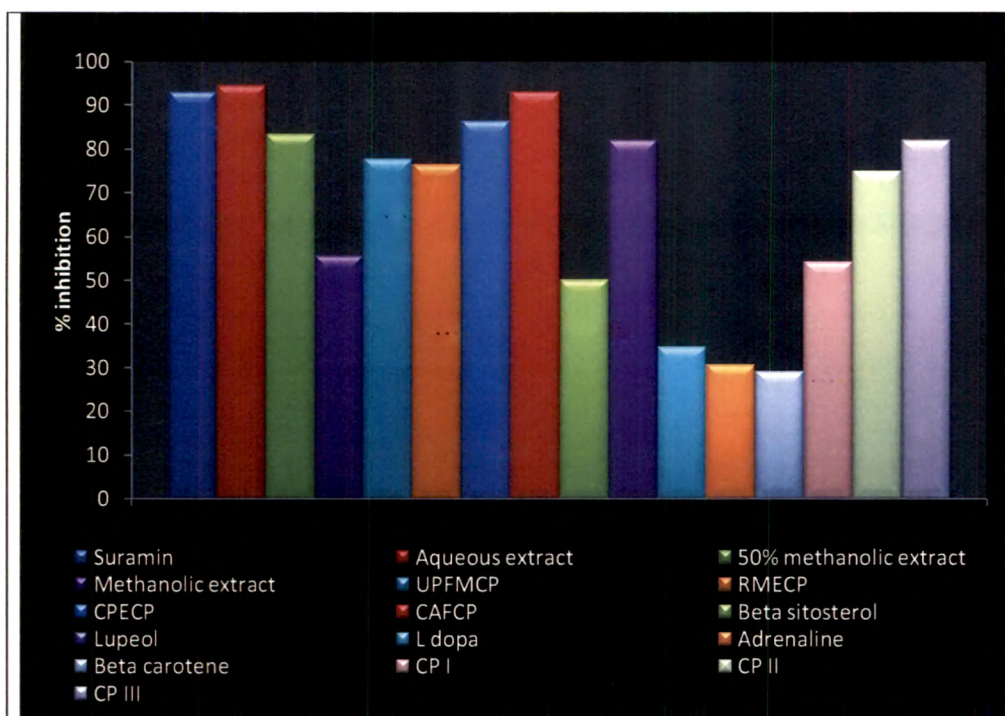


Figure 4.1.72: % inhibition of PTP1B by extracts / fractions / compounds of *C. phlomidis*

Aqueous extract exhibited highest inhibition, CAFCP and suramin equally inhibited PTP1B (Table 4.1.30, Figure 4.1.72). Steroids, coumarins, flavonoids, phenolics were detected in aqueous extract and many steroids and flavonoids has been reported for their PTP1B inhibition (Chen et al., 2002; Cui et al., 2007). Many individual alkaloids have been previously reported for their PTP1B inhibition (Cao et al., 2005; Bustanji et al., 2006) CAFCP being a crude alkaloidal fraction explains its equipotency with suramin. CPECP showed 86.39 % inhibition but STZ-NAD model showed indication that it may involve an insulin-independent-mechanism, which is contradictory. Highest inhibition by aqueous extract explains the 83.33% inhibition of 50 % methanolic extract. Lupeol and CP III showed 81.94 % inhibition but lupeol has been previously reported for PTP1B inhibition (Na et al., 2009). The presence of lupeol and CP III gives explanation for the inhibitory activity of UPFMCP, their less quantitative presence may have decreased the % inhibition. Conversely UPFMCP exhibited maximum antidiabetic activity in STZ-

NZD model. CP II, the palmityl ester exhibited less % inhibition than CPIII, suggesting that the presence of fatty chain may have hindered the activity. RMECP in spite of showing inactiveness in STZ-NAD model still inhibited 76.39 % inhibition of PTP1B, which is paradoxical. In spite of the presence of lupeol, CP III and CPII, methanolic extract exhibited modest activity. CP I and β -sitosterol exhibited 54.17 and 50 % respectively. β -sitosterol has been previously reported for less/no PTP1B inhibition (Zhang et al., 2010) but the 50 % inhibition in this study may be due to its higher concentration. L-dopa, adrenaline and β -carotene showed less than 50 % inhibition, which were considered as inactive. β -carotene has been previously reported to be inactive (Liu et al., 1999) in PTP1B Inhibition.

4.1.16 Brine shrimp lethality bioassay

The study of bioactive compounds from plant sources and extracts in the chemical laboratory is often hampered by the lack of a suitable, simple, and rapid screening procedure. There are, of course, many procedures for bioassay, but unless collaborative programs with biologists or pharmacologists are in place, the typical chemical laboratory is not suitably equipped to perform the usual bioassays with whole animals or isolated tissues and organs, as well aseptic techniques.

This method, utilizing brine shrimp (*Artemia salina*), is a simple bioassay for natural product research. The procedure determines lethal concentrations of active compounds in brine medium. The activities of a broad range of active compounds are manifested as toxicity to the shrimp. The method is rapid, reliable and has been used for over thirty years in toxicological studies. The commercial availability of inexpensive brine shrimp eggs, the low cost and ease of performing the assay make brine shrimp lethality assay, a very useful bench-top method (McLaughlin et al., 1991). The shrimp lethality assay was proposed by Michael et al., (1956), and later developed by Vanhaecke et al., (1981), and Sleet and Brendel (1983). It is based on the ability to cause death in the laboratory cultured *Artemia nauplii* brine shrimp.

Results and Discussion

The assay is considered a useful tool for preliminary assessment of toxicity (Solis et al., 1993), and it has been successfully used for studying fungal toxins (Harwig and Scott, 1971), plant extract toxicity (McLaughlin et al., 1991), teratology screens (Carballo et al., 2002), ecotoxicology studies (Carballo et al., 2002), heavy metal toxicity (Martinez et al., 1998), cyanobacteria toxins (Jaki et al., 1999), pesticide toxicity (Barahona et al., 1999), cytotoxic compounds (Siqueira et al., 1998), antimalaria compounds (Perez et al., 1997), insecticidal compounds (Oberlies et al., 1998), antifeedent compounds (Labbe et al., 1993) and cytotoxicity testing of dental materials (Pelka et al., 2000).

The brine shrimp assay has also been used for the isolation of biogenic compounds from plant extracts (Sam, 1993). This method allows the use of smaller quantity of the samples and permits large number of samples and dilutions within short time (Sam, 1993).

Brine shrimp bioassay has good correlation with the human solid tumour cell lines (Anderson et al., 1991). Considering the Brine shrimp lethality as a simple bioassay useful for drug discovery process, the procedure of Mayer et al., (1982), was adopted to determine the lethality of plant extracts to brine shrimp. The nauplii immediately after hatching and after 24 h are shown in Figure 4.1.73.

The degree of lethality was found to be directly proportional to the concentration of the samples. The LC₅₀ values of the brine shrimp obtained for extracts/fractions or isolated/identified compounds have been presented in Table 4.1.31.

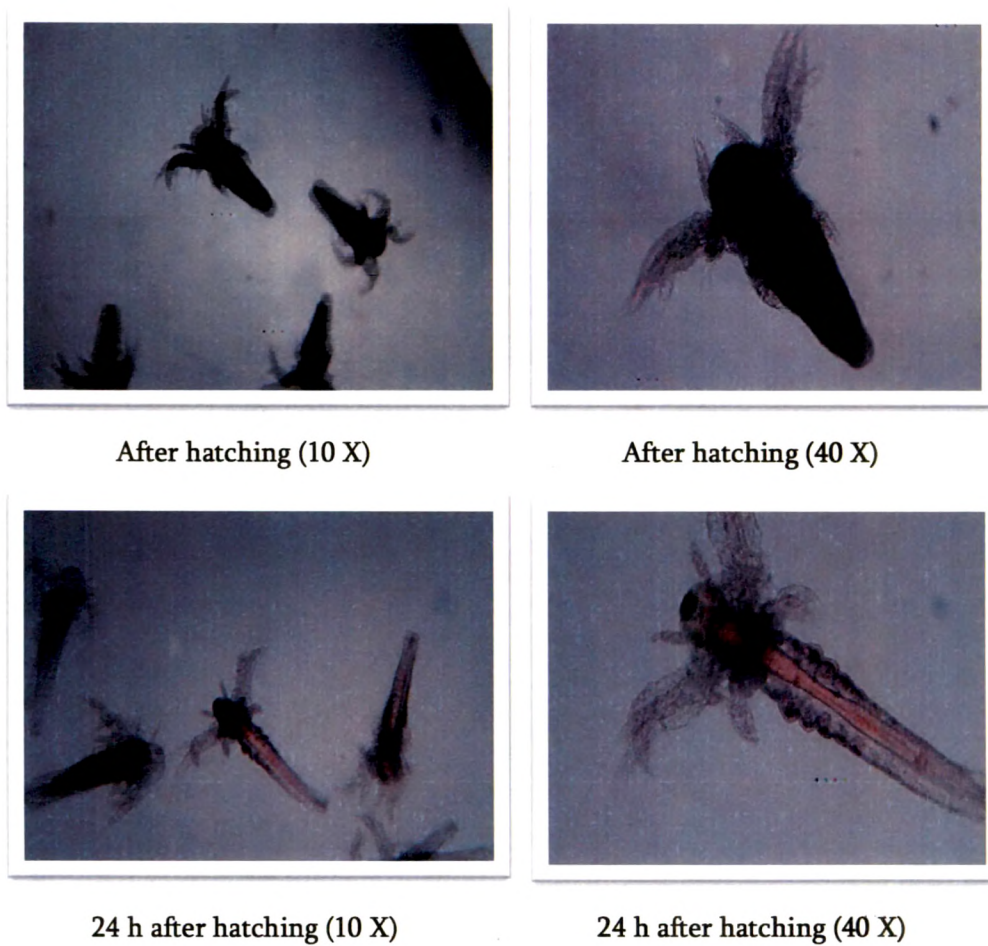


Figure 4.1.73: Brine shrimp nauplii immediately after hatching and 24 h after hatching

LC₅₀ values < 1000 µg/ml are considered significant for crude extracts (Garza et al., 2007). The tested compounds followed the order CP III>CP II>β-carotene>CP I>β-sitosterol in lethality to brine shrimps. Lupeol, l-dopa and adrenaline showed no significant effect till 2000 µg/ml. As expected UPFMCP showed highest lethality followed by methanolic extract and CAFCP among the extracts/fractions. All the compounds (CP III, CP II, β-carotene, CP I, β-sitosterol) that exhibited significant effect are ingredients of UPFMCP and methanolic extract. 50 % methanolic extract, aqueous extract, CPECP and RMECP showed no lethality even at 4000 µg/ml.

Table 4.1.31: LC₅₀ values of extracts/fractions/compounds of *C. phlomidis*

Extracts/fractions/isolated or identified compounds	LC ₅₀ values (µg/ml)
Methanolic extract	1340
50 % methanolic extract	> 4000
Aqueous extract	> 4000
CPECP (Crude polyamine extract)	> 4000
CAFCP (Crude alkaloidal fraction)	2450
UPFMCP (Unsaponified petroleum ether fraction of methanol extract)	1130
RMECP (Residual methanolic extract)	> 4000
CP I	600
CP II	450
CP III	330
β-sitosterol	750
Lupeol	> 2000
L-dopa	> 2000
Adrenaline	> 2000
β-carotene	520

4.1.17 Anti-platelet aggregation activity

An association between overt diabetes and cardiovascular disease has been observed in many studies (Kannel et al., 1979; Connor and Wingard, 1983; Donahue et al., 1987). Among persons with NIDDM in the United States, up to

75% of deaths are attributed to ischemic heart disease or other heart and vascular disease (Harris and Entmacher, 1985). Several cardiovascular complications have been associated with diabetes. These include acute myocardial infarction (Connor and Wingard, 1983; Kannel and McGee, 1979; Donahue et al., 1987), acute myocardial infarction (Smith et al., 1984) chronic congestive heart failure (Kannel et al., 1974), cerebrovascular disease (Abbott et al., 1987), and peripheral vascular disease (Melton et al., 1980). Platelet hyperaggregability is considered as one of the important risk factors for CVD in diabetic patients (Trovati and Anfossi, 1998; Sowers et al., 2001). Several hemostatic abnormalities involving levels of coagulation factors, platelet dysfunction, and increased blood viscosity have also been described as causes of the high risk for cardiovascular disease in diabetic patients.

Patients with type II diabetes mellitus were found to be associated with increased platelet aggregation and higher thromboxane A₂ and von Willebrand factor activity (Gresele et al., 2003). Acute hypoglycemia induces a shortening of the half-life of fibrinogen and platelet aggregation and results in increased levels of fibrinopeptide A, prothrombin fragments, and factor VII, all these facts suggest increased activation of prothrombotic factors (Jones and Peterson, 1979; Ceriello et al., 1988; Ceriello et al., 1989; Ceriello et al., 1995 ; Sakamoto et al., 2000).

Insulin is reported to attenuate platelet functions by interfering with cAMP suppression through IRS-1 and Gi (Ferreira et al., 2004). Anti-platelet therapy is recommended by The American Heart Association (AHA) and the American Diabetes Association (ADA) as a primary prevention strategy in those with diabetes at increased cardiovascular risk, including those who are >40 years of age or who have additional risk factors (family history of CVD, hypertension, smoking, dyslipidemia, or albuminuria) (Antiplatelet Trialists Collaboration, 1994). Aspirin as anti-platelet agent is widely used to reduce CVD in the general population and in patients with diabetes (James CN et al., 2004; Antiplatelet

Trialists Collaboration, 1994; Hayden et al., 2002). Numerous epidemiological studies support the early treatment of diabetic cardiovascular complications with anti-platelet agents (SCPHSRG Report, 1989; ETDRS Investigators, 1992; Sacco et al., 2003; Ridker et al., 2005). *Clerodendrum phlomidis* is widely used in Ayurveda and Siddha system of medicines for the treatment of diabetes (Mohan Maruga Raja and Mishra, 2010). The ethanolic leaf extract is hypoglycemic and also corrected the elevated cholesterol and triglycerides levels (Dhanabal et al., 2007). An antidiabetic drug with antiplatelet activity could be more significant, hence the antiplatelet study was carried out.

Cardinal and Flower (1980) described the impedance method for measuring platelet aggregation in described Whole blood. A cuvette of whole blood is continuously stirred and maintained at 37 °C. A very small electric current is passed between two electrodes immersed in the sample. During initial contact with the sample, the electrodes become coated with a monolayer of platelets. When ADP is added, platelets aggregate on the monolayer, increasing the impedance. The extent of aggregation in terms of change in impedance is reported in ohms. Platelet aggregation is a consequence of complex signal transduction cascade reactions, which can be induced by a variety of stimulants. Platelet membrane GPIIb and IIIa exist as a heterodimeric complex that is important in platelet plug formation after vascular injury (Coller et al., 1995). This complex acts as a receptor for fibrinogen, fibronectin, von Willebrand factor, and vitronectin, and its binding of these adhesive proteins mediates platelet aggregation, adhesion, and spreading (Bennett et al., 1979; Ruggeri et al., 1982; Ginsberg et al., 1983).

The common final step in the formation of platelet aggregates involves fibrinogen binding to platelet GPIIb/IIIa (Dejana et al., 1988; Phillips et al., 1988). Platelet aggregation is mediated by the formation of fibrinogen bridges between GPIIb/IIIa molecules on adjacent platelets as shown in Figure 4.1.74.

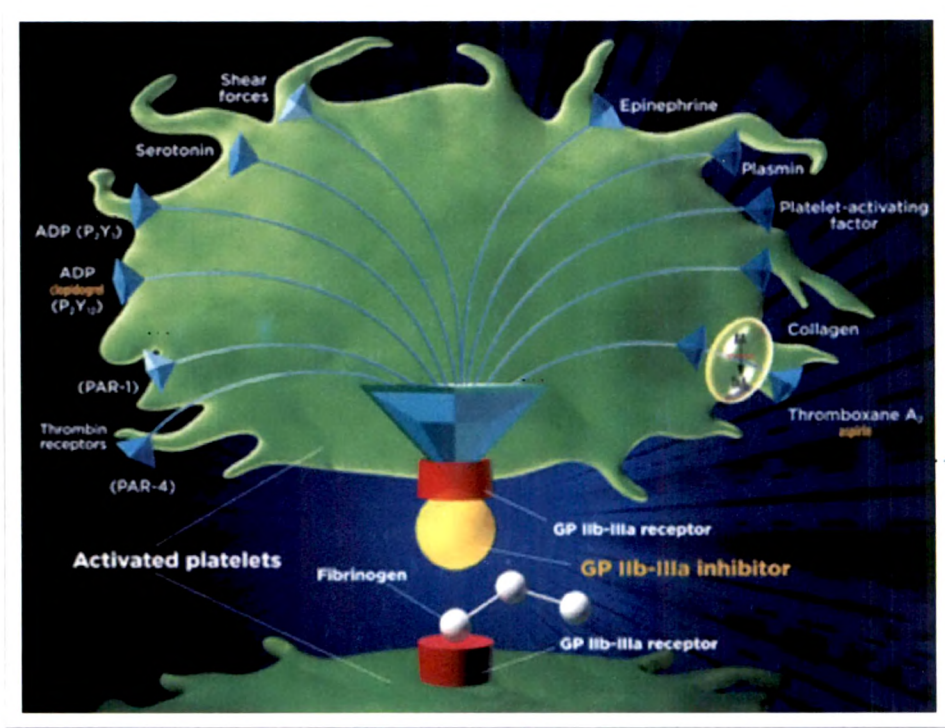


Figure 4.1.74: Platelet thrombus formation

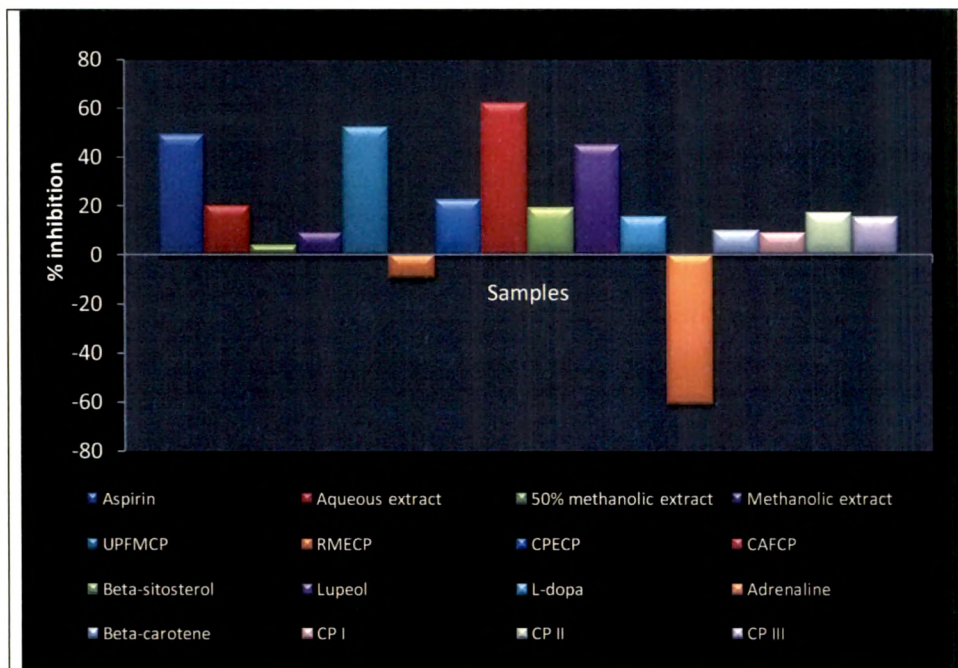


Figure 4.1.75: Percentage inhibition of platelet aggregation of extracts / fractions / compounds of *C. phlomidis*

Table 4.1.32: Effects of *C. phlomidis* extracts/fractions/compounds on ADP induced platelet aggregation

Extracts/fractions/isolated or identified compounds	Change in impedance Mean±SD (Ω)	% Inhibition of platelet aggregation
Control	12.17±1.14	-
Aspirin (10 μM)	6.17±0.95 **	49.3
Aqueous extract (4000 μg/ml)	9.73±0.91 *	20.04
50 % methanolic extract (4000 μg/ml)	11.7±10.82 ^{ns}	3.86
Methanolic extract (4000 μg/ml)	11.03±0.72 ^{ns}	9.36
UPFMCP (Unsaponified petroleum ether fraction of methanol extract) (4000 μg/ml)	5.8±0.95 **	52.34
RMECP (Residual methanolic extract) (4000 μg/ml)	13.33±0.8 ^{ns}	-9.53
CPECP (Crude polyamine extract) (4000 μg/ml)	9.4±0.85 **	22.76
CAFCEP (Crude alkaloidal fraction) (4000 μg/ml)	4.63±1.05 **	61.96
β-sitosterol (400 μg/ml)	9.83±1.07 *	19.22
Lupeol (400 μg/ml)	6.7±1.05 **	44.95
L-dopa (400 μg/ml)	10.3±0.56 ^{ns}	15.37
Adrenaline (400 μg/ml)	19.6±0.95 **	-61.05
β-carotene (400 μg/ml)	10.97±0.40 ^{ns}	9.86
CP I (400 μg/ml)	11.07±0.76 ^{ns}	9.04
CP II (400 μg/ml)	10.07±0.42 ^{ns}	17.26
CP III (400 μg/ml)	10.30±0.95 ^{ns}	15.37

Values are expressed as Mean ± SD; n=3; *-p<0.05; **-p<0.01; ^{ns}-not significant

The normal platelet aggregation (viz. Control) was found to be $12.17 \pm 1.14 \Omega$ and the platelet aggregation inhibition by of aspirin ($10 \mu\text{M}$) was $6.17 \pm 0.95 \Omega$. The standard inhibition range of ADP ($10 \mu\text{M}$) induced platelet aggregation for aspirin is $6-24 \Omega$. Aspirin irreversibly inactivates cyclooxygenase (COX-1) by acetylating the hydroxy group of Ser-529 near the active site, thereby blocking the binding of its substrate arachadonic acid. COX-1 in the platelet normally converts arachadonic acid to PGH, a precursor of the potent platelet activator thromboxane A₂. 50 % methanolic extract, methanolic extract, RMECP, l-dopa, β -carotene, CP I, CP II and CP III showed no significant change in impedance (Table 4.1.32). Further RMECP showed increase in impedance more than the control. Adrenaline, a known platelet sensitizer and antagonist of insulin, abolishes the effect of insulin on $[\text{Ca}^{2+}]$; tyrosine phosphorylation of $\text{G}\alpha_2$, and causes aggregation by interfering with the phosphorylation of the insulin receptor β subunit and by activating $\alpha_2\text{A}$ adrenergic receptor. Although ADP has initiated aggregation adrenaline plays a prominent role in the process of extension of the platelet plug (Rivera et al., 2009), hence a negative inhibition of -61.05 % (Figure 4.75). Traces of adrenaline in RMECP may be responsible for its negative inhibition of -9.53 %.

Aqueous extract and β -sitosterol showed significant ($p < 0.05$) change in impedance with 20.04 and 19.22 % inhibition respectively. Aqueous extract was expected to contain quantitatively higher adrenaline showed positive inhibition (20.04 %), may be due to the counteract effect of other water soluble constituents. Considering this hypothesis the aqueous extract without adrenaline would exert higher platelet aggregation inhibition. β -sitosterol has been previously reported for anti-platelet activity (Saeed et al., 1993). Aspirin, CAFCP, UPFMCP, lupeol and CPECP showed significant ($p < 0.01$) change in impedance with 49.3, 61.96, 52.34, 44.95 and 22.76 % inhibition of ADP induced platelet aggregation respectively. CAFCP and UPFMCP showed higher inhibition than the standard drug, aspirin. β -sitosterol and lupeol inhibits platelet aggregation, both being constituents of

UPFMCP explains the higher platelet aggregation inhibition, vitamin E has been reported for its anti-thromboxane action (Davi et al., 1999). Conversely the inhibition may also be due to unidentified constituent/s in UPFMCP. CAFCP has exhibited maximum inhibition and many alkaloidal compounds have been previously reported for their anti-platelet activity (Watson et al., 2010; Brossi et al., 1987; Sheu et al., 1998; Chen et al., 1991; Chen et al., 2000; Chen et al., 1996).

ADP causes a full range of activation events including intraplatelet Ca^{2+} elevation, TxA^2 synthesis, protein phosphorylation, shape change, granule secretion, activation of $\alpha_{IIb}\beta_3$, and aggregation. All these events are mediated by interaction with two classes of purinergic GPCR, $P2Y_1$ and $P2Y_{12}$ (Gachet, 2008). Stimulation of $P2Y_1$ activates phospholipase C, whereas stimulation of $P2Y_{12}$ downregulates adenylate cyclase activity, leading to lower levels on cAMP, an inhibitor of platelet activation. At cellular level, stimulation of $P2Y_1$ generates an initial transient aggregation response, whereas agonism of $P2Y_{12}$ generates sustained aggregation. Inhibition of ADP induced platelet aggregation by CAFCP, UPFMCP and lupeol may be due to activation of $P2Y_1$ or $P2Y_{12}$ or both.

4.1.18 Anti-acetylcholinesterase study

Alzheimer's disease (AD) is the most common age-related neuro-degenerative disorder that affects regions of the brain that control cognition (memory, language, speech and awareness to one's physical surroundings) and neuropsychiatric manifestations that result in progressive disability and eventual incapacitation (Farlow, 1998; Holden and Kelly, 2002). In recent decades, studies have shown that AD is a multifactorial pathology caused by genetic, environmental, and endogenous factors. These include excessive protein misfolding and aggregation, oxidative stress and free radical formation, impaired bioenergetics and mitochondrial abnormalities, neuroinflammatory processes and cholinergic neuron loss in the basal nucleus of Meynert (Selkoe, 1989). Of the many pathogenic hypotheses of AD, an alteration of cell Ca^{2+} homeostasis might be

at the centre of the metabolic crossroad leading neurons to apoptotic death (Mattson and Pedersen, 1998; Mattson et al., 2000). Amyloid β ($A\beta$) peptide aggregates ($A\beta$ plaques), and neurofibrillary tangles (NFTs) of hyperphosphorylated τ protein, represent the two main hallmarks of AD correlated with the severity of the disease. It is well-known that AD is characterized by degradation of the cholinergic system together with alteration of glutamatergic and serotonergic receptors (Salloway et al., 2008). The neuropsychiatric symptoms associated with the illness are also related to the reduction in the number of functional neuronal nicotinic receptors (nAChR) (Schroder et al., 1991) for this reason the only therapeutical strategy that, up to now, has proven to have some efficacy in slowing progression of AD is that which improves cholinergic neurotransmission, counteracting the deficit of cerebral acetylcholine (Relman, 1990; Standaert and Young, 1996). A decrease of acetylcholine in the brain of patients with AD appears to be a critical element in producing dementia (Becker et al., 1988). Cholinesterases are polymorphic enzymes that hydrolyse the synaptic acetylcholine and terminate neuronal signaling. Vertebrates have two cholinesterases: acetylcholinesterases (AChE; EC 3.1.1.7) and butyrylcholinesterase (BChE; EC 3.1.1.8). AChE inhibition remains the most important strategy for designing new potential anti-AD agents. This is because, in addition to its role in degradation of acetylcholine (ACh), AChE can accelerate $A\beta$ aggregation through direct interaction with its peripheral anionic site (PAS) (Inestrosa et al., 1996). AChE inhibitors increase the availability of acetylcholine in central cholinergic synapses and are the most promising currently available drugs for the treatment of AD (Giacobini, 2000). Cholinesterase inhibition is not only the mainstay treatment for AD but also considered as promising strategy for the therapy of dementia, myasthenia gravis and Parkinson's disease.

Alzheimer's disease and type 2 diabetes mellitus: the cholinesterase connection:
Insulin signaling abnormalities could be the underlying mechanism affecting the

outcome of Alzheimer's disease; insulin resistance and disordered degradation of amyloid seem to link diabetes mellitus with Alzheimer's disease (Sun and Alkon, 2006). Insulin dysregulation could act in a variety of ways including decreased cortical glucose utilization, oxidative stress formation of advanced glycated proteins, increased neurofibrillary formation and increased amyloid β aggregation through inhibition of insulin-degrading enzyme (Grossman, 2003). Insulin resistance could therefore be a link between Alzheimer's disease and type 2 diabetes mellitus (Craft et al., 2006). It has been hypothesized that peripheral insulin resistance can affect CNS insulin levels, cognition and amyloid β levels (Craft et al., 2006). Peripheral insulin resistance downregulate insulin uptake at the blood brain barrier and lead to CNS insulinopenia. Since insulin promotes intracellular amyloid β release and alters expression of insulin degrading enzyme, low brain insulin levels can lead to amyloid β accumulation in neurons. Peripheral insulin resistance may also inhibit clearance of amyloid β from the brain to the periphery, either by blocking its transport from the brain or by interference with clearance in peripheral sites. Thus there could be a combination of accumulation of amyloid β , with decreased clearance, both due to insulin resistance (Craft et al., 2006).

Antidiabetic drugs could be potentially useful in treating Alzheimer's disease: PPAR γ agonists, by improving insulin sensitivity, decreasing inflammation and improving cerebral energy metabolism; intranasal insulin, by restoring brain insulin levels in Alzheimer's disease (Craft et al., 2006). Esterase group of enzymes may be an underlying thread in the coexistence of Alzheimer's disease and diabetes mellitus. At present however, one cannot impute a direct cause effect relationship between Alzheimer's disease, type 2 diabetes mellitus and insulin resistance, although there are epidemiological, biochemical, pathological and computational biological leads pointing to an association. Figure 4.1.76 shows the common pathological processes in Alzheimer's disease and type 2 diabetes mellitus.

Butyrylcholinesterase and acetylcholinesterase related proteins were found common to both Alzheimer's disease and diabetes; they may play an etiological role via influencing insulin resistance and lipid metabolism (Allam et al., 2006). The effect of streptozotocin-induced diabetes on cholinesterases activities was studied in the retina and, for comparison, in other nervous and non-nervous tissues. The results suggest that diabetes might influence a specific subset of cells and isoforms of cholinesterases (Chavez and Salceda, 2000). AChE inhibitory activity has also been observed for several classes of phytoconstituents such as steroidal, indole and isoquinoline alkaloids, pregnane glycosides (cynantrosides, norswertianolin and swertianolin), stilbene, xanthenes, ursane (Mukherjee et al., 2007) and other triterpenes (Gurovic et al., 2009). Galanthamine, an alkaloid obtained from *Galanthus* and *Narcissus* species (Amaryllidaceae) and (-)-huperzine A, an alkaloid isolated from Chinese herb *Huperzia serrata* (Thumb.) are selective, reversible and competitive acetylcholinesterase inhibitors (Liu et al., 1986; Sweeney et al., 1989; Thomsen and Kewitz, 1990; Kozikowski et al., 1992).

Acetylcholinesterase micro plate inhibition assay: Acetylcholinesterase inhibition was measured using the analogue acetylthiocholine iodide, which is converted to thiocholine in the presence of AChE. The reaction of thiocholine with the chromogenic substrate dithionitrobenzoic acid (DTNB) leads to the formation of 2-nitrobenzoate-5-mercaptothiocholine and 5-thio-2-nitrobenzoate (yellow color), which absorbs strongly at 405 nm.

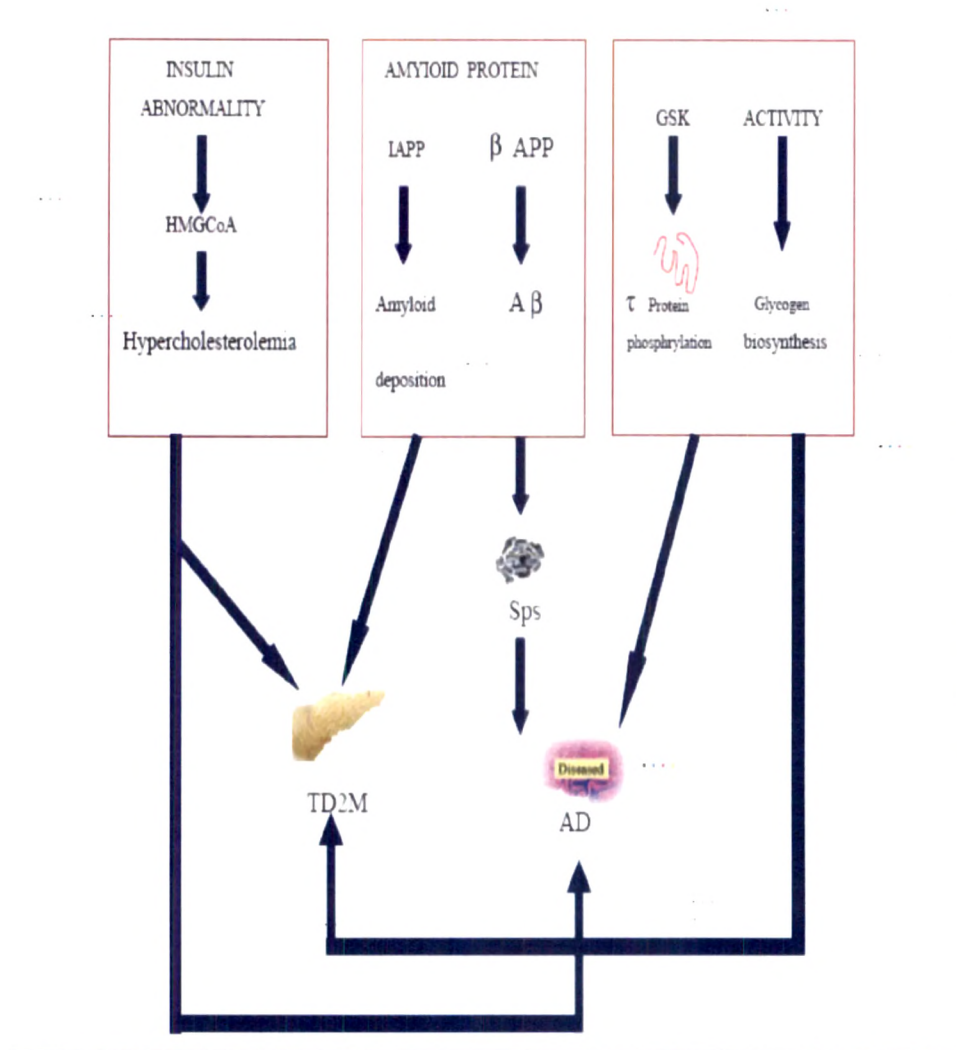


Figure 4.1.76: Common pathological processes in AD and type 2 DM. Ninety percent homologous structure has been observed between amyloid β which is a hallmark pathology in AD and islet amyloid polypeptide (IAPP) which is involved in type 2 diabetes mellitus. Insulin abnormality is attributed to AD by promoting amyloid β deposit and τ protein hyperphosphorylation. GSK3 is a key kinase to promote τ protein hyperphosphorylation and glycogen biosynthesis.

AD - Alzheimer's disease; T2DM - Type 2 diabetes mellitus; IAPP - islet amyloid polypeptide; $A\beta$ - Amyloid β ; GSK3 - glycogen synthase kinase; Sps - senile plaques.

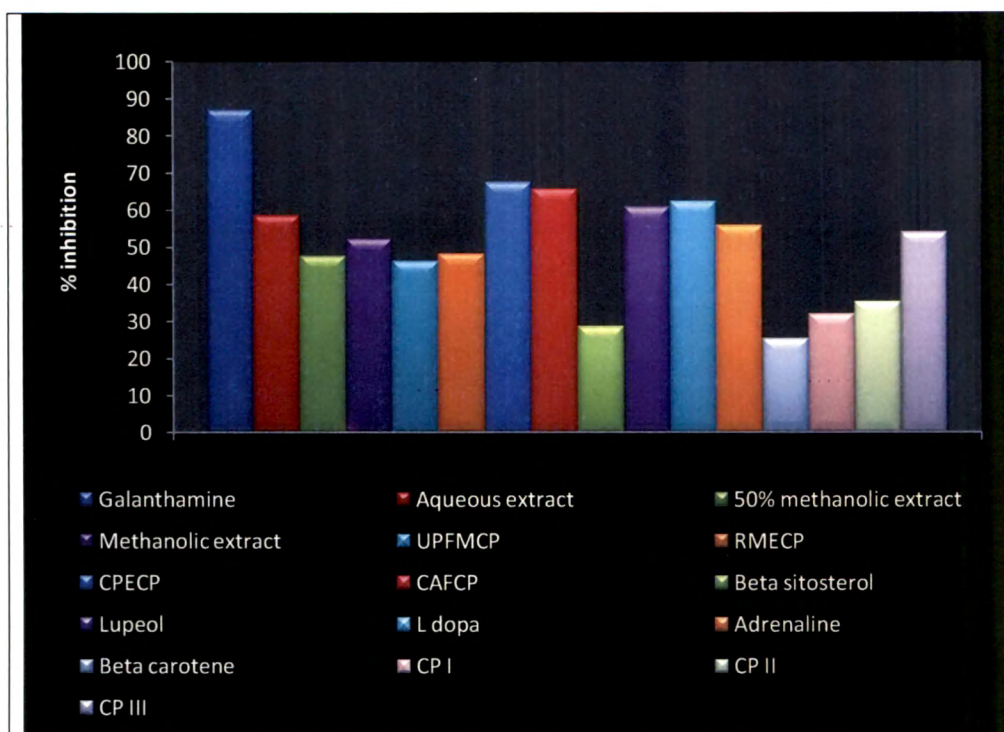


Figure 4.1.77: Comparison of % inhibition of acetylcholinesterase of extracts/fractions/compounds of *C. phlomidis*

Galanthamine showed highest % inhibition of 87.01 (Figure 4.1.77). Galanthamine has the added advantage of stimulating nicotinic receptors, preventing cell death induced by amyloid β , as well as inhibiting AChE (Pearson, 2001; Arias et al., 2004). CPECP inhibited acetylcholinesterase 67.38 % (Table 4.1.33). Polyamines inhibit acetylcholinesterase on substrate-concentration-dependent activation and is similar to that by Na^+ , K^+ , Ca^{2+} , Mg^{2+} and certain quaternary and bisquaternary amines (Kossorotow et al., 1974). Polyamines bind to neurotransmitter receptors and enzymes, such as muscarinic receptor subtypes, muscle-type nicotinic receptors and acetylcholinesterase (Minarini et al., 2010). Inhibitory effects on acetylcholinesterase by spermine and spermidine has been reported (Anand et al., 1976). CAFCP showed 65.64 % inhibition. Many alkaloids including galanthamine and huperzine A have been reported previously for acetylcholinesterase inhibition (Lopez et al., 2002; Houghton et al., 2004; Rijn et al., 2010; Serrano et al., 2010).

Table 4.1.33: % inhibition of acetylcholinesterase by extracts/fractions/compounds of *C. phlomidis*

Extracts/fractions/isolated or identified compounds	% Inhibition of acetylcholine esterase
Galanthamine (1 μ M)	87.01
Aqueous extract (4000 μ g/ml)	58.46
50 % methanolic extract (4000 μ g/ml)	47.66
Methanolic extract (4000 μ g/ml)	52.31
UPFMCP (Unsaponified petroleum ether fraction of methanol extract) (4000 μ g/ml)	46.16
RMECP (Residual methanolic extract) (4000 μ g/ml)	48.16
CPECP (Crude polyamine extract) (4000 μ g/ml)	67.38
CAFCP (Crude alkaloidal fraction) (4000 μ g/ml)	65.64
β -sitosterol (400 μ g/ml)	28.53
Lupeol (400 μ g/ml)	60.88
L-dopa (400 μ g/ml)	62.23
Adrenaline (400 μ g/ml)	55.84
β -carotene (400 μ g/ml)	25.30
CP I (400 μ g/ml)	31.98
CP II (400 μ g/ml)	35.36
CP III (400 μ g/ml)	53.93

L-dopa inhibited AchE 62.23 %, it has been reported to decrease acetylcholinesterase activity (Messripour and Shahidi, 1990). Kosmulalage et al., (2007) reported moderate acetylcholinesterase inhibition by lupeol, which explains the 60.88 % inhibition. Adrenaline has been reported to non-competitively inhibit acetylcholinesterase (Diadiusha and Poliakova, 1981.), in the present study it showed 55.84 % inhibition. The aqueous extract showed 58.46 %

Results and Discussion

inhibition. The acetylcholinesterase inhibition of aqueous extract may be influenced by polyamines, l-dopa or adrenaline or other unidentified polar compound/s. Of the isolated compounds tested CP III alone showed higher inhibition (53.93 %). The methanolic extract showed only 52.31 % inhibition of acetylcholinesterase, in spite of lupeol, alkaloids, polyamines and CP III being constituents of the extract. 50 % methanolic extract, UPFMCP, RMECP, β -sitosterol, β -carotene, CP I and CP II showed less than 50 % inhibition. No synergistic effect was observed of lupeol and CP III as UPFMCP showed only 46.16 % inhibition.

β -sitosterol and β -carotene showed 28.53 and 25.30 % inhibition respectively, both the constituents have been reported for nil activity against acetylcholinesterase (El-Demerdasha et al., 2004; Kolak et al., 2009). Apart from lupeol and CP III, increased acetylcholinesterase inhibition was observed in polar to moderate polar extracts/fractions.

4.2 *Nymphaea stellata*

4.2.1 Development of quality control parameters

Based on the literatures and preliminary hypoglycemic report, leaf was selected as the morphological part of study. It is essential to develop quality control parameters by using modern techniques.

4.2.2 Plant Profile

Nymphaea stellata Willdenow (Nymphaeaceae) (Figure 4.2.1)

Synonyms: *Nymphaea nouchali* Burman f.



Figure 4.2.1: *Nymphaea stellata*

4.2.3 Determination of foreign matter

Macroscopic examination can conveniently be employed for determining the presence of foreign matter in whole or cut plant materials. However, microscopy is indispensable for powdered materials. The leaf material showed 1.6 %w/w of total foreign matter (Table 4.2.1). 0.28 %w/w of mineral admixture indicates the presence of appreciable quantity of soil, stones, sand and dust. 0.445 %w/w of

other plant materials indicates the presence of other morphological parts of *N. stellata*. 0.864 %w/w of other organic matter includes moulds or insects, and other animal contamination, including animal excreta.

Table 4.2.1: Foreign matter in *N. stellata* leaves

Mineral admixture	Other plant materials	Other organic matter	Total foreign matter
0.28 % w/w	0.445 %w/w	0.864 %w/w	1.6 %w/w

4.2.4 Morphology, anatomy, histology and powder microscopy

The plant is an aquatic herb with underground perennial rhizome. The leaves are floating, orbicular, marginious smooth or bluntly deutate, glabrous beneath: Flowers – large borne on long pedicel: sepals – 4, greenish, white: petals – numerous blue of white, oblanceolate, spirally arranged. Stamens – numerous flattened, spiral, appendaged at the apex. Ovary: many celled, ovules many, stigma sessile, radiating, unappendaged (Figure 4.2.2). The morphological features matched with details available in the literature.



Figure 4.2.2: Leaves of *N. stellata*

The leaf is hydromorphic with wide air-chambers, reduced vascular strands and sclerenchyma. The lamina is 400 μm thick. It consists of thin adaxial and abaxial epidermal layers which are less conspicuous; the cells are small and squarish (Figure 4.2.3). The mesophyll tissues are differentiated in to adaxial palisade zone and abaxial arenchyma zone. The palisade zone is 100 μm in height and consists of

two layers of cells. The aerenchyma zone consists of wide air-chambers separated by thin, one-cell thick partitions walls (Figure 4.2.4, 4.2.5). All along the partition filaments, there are stellately branched, long armed sclerenchyma cells called 'trichosclereids'. These sclereide have pointed arms on the surface of which minute prismatic crystals are densely deposited (Figure 4.2.6, 4.2.7). These sclereids give mechanical support to the mesophyll tissue.

The vascular bundles differ in size from different zones of the lamina. The largest vascular of the major veins occur in the abaxial part of the lamina (Figure 4.2.4). The bundle is surrounded by a thin parenchymatous cells; a large mass of collenchyma is situated at the base of the bundles. The xylem consists of a cluster of wide vessels and large mass phloem. There are also slightly smaller vascular bundles placed in the median part of the lamina (Figure 4.2.3) these bundles are also collateral with a small cluster of xylem and a mass of phloem, the bundles being surrounded by parenchymatous sheath.

Along the adaxial part and beneath, the palisade zone are still smaller vascular bundles (Figure 4.2.4). These adaxial bundles are circular, collateral and have small groups of xylem and phloem surrounded by dialted hyaline bundle sheath cells. The leaf powder shows abundant trichosclereids of either entire or broken pieces (Figure 4.2.8). The trichosclereids have central wide body and several pointed arms spreading in all directions. The surface of the sclereid is warty due to deposition of minute prismatic crystals. These are also large masses of calcium oxalate crystals in the powder (Figure 4.2.9).

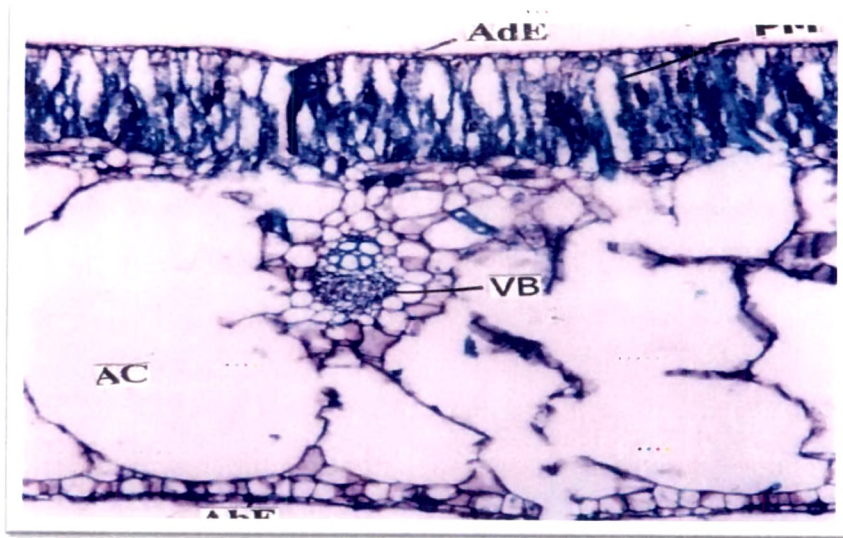


Figure 4.2.3: TS of *N. stellata* showing smaller vascular bundles in the median part of the lamina

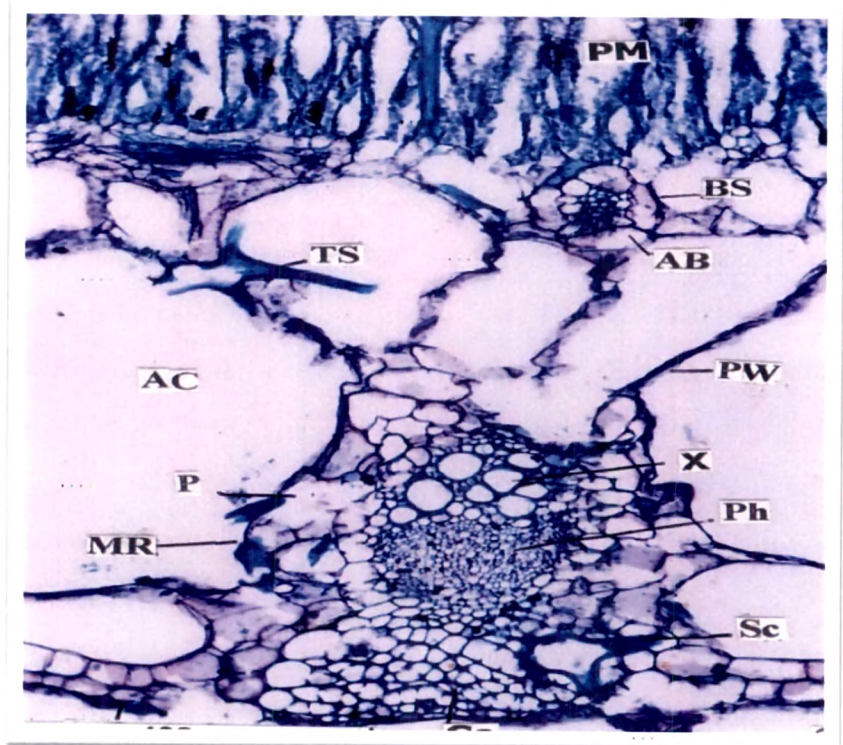


Figure 4.2.4: TS of *N. stellata* showing smaller vascular bundles beneath the palisade zone

Legend for figures: AbE- Abaxial epidermis; AC- Air chamber; AdE- Adaxial epidermis; BS- Bundle sheath; Co- Collenchyma; Mr- Midrib; P- Parenchyma; Ph- Phloem; PW- Phloem wall; PM- Palisade mesophyll; Scl- Sclerenchyma; Tr- Trichosclereids; VB- Vascular bundle; X- Xylem; AB- Accessory bundle.

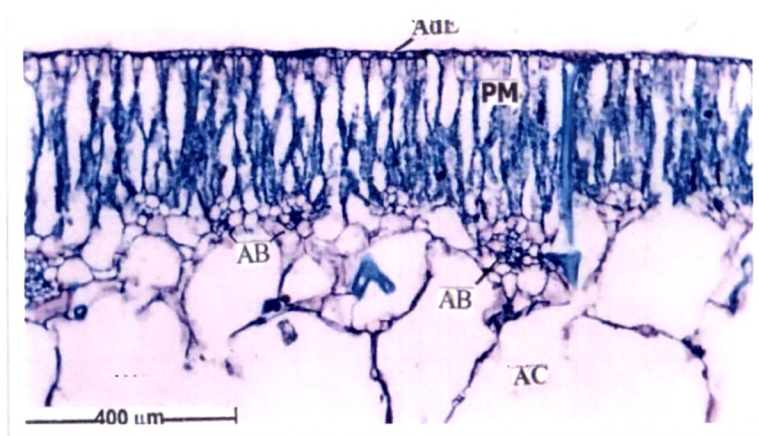


Figure 4.2.5: TS of *N. stellata* showing the arenchyma zone

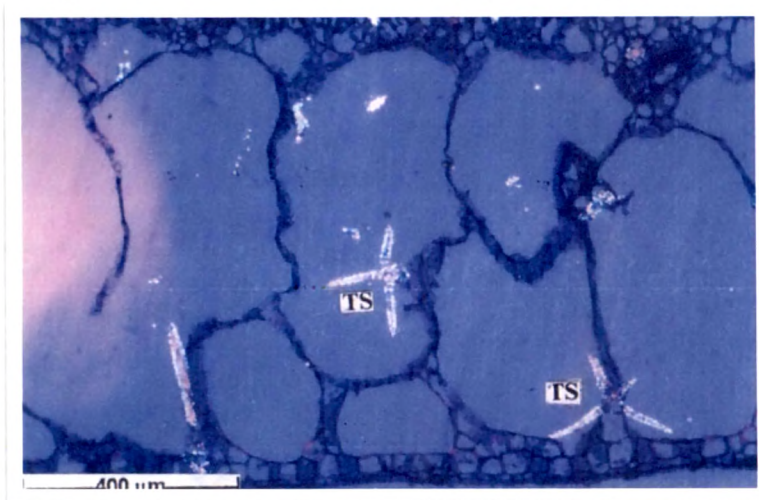


Figure 4.2.6: TS of *N. stellata* showing stellately branched, long armed trichosclereids

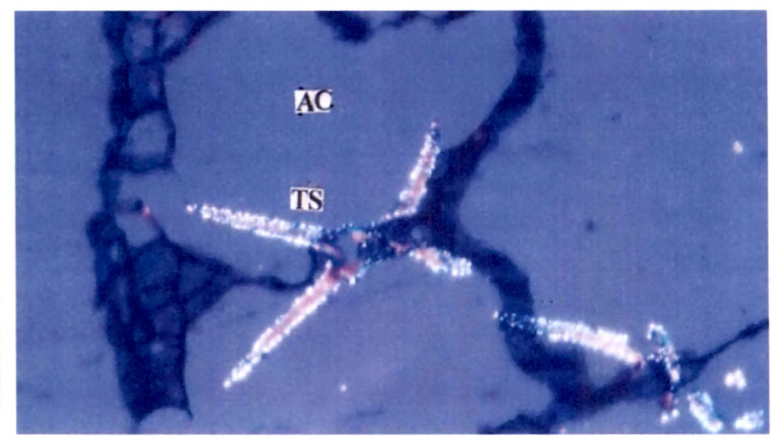


Figure 4.2.7: TS of *N. stellata* showing trichosclereid in higher magnification
Legend for figures: AB- Accessory bundle; Ac- Air chamber; AdE- Adaxial epidermis; PM- Palisade mesophyll; Ts- Trichosclereids.



Figure 4.2.8: Powder analysis of *N. stellata* showing abundant trichosclereids

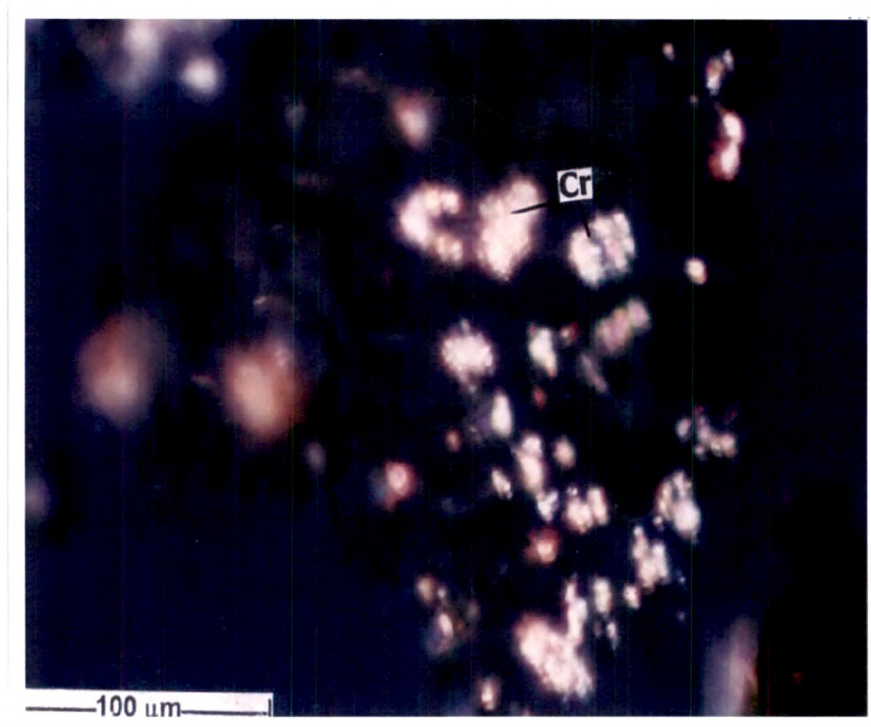


Figure 4.2.9: Powder analysis of *N. stellata* showing large masses of calcium oxalate crystals

Legend for figures: Cr- Crystals; Ts- Trichosclereide.

4.2.5 Proximate analysis

N. stellata leaves shows total ash value of 1.62 % and high sulphated ash, which indicates high quantity of carbonates and oxides. Low acid insoluble ash indicates less silicious materials like earth or sand (Table 4.2.2). Extractive values of *N. stellata* leaves show very high quantity of polar constituents than non-polar constituents (Table 4.2.2). The LOD was found to be 15.72 %w/w (Table 4.2.2). *N. stellata* being an aquatic plant has showed a relatively high value. The bitterness value of *N. stellata* leaves was found to be 125.71 (Table 4.2.2).

Table 4.2.2: Proximate analysis of *N. stellata* leaves

Parameters	Values
Total ash	2.21%w/w
Acid-insoluble ash	1.09 %w/w
Water-soluble ash	0.88 %w/w
Sulphated ash	1.62 %w/w
Water-soluble extractive	25.17 %w/w
Ethanol-soluble extractive	17.28 %w/w
Ether-soluble extractive	4.12 %w/w
Loss on drying (LOD)	15.72 %w/w
Bitterness value	125.71

4.2.6 Elemental analysis

N. stellata leaves shows 15. 240 g/kg of potassium level (Table 4.2.3) suggesting the presence of higher quantity of salts.

Table 4.2.3: Elemental analysis of *N. stellata* leaves

Elements	Quantity present
Potassium	15.240 g/kg
Zinc	117.39 ppm
Calcium	8.98 ppm
Manganese	40.85 ppm
Iron	1000 ppm
Magnesium	518.34
Nickel	Nil

4.2.7 Preliminary qualitative phytochemical screening

N. stellata leaves shows terpenoids and phenolics as major secondary metabolites. Steroids were detected in petroleum ether, unsaponified matter of petroleum ether, benzene, diethyl ether and chloroform extract. Flavonoids were detected in acetone, methanol and water extract. The % yield, appearance and nature of different extracts are shown in Table 4.2.4

Table 4.2.4: Preliminary qualitative phytochemical screening of *N. stellata* extracts

Successive extract	Yield % w/w	Appearance	Odour	Secondary metabolites
Petroleum ether	5.17	Brown sticky mass	No characteristic odour	Steroids
Unaponified matter of petroleum ether extract	0.43	Yellowish brown sticky mass	No characteristic odour	Steroids
Benzene	2.12	Green sticky mass	Faint odour	Steroids
Diethyl ether	0.85	Green sticky mass	Faint odour	Steroids, saponins
Chloroform	0.98	Blackish green sticky mass	Characteristic odour	Steroids, saponins, phenolics
Ethyl acetate	0.42	Blackish Green sticky mass	Characteristic odour	Phenols, saponins
Acetone	1.1	Blackish green mass	Characteristic odour	Flavanoids, phenolics
Methanol	12.67	Dark brown sticky mass	Characteristic odour	Flavonoids, phenolics
Water	20.54	Light brown powder	Pleasant odour	Flavonoids, phenolics

4.2.8 Thin layer chromatographic study

4.2.8.1 Identification and quantification of lupeol

Preliminary TLC finger printing and co-TLC studies (with marker compound) of *N. stellata* leaves revealed the presence of lupeol. Further, their presence was confirmed by R_f comparison, multi-wavelength scanning and spectral overlay.

Table 4.2.5: Method validation parameters for quantification of lupeol in *N. stellata* leaves

S. No.	Parameter	Results
1	R_f	0.40
2	Dynamic range (ng spot ⁻¹)	100 - 500
3	Equation	$y=553.192+10.463x$
4	Slope	10.463
5	Intercept	553.192
6	Linearity (correlation coefficient)	0.99646

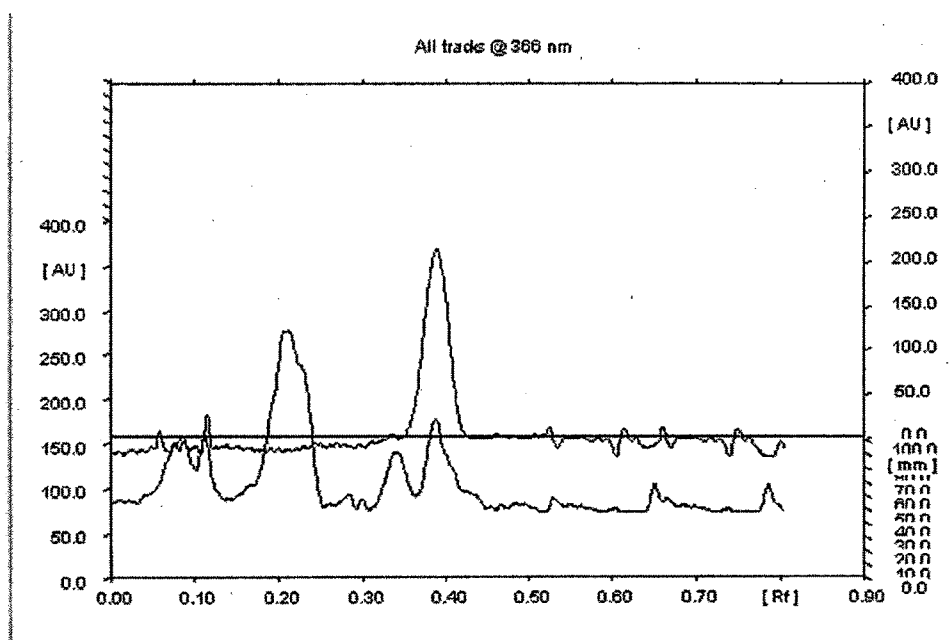


Figure 4.2.10: *N. stellata* leaf extract showing identical peak with standard lupeol

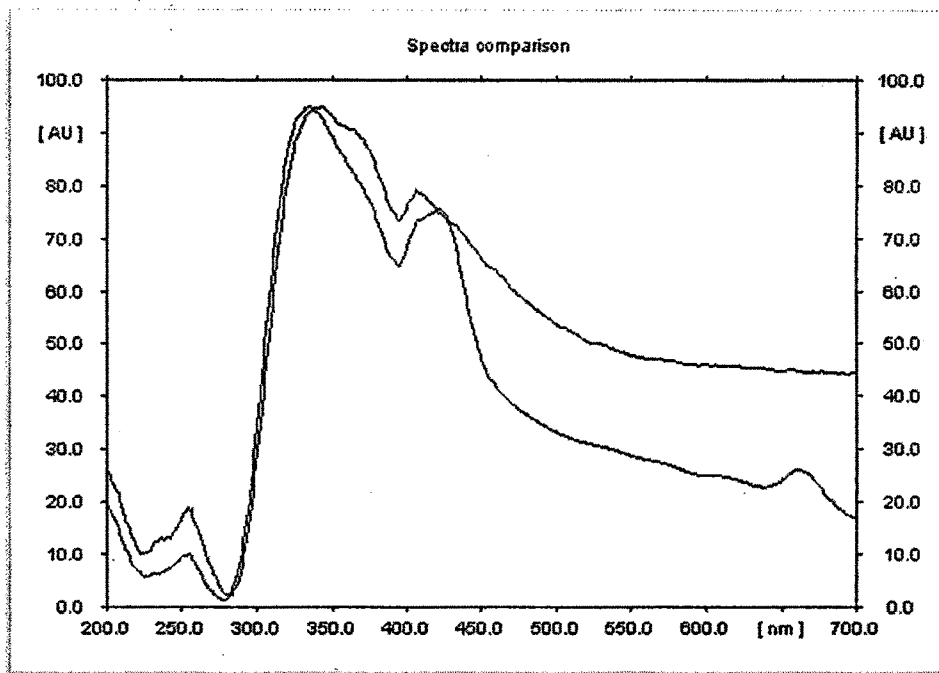


Figure 4.2.11: Spectral comparison for the peaks of standard lupeol and *N. stellata* leaf extract

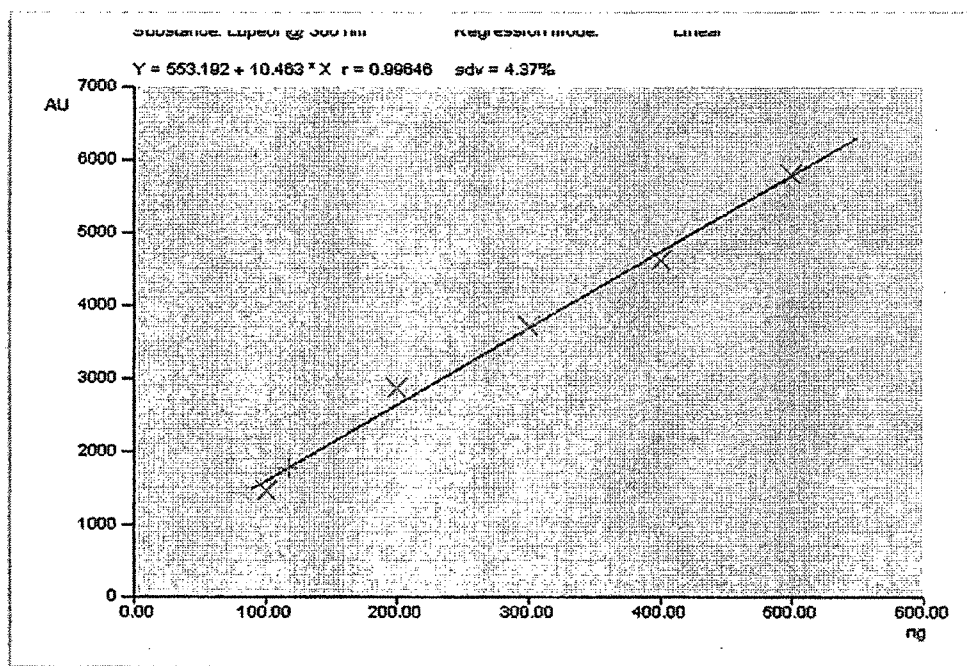


Figure 4.2.12: Calibration curve of peak area versus concentration for lupeol

Table 4.2.6: Calibration curve parameters for quantification of lupeol in *N. stellata* extract

R _f	Amount/Fraction	Area	X(calc)
0.40	100 ng	1457.42	-
0.41	200 ng	2856.83	-
0.40	300 ng	3714.96	-
0.40	400 ng	4627.37	-
0.40	500 ng	5803.54	-
0.39	-	1778.82	117.14 ng

TLC separation optimization: The leaves of *N. stellata* when subjected to TLC showed the presence of lupeol peak (Figure 4.2.10). A comparison of the spectral characteristics of the peak for standard compound and that of the sample further confirmed the identity of lupeol present in the sample (Figure 4.2.11). Good resolution with symmetrical and reproducible peak was obtained.

Linearity: The peak area versus concentration plot was found to be linear in the range of 100-500 ng spot⁻¹ for lupeol (Table 4.2.5, Figure 4.2.12). The regression equation and correlation coefficient for lupeol indicated good linearity.

Sample analysis: The lupeol content of the leaves calculated from the area calibration curve (Table 4.2.6) by this method was found to be 0.013016 %w/w (plant dry weight basis).

This TLC procedure may be used effectively for identity, quality evaluation as well as quantitative determination for this plant or its derived products.

4.2.8.2 Identification and quantification of β -sitosterol

Considering the wide therapeutic application of β -sitosterol and to ensure identity, quality of the plant material, this study was planned to quantify this marker constituents by TLC method.

Table 4.2.7: Method validation parameters for quantification of β -sitosterol in *N. stellata* leaves

S. No.	Parameter	Results
1	R _f	0.57
2	Dynamic range (ng spot ⁻¹)	100-500
3	Equation	y=280.581+8.778x
4	Slope	8.778
5	Intercept	280.581
6	Linearity (correlation coefficient)	0.98515

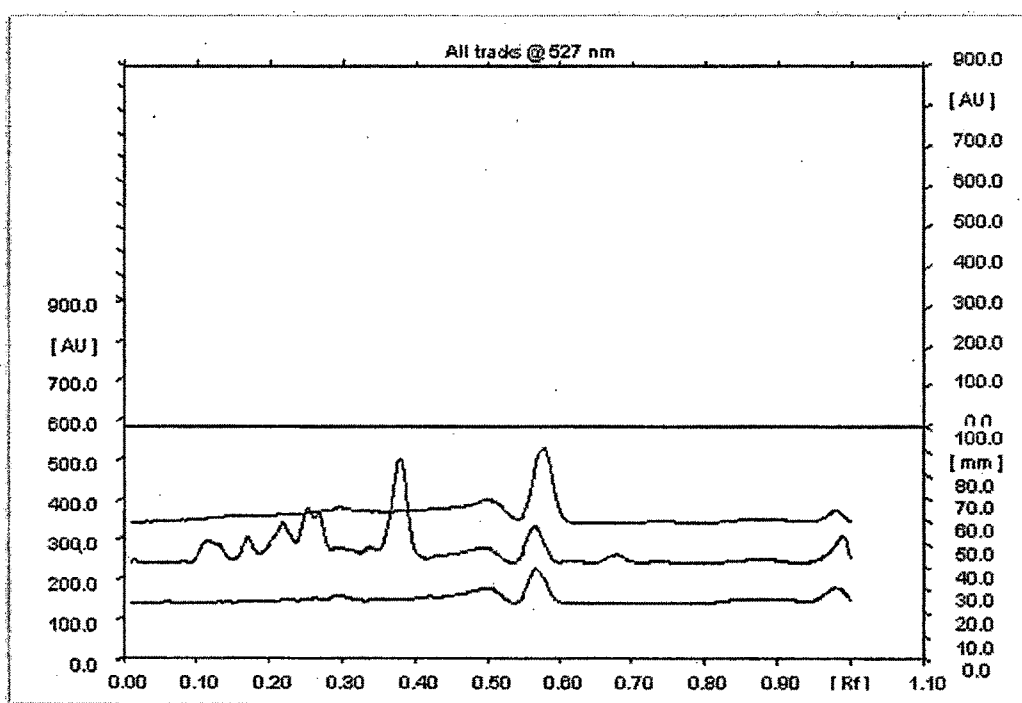


Figure 4.2.13: *N. stellata* leaf extract showing identical peak with standard β -sitosterol

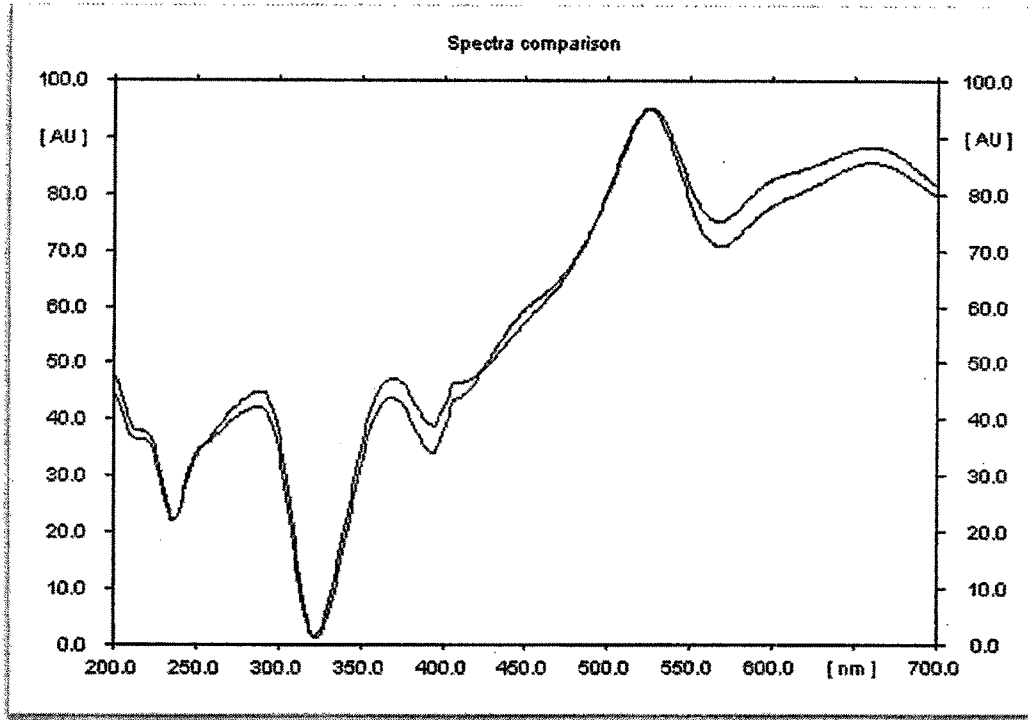


Figure 4.2.14: Spectral comparison for the peaks of standard β -sitosterol and *N. stellata* leaf extract

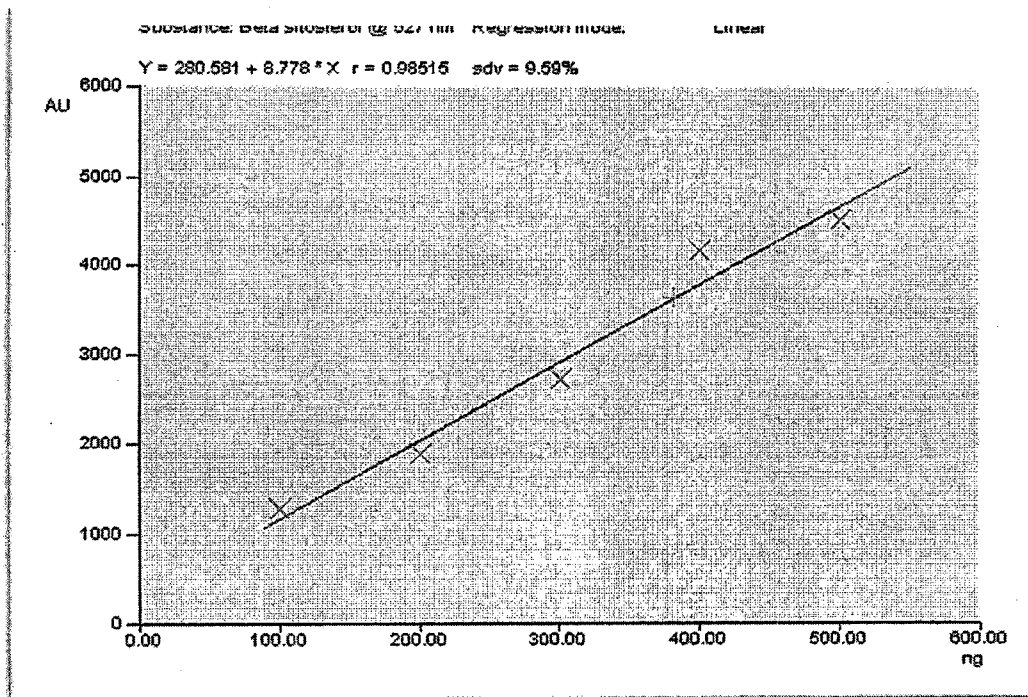


Figure 4.2.15: Calibration curve of peak area versus concentration for β -sitosterol

Table 4.2.8: Calibration curve parameters for quantification of β -sitosterol in *N. stellata* extract

R _f	Amount/Fraction	Area	X(calc)
0.58	100 ng	1270.61	-
0.57	200 ng	1892.08	-
0.56	300 ng	2717.87	-
0.57	400 ng	4166.66	-
0.58	500 ng	4522.15	-
0.58	-	3630.27	381.62 ng

TLC separation optimization: The leaves of *N. stellata*, when subjected to TLC showed the presence of β -sitosterol peak (Figure 4.2.13). A comparison of the spectral characteristics of the peak for standard compound and that of the sample further confirmed the identity of β -sitosterol present in the sample (Figure 4.2.14). Good resolution with symmetrical and reproducible peak was obtained.

Linearity: The peak area versus concentration plot was found to be linear in the range of 100-500 ng spot⁻¹ for β -sitosterol (Figure 4.2.15). The regression equation and correlation coefficient for β -sitosterol indicated good linearity (Table 4.2.7).

Sample analysis: The β -sitosterol content of the leaves calculated from the area calibration curve (Table 4.2.8) by this method was found to be 0.047703 %w/w (plant dry weight basis). This TLC procedure may be used effectively for identity, quality evaluation as well as quantitative determination for this plant or its derived products.

4.2.8.3 Identification and quantification of β -carotene

β -carotene as an antioxidant provides protection against cancer, heart disease, macular degeneration and ageing (Burri, 1997).

Table 4.2.9: Validation parameters for quantification of β -carotene in *N. stellata* leaves

S. No.	Parameter	Results
1	R_f	0.39
2	Dynamic range (ng spot ⁻¹)	100 – 500
3	Equation	$y=169.086+4.235x$
4	Slope	4.235
5	Intercept	169.086
6	Linearity (correlation coefficient)	0.99808

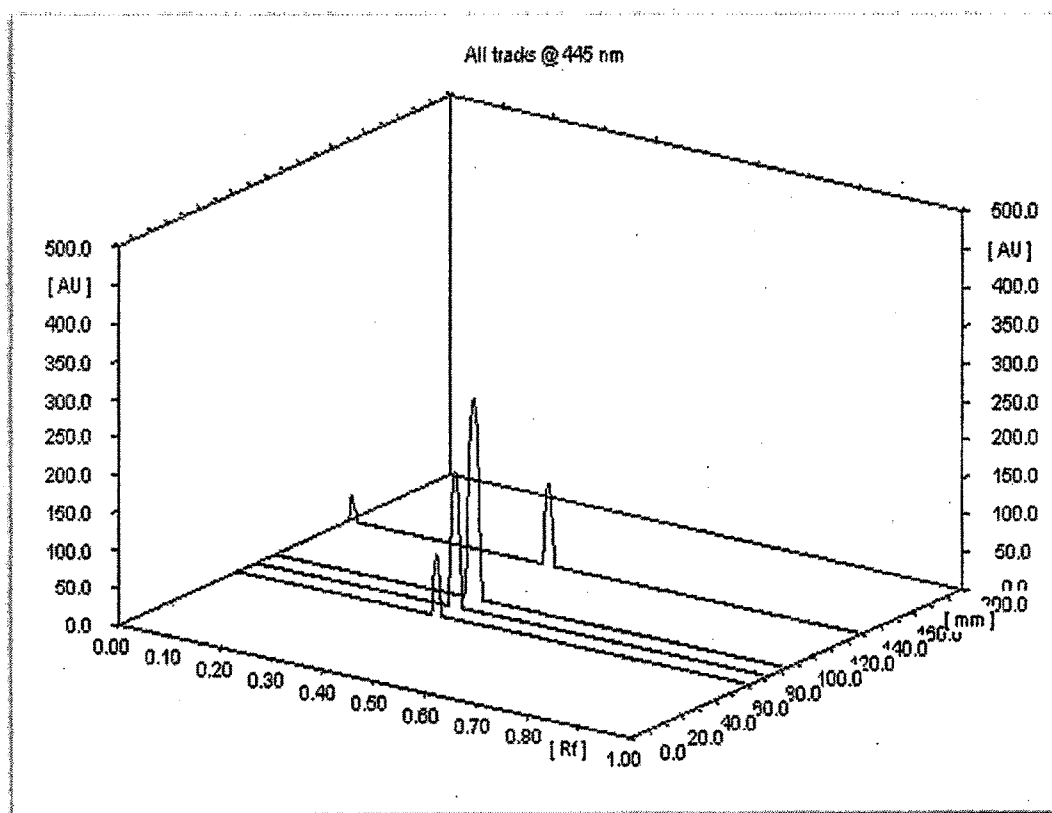


Figure 4.2.16: *N. stellata* leaf extract showing identical peak with standard β -carotene

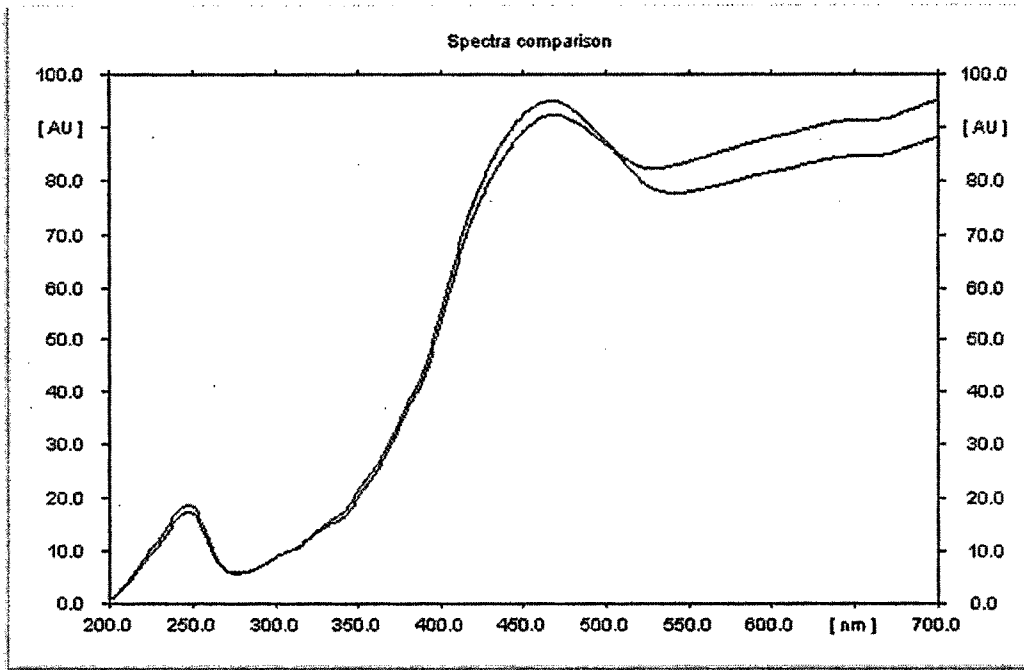


Figure 4.2.17: Spectral comparison for the peaks of standard β -carotene and *N. stellata* leaf extract

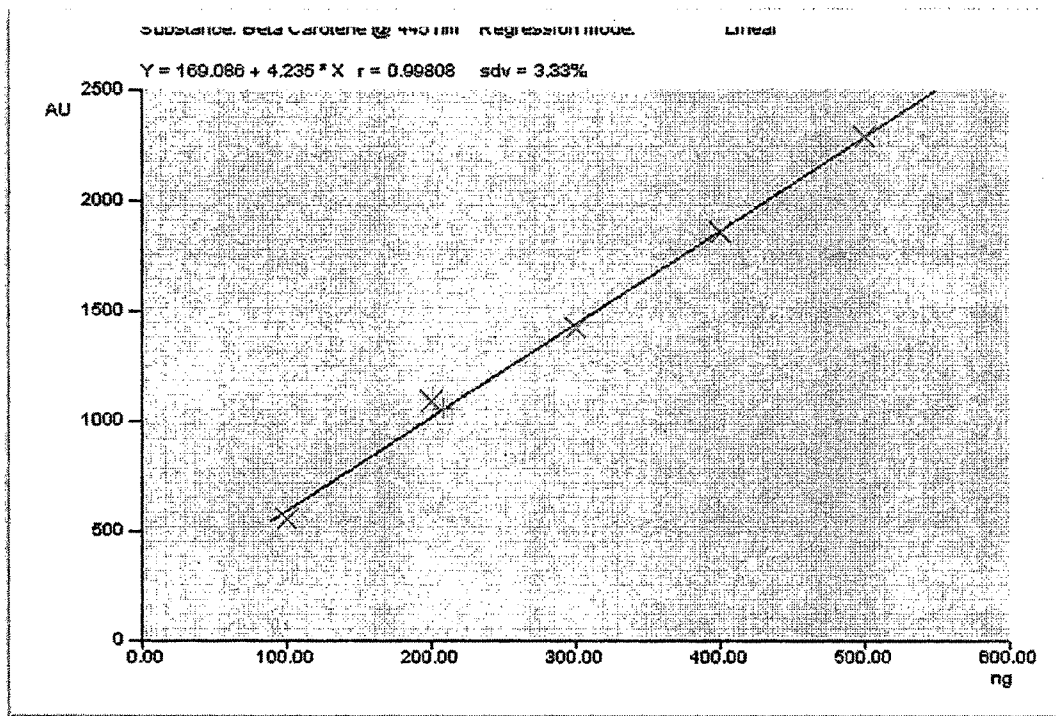


Figure 4.2.18: Calibration curve of peak area versus concentration for β -carotene

Table 4.2.10: Calibration curve parameters for quantification of β -carotene in *N. stellata* extract

R _f	Amount/Fraction	Area	X(calc)
0.39	100 ng	553.32	-
0.39	200 ng	1085.44	-
0.39	300 ng	1417.91	-
0.39	400 ng	1854.58	-
0.40	500 ng	2286.05	-
0.39	-	1054.13	209.00 ng

TLC separation optimization: The leaves of *N. stellata*, when subjected to TLC showed the presence of β -carotene peak (Figure 4.2.16). A comparison of the spectral characteristics of the peak for standard compound and that of the sample further confirmed the identity of β -carotene present in the sample (Figure 4.2.17). Good resolution with symmetrical and reproducible peak was obtained.

Linearity: The peak area versus concentration plot was found to be linear in the range of 100-500 ng spot⁻¹ for β -carotene (Figure 4.2.18). The regression equation and correlation coefficient for β -carotene indicated good linearity (Table 4.2.9).

Sample analysis: The β -carotene content of the leaves calculated from the area calibration curve (Table 4.2.10) by this method was found to be 0.01045 %w/w (plant dry weight basis). This TLC procedure may be used effectively for identity, quality evaluation as well as quantitative determination for this plant or its derived products.

4.2.8.4 Identification and quantification of oleanolic acid in *N. stellata*

TLC separation optimization: The leaves of *N. stellata*, when subjected to TLC showed the presence of oleanolic acid peak (Figure 4.2.19, 4.2.20). A comparison of the

Results and Discussion

spectral characteristics of the peak for standard compound and that of the sample further confirmed the identity of oleanolic acid present in the sample (Figure 4.2.21). Good resolution with symmetrical and reproducible peak was obtained.

Table 4.2.11: Validation parameters for quantification of oleanolic acid in *N. stellata* leaves

S. No.	Parameter	Results
1	R _f	0.53
2	Dynamic range (ng spot ⁻¹)	100 - 500
3	Equation	y=3397.724+7.504x
4	Slope	7.504
5	Intercept	3397.724
6	Linearity (correlation coefficient)	0.99613

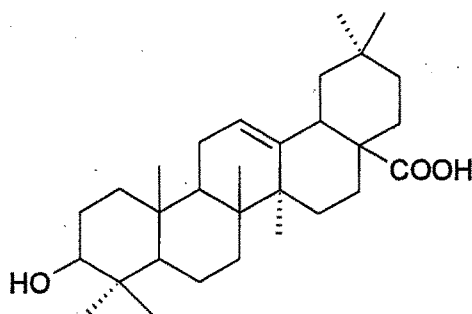


Figure 4.2.19: Chemical structure of oleanolic acid

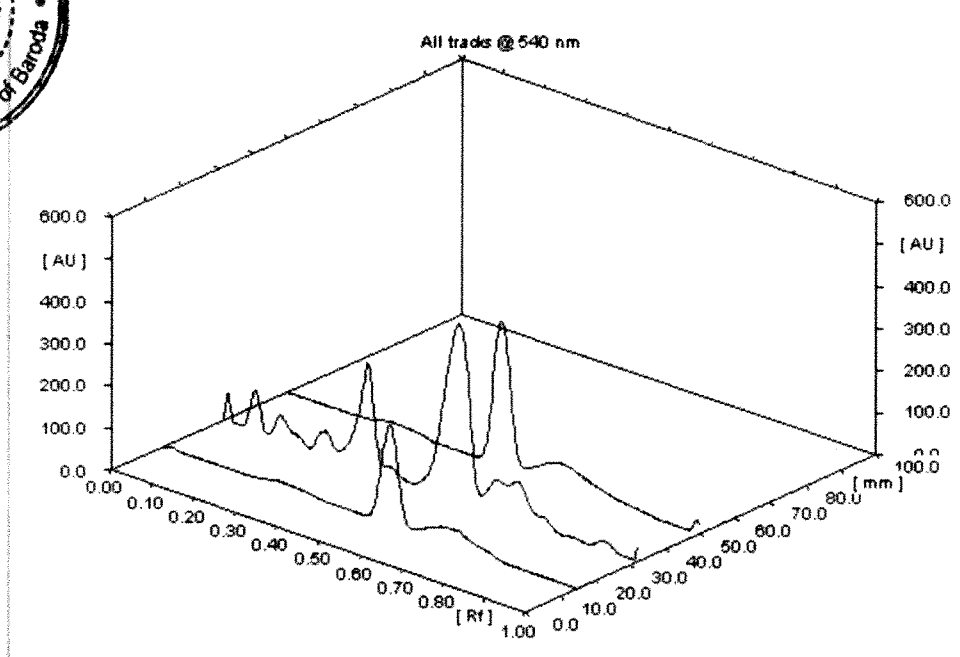


Figure 4.2.20: *N. stellata* leaf extract showing identical peak with standard oleanolic acid

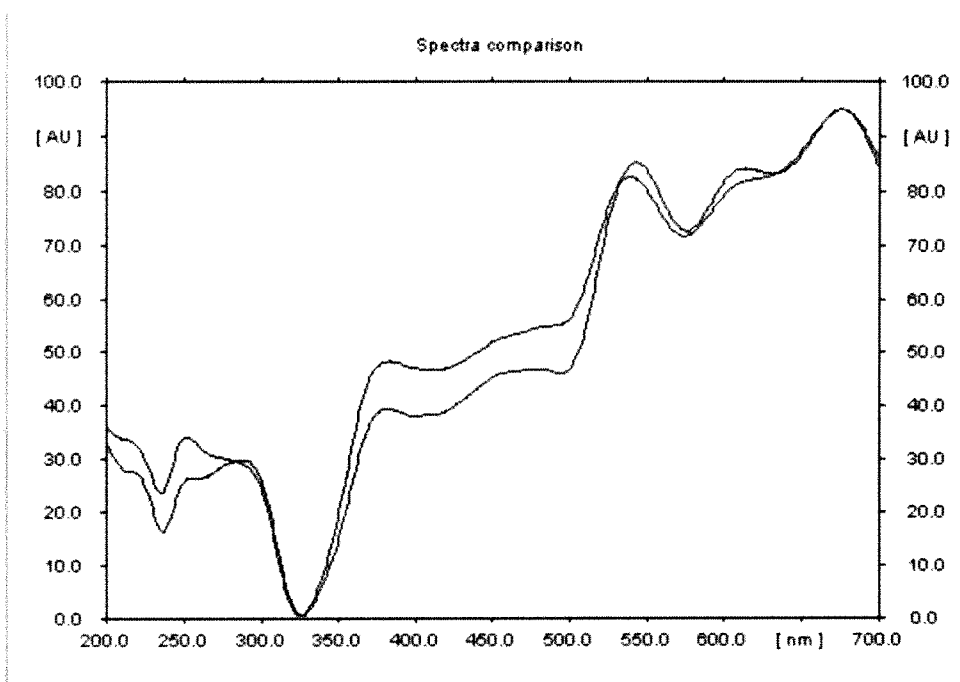


Figure 4.2.21: Spectral comparison for the peaks of standard oleanolic acid and *N. stellata* leaf extract

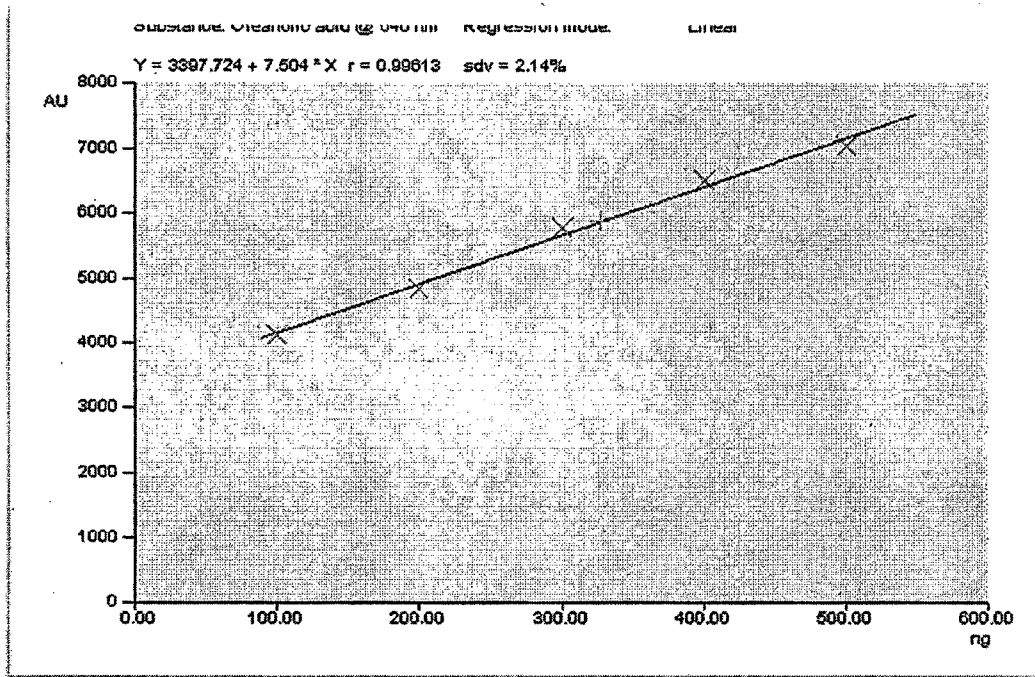


Figure 4.2.22: Calibration curve of peak area versus concentration for oleanolic acid

Table 4.2.12: Calibration curve parameters for quantification of oleanolic acid in *N. stellata* extract

R _f	Amount/Fraction	Area	X(calc)
0.54	100 ng	4120.42	-
0.54	200 ng	4825.23	-
0.53	300 ng	5761.18	-
0.53	400 ng	6505.68	-
0.53	500 ng	7032.25	-
0.54	-	5854.78	327.43 ng

Linearity: The peak area versus concentration plot was found to be linear in the range of 100-500 ng spot⁻¹ for oleanolic acid (Figure 4.2.22). The regression equation and correlation coefficient for oleanolic acid indicated good linearity (Table 4.2.11).

Sample analysis: The oleanolic acid content of the leaves calculated from the area calibration curve (Table 4.2.12) by this method was found to be 0.008186 %w/w (plant dry weight basis). This TLC procedure may be used effectively for identity, quality evaluation as well as quantitative determination for this plant or its derived products.

4.2.8.5 Identification and quantification of betulinic acid in *N. stellata*

TLC separation optimization: The leaves of *N. stellata*, when subjected to TLC showed the presence of betulinic acid peak (Figure 4.2.23, 4.2.24). A comparison of the spectral characteristics of the peak for standard compound and that of the sample further confirmed the identity of betulinic acid present in the sample (Figure 4.2.25). Good resolution with symmetrical and reproducible peak was obtained.

Table 4.2.13: Validation parameters for quantification of betulinic acid in *N. stellata* leaves

S. No.	Parameter	Results
1	R _f	0.56
2	Dynamic range (ng spot ⁻¹)	100 - 500
3	Equation	y=510.618+7.004x
4	Slope	7.004
5	Intercept	510.618
6	Linearity (correlation coefficient)	0.99670

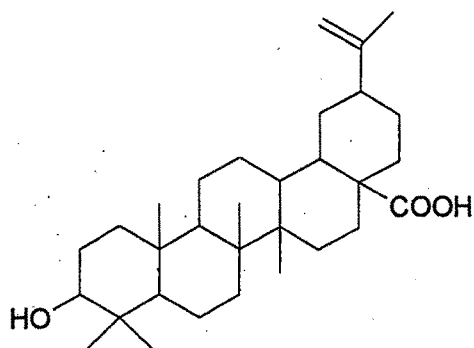


Figure 4.2.23: Chemical structure of betulinic acid

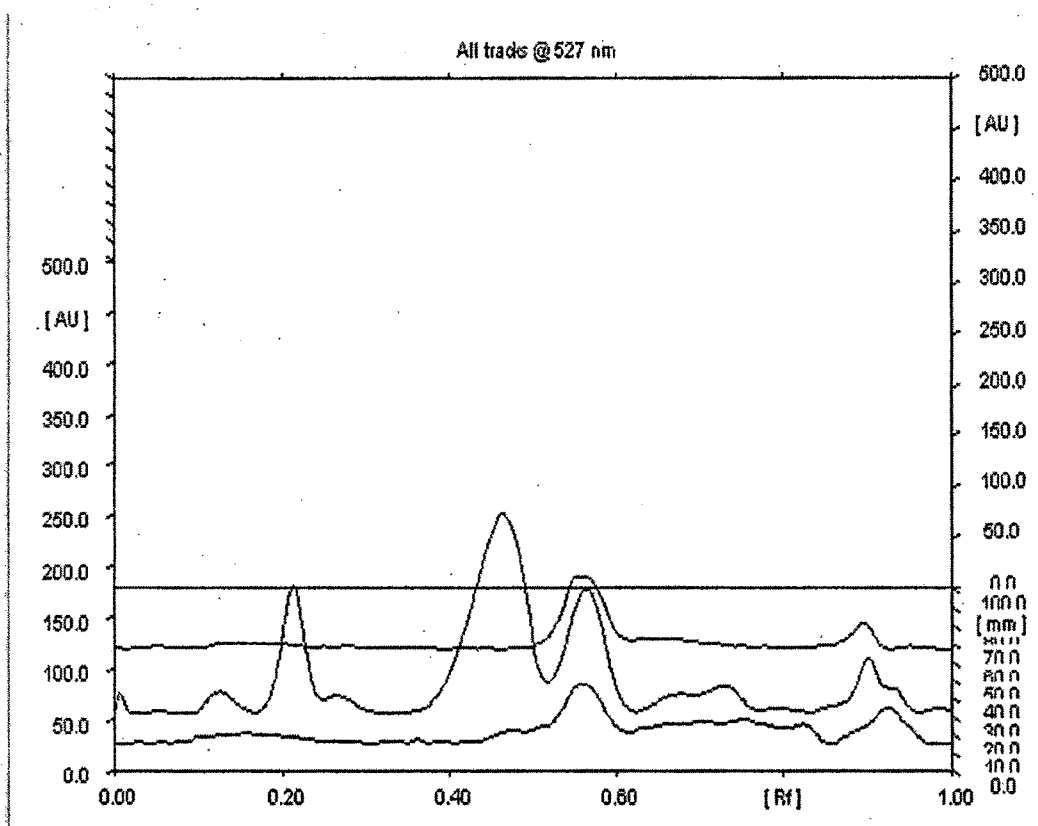


Figure 4.2.24: *N. stellata* leaf extract showing identical peak with standard betulinic acid

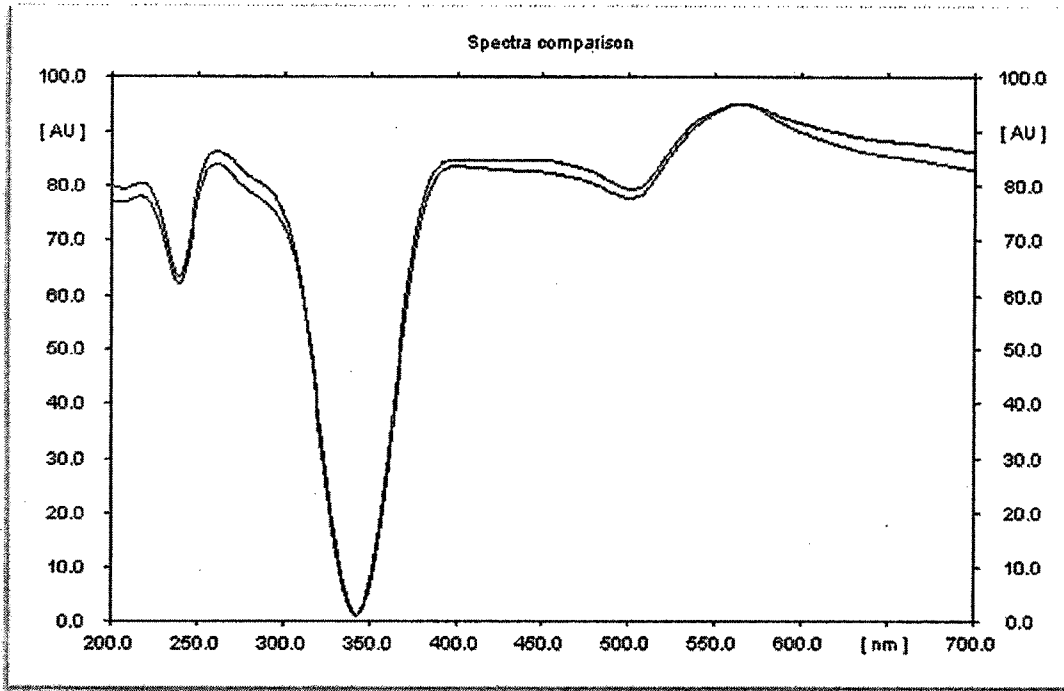


Figure 4.2.25: Spectral comparison for the peaks of standard betulinic acid and *N. stellata* leaf extract

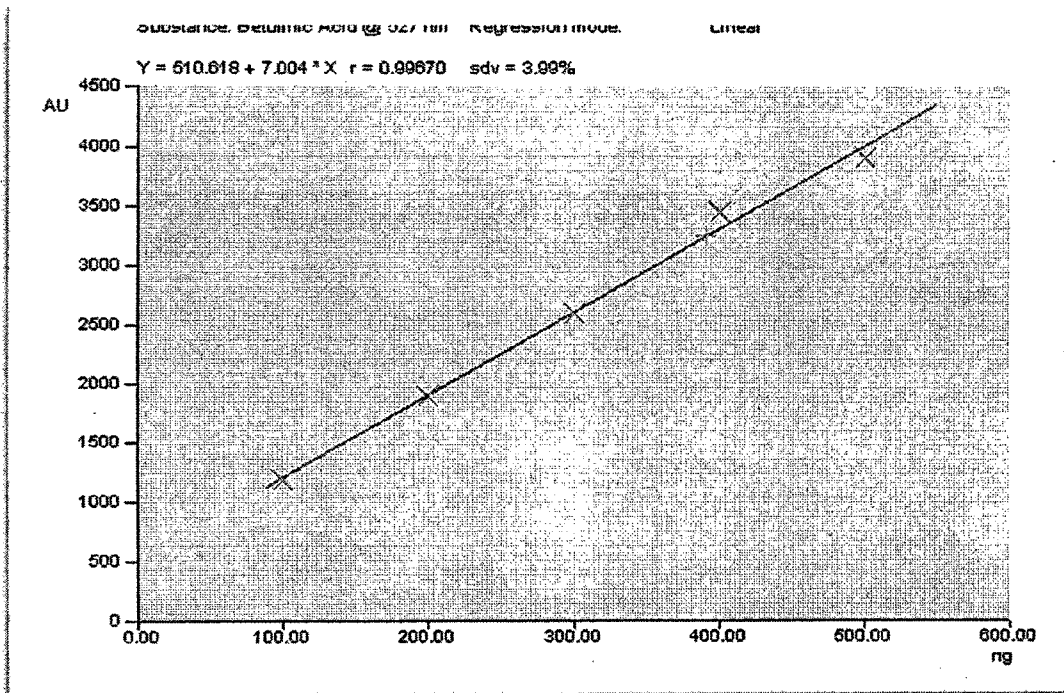


Figure 4.2.26: Calibration curve of peak area versus concentration for betulinic acid

Table 4.2.14: Calibration curve parameters for quantification of betulinic acid in *N. stellata* extract

R _f	Amount/Fraction	Area	X(calc)
0.57	100 ng	1186.99	-
0.56	200 ng	1898.54	-
0.56	300 ng	2606.62	-
0.56	400 ng	3457.63	-
0.56	500 ng	3909.49	-
0.58	-	3250.56	391.19 ng

Linearity: The peak area versus concentration plot was found to be linear in the range of 100-500 ng spot⁻¹ for betulinic acid (Figure 4.2.26). The regression equation and correlation coefficient for betulinic acid indicated good linearity (Table 4.2.13).

Sample analysis: The betulinic acid content of the leaves calculated from the area calibration curve (Table 4.2.14) by this method was found to be 0.078238 %w/w (plant dry weight basis).

This TLC procedure may be used effectively for identity, quality evaluation as well as quantitative determination for this plant or its derived products.

4.2.8.6 Identification and quantification gallic acid in *N. stellata*

TLC Separation Optimization: The leaves of *N. stellata*, when subjected to TLC showed the presence of gallic acid peak (Figure 4.2.27, 4.2.28). A comparison of the spectral characteristics of the peak for standard compound and that of the sample further confirmed the identity of gallic acid present in the sample (Figure 4.2.29). Good resolution with symmetrical and reproducible peak was obtained.

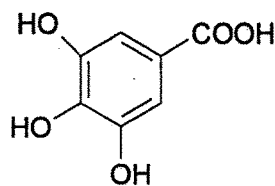
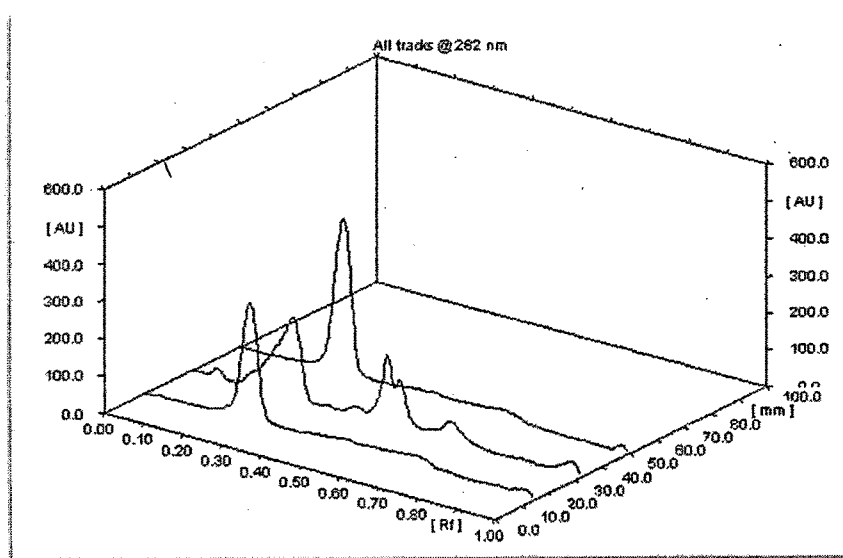


Figure 4.2.27: Chemical structure of gallic acid

Table 4.2.15: Validation parameters for quantification of gallic acid in *N. stellata* leaves

S. No.	Parameter	Results
1	R _f	0.26
2	Dynamic range (ng spot ⁻¹)	500 - 900
3	Equation	y=2732.345+6.654x
4	Slope	6.654
5	Intercept	2732.345
6	Linearity (correlation coefficient)	0.99941

Figure 4.2.28: *N. stellata* leaf extract showing identical peak with standard gallic acid

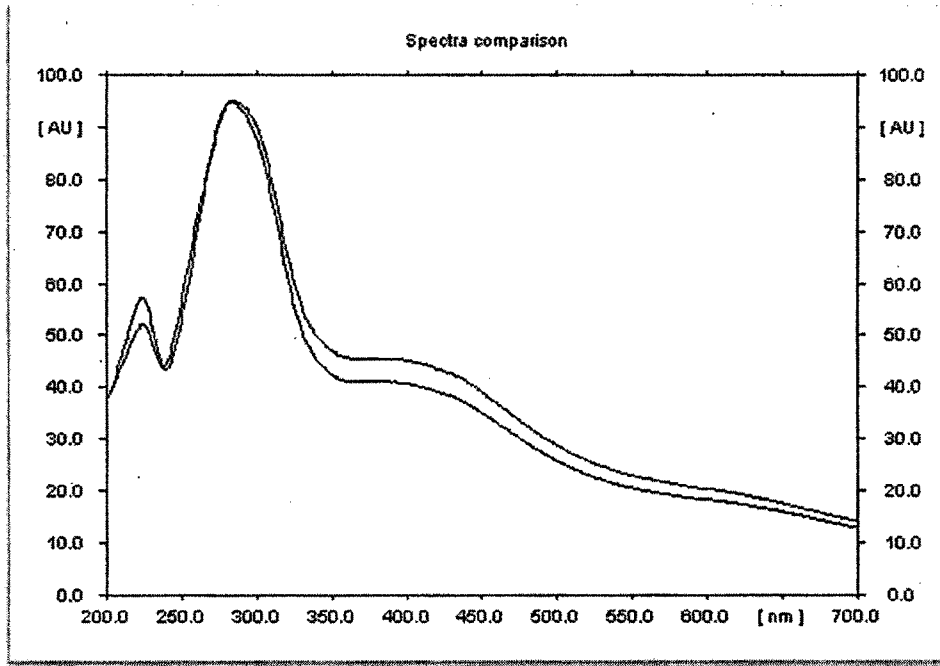


Figure 4.2.29: Spectral comparison for the peaks of standard gallic acid and *N. stellata* leaf extract

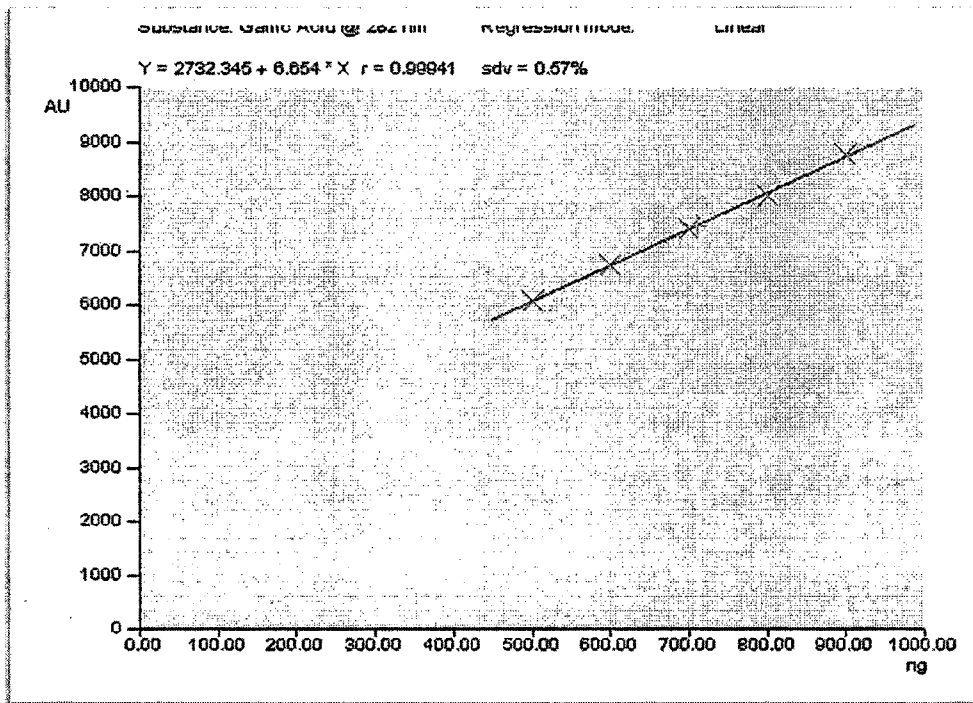


Figure 4.2.30: Calibration curve of peak area versus concentration for gallic acid

Table 4.2.16: Calibration curve parameters for quantification of gallic acid in *N. stellata* extract

R _f	Amount/Fraction	Area	X(calc)
0.27	500 ng	6054.21	-
0.27	600 ng	6741.45	-
0.26	700 ng	7406.67	-
0.27	800 ng	7995.71	-
0.26	900 ng	8754.31	-
0.27	-	7457.64	710.09 ng

Linearity: The peak area versus concentration plot was found to be linear in the range of 100-500 ng spot⁻¹ for gallic acid (Figure 4.2.30). The regression equation and correlation coefficient for gallic acid indicated good linearity (Table 4.2.15).

Sample analysis: The gallic acid content of the leaves calculated from the area calibration curve (Table 4.2.16) by this method was found to be 0.094679 %w/w (plant dry weight basis).

This TLC procedure may be used effectively for identity, quality evaluation as well as quantitative determination for this plant or its derived products.

4.2.9 Acute toxicity study

The fractions showed no signs of toxicity up to the dose of 2000 mg/kg. One-tenth of the maximum tested dose was considered as effective dose.

4.2.10 Anti-diabetic study

Defatted ethanol extract of leaves has been reported for antidiabetic activity (Dhanabal et al., 2007). The methanolic extract was fractioned to petroleum ether

fraction, chloroform fraction (CFMNS). Unsaponified matter of petroleum ether fraction of methanol extract (UPFMNS) was prepared based on the earlier report of hypoglycemic activity of defatted ethanol extract. UPFMNS, CFMNS and the residual methanol extract left out after fraction (RFMNS) were considered for the antidiabetic study.

Table 4.2.17: Changes in plasma glucose and insulin in control and experimental groups of *N. stellata*

Groups	Plasma glucose (mg/dl)	Plasma insulin (μ U/ml)
Diabetic control (2 % gum acacia solution)	275.34 \pm 28.86	4.86 \pm 1.05
Standard control (Metformin, 11.3 mg/kg)	145.26 \pm 24.22 **	14.56 \pm 1.54 **
UPFMNS 100 mg/kg	240.54 \pm 14.34 *	7.01 \pm 0.89 *
UPFMNS 200 mg/kg	190.57 \pm 21.57 **	11.58 \pm 1.07 **
CFMNS 100mg/kg	262.59 \pm 12.19 ^{ns}	6.47 \pm 0.87 ^{ns}
CFMNS 200mg/kg	250.67 \pm 13.51 ^{ns}	6.01 \pm 1.47 ^{ns}
RFMNS 100mg/kg	265.49 \pm 10.53 ^{ns}	5.16 \pm 1.27 ^{ns}
RFMNS 200mg/kg	255.31 \pm 15.11 ^{ns}	5.94 \pm 1.01 ^{ns}

Values are expressed as Mean \pm SD; n=6; *-p<0.05; **-p<0.01; ns-not significant

The diabetic control group showed a marked increase in plasma glucose and a reduction in insulin level while the metformin treated group restored the elevated glucose level to near normal level and also increased the reduced insulin level. UPFMNS 200 mg/kg and metformin treated groups showed significant change (p<0.01) in restoring the glucose and insulin levels (Table 4.2.17) when compared to

the diabetic control. But UPFMNS 100 mg/kg treated groups showed less significant change ($p < 0.05$) in restoring the glucose and insulin levels. CFMNS and RFMNS treated groups at both dose levels did not show any significant change in glucose and insulin levels.

UPFMNS 200 mg/kg treated group showed restoration of both glucose and insulin levels relatively comparable to the standard drug than other treated groups (Figure 4.2.31, 4.2.32). The significant decrease in the glucose levels of diabetic rats treated with UPFMNS may be by stimulation of the residual pancreatic mechanism like stimulating insulin secretion from the remnant β -cells or regenerated β -cells or probably by increasing peripheral utilization of glucose or both (Erah et al., 1996). The significant hyperglycemic effect of UPFMNS may also be due to its insulin-like effects (Akhtar and Ali, 1985; Day et al., 1990), including stimulation of glycogen synthesis and improvement of glucose homeostasis.

The increase in the insulin levels of treated groups also showed same pattern as in glucose levels (Table 4.2.17). Considerable increase in insulin level of UPFMNS (Figure 4.2.32) treated diabetic animals may be attributed to the stimulation of the surviving β -cells and increasing the secretion of insulin (Pari and Latha, 2002). Reports are available to show that antidiabetic plants may affect circulating insulin levels (Lamela et al., 1985). Thus, it may also be suggested that UPFMNS may induce the release of insulin from the bound form thereby potentiating its effect. It has been suggested that bioactive compounds from plants sources having antihyperglycemic activities might act by several mechanisms such as stimulating insulin secretion, increasing repair or proliferation of β -cells and enhancing the effects of insulin (Shanmugasundaram et al., 1990; Fayed et al., 1998).

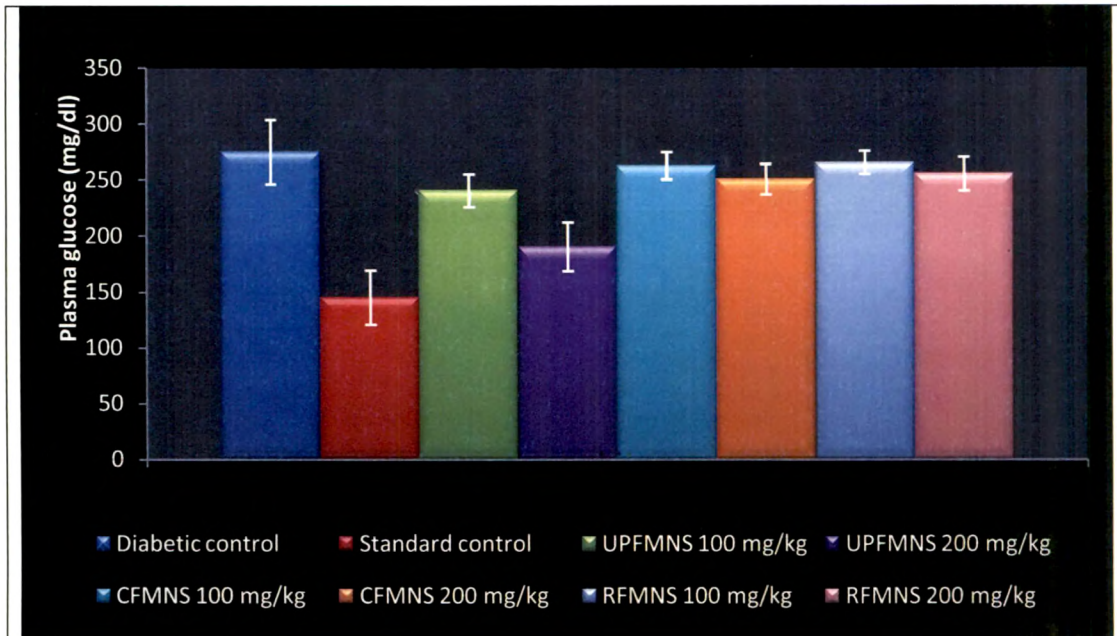


Figure 4.2.31: Comparison of changes in plasma glucose level in control and experimental groups of *N. stellata*

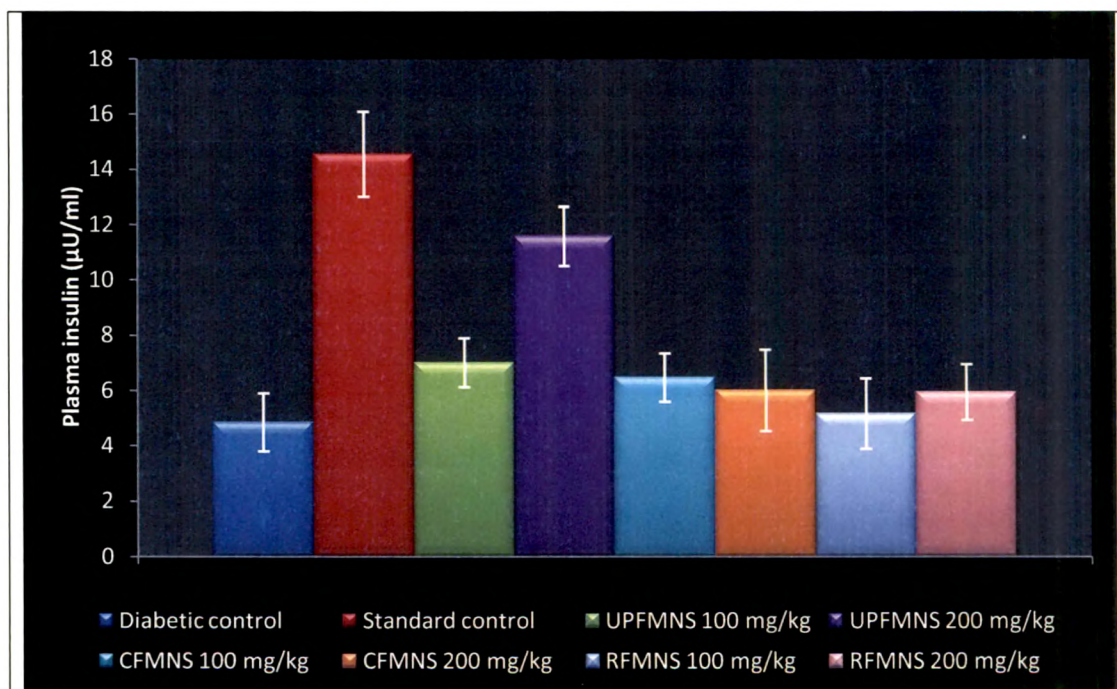


Figure 4.2.32: Comparison of changes in plasma insulin level in control and experimental groups of *N. stellata*

Table 4.2.18: Changes in hepatic hexokinase, glucose-6-phosphatase and liver glycogen levels in control and experimental groups of *N. stellata*

Groups	Hexokinase (U/g/min)	Glucose-6-phosphatase (U/g/min)	Liver glycogen (µg of glucose/mg of wet tissue)
Diabetic control	2.24±1.69	35.38±6.54	25.13±3.21
(2 % gum acacia solution)			
Standard control	8.54±1.1 **	19.35±5.67 **	52.24±1.28 **
(Metformin, 11.3 mg/kg)			
UPFMNS 100 mg/kg	3.12±0.85 ^{ns}	26.15±4.57 *	34.15±3.31 **
UPFMNS 200 mg/kg	5.67±0.48 **	23.68±3.58 **	40.11±2.12 **
CFMNS 100mg/kg	2.75±1.12 ^{ns}	33.65±5.47 ^{ns}	27.94±4.11 ^{ns}
CFMNS 200mg/kg	3.12±1.87 ^{ns}	30.27±3.69 ^{ns}	28.12±3.21 ^{ns}
RFMNS 100mg/kg	2.98±1.68 ^{ns}	34.65±4.19 ^{ns}	28.04±5.27 ^{ns}
RFMNS 200mg/kg	3.15±0.81 ^{ns}	29.68±3.31 ^{ns}	29.11±5.61 ^{ns}

Values are expressed as Mean ± SD; n=6; *p<0.05; **p<0.01; ^{ns}-not significant

Metformin and UPFMNS 200 mg/kg treated groups showed a significant ($p < 0.01$) increase (Table 4.2.18). The activation of glycolysis and increase the utilization of glucose for energy production may be the reason for the significant increase of hexokinase in UPFMNS 200 mg/kg treated. Conversely the mechanism played by UPFMNS 200 mg/kg treated in enhancing the hexokinase activity could also be due to glycogen synthesis activation or activation of mRNA coding for hexokinase in diabetic rats (Spence, 1983).

Metformin and UPFMNS 200 mg/kg treated groups showed significant ($p < 0.01$) decreased activity of glucose-6-phosphatase, while the UPFMNS 100 mg/kg treated groups showed less significant change ($p < 0.05$) (Table 4.2.18). The decreased levels observed in UPFMNS treated diabetic animals may be due to its primarily modulating and regulating the gluconeogenic enzyme activity either through the regulation by 3'5'-cyclic adenosine monophosphate (cyclic AMP) and any other metabolic activation or inhibition of glycolysis and gluconeogenesis.

The hepatic glycogen content of diabetic control was reduced significantly as compared to other treated groups. Metformin and UPFMNS treated (100 mg/kg and 200 mg/kg) groups showed significant ($p < 0.01$) change and restored the depleted glycogen level better than other treated groups (Table 4.2.18). Accumulation of glycogen in liver of UPFMNS treated animals is somewhat similar to that reported during insulin therapy (Spiro et al., 1958; Anderson, 1974). UPFMNS treated groups prevented the alteration in glycogen content but could not normalise it. This prevention of depletion of glycogen in liver may be possibly due to decreased activity of glycogen phosphorylase and increased activity of glycogen synthase. Conversely it may also be possible due to either stimulation of insulin release from β -cells (Lolitkar and Rao, 1966) or due to insulinomimetic activity (Broadhurst et al., 2000) or direct peripheral glucose uptake or due to a combination of the two (Lolitkar and Rao, 1966). Therefore, the mechanism of

action appears to be both pancreatic (Bansal et al., 1981) and extra pancreatic effect (Achrekar et al., 1991).

Table 4.2.19: Changes in body weight in control and experimental group of *N. stellata*

Groups	Body weight (g)
Diabetic control (2 % gum acacia solution)	165.24±9.56
Standard control (Metformin, 11.3 mg/kg)	220.35±4.87 **
UPFMNS 100 mg/kg	174.84±5.66 ^{ns}
UPFMNS 200 mg/kg	190.22±5.12 **
CFMNS 100mg/kg	170.35±7.11 ^{ns}
CFMNS 200mg/kg	171.94±4.59 ^{ns}
RFMNS 100mg/kg	168.22±3.67 ^{ns}
RFMNS 200mg/kg	171.41±6.66 ^{ns}

Values are expressed as Mean ± SD; n=6; **-p<0.01; ^{ns}-not significant

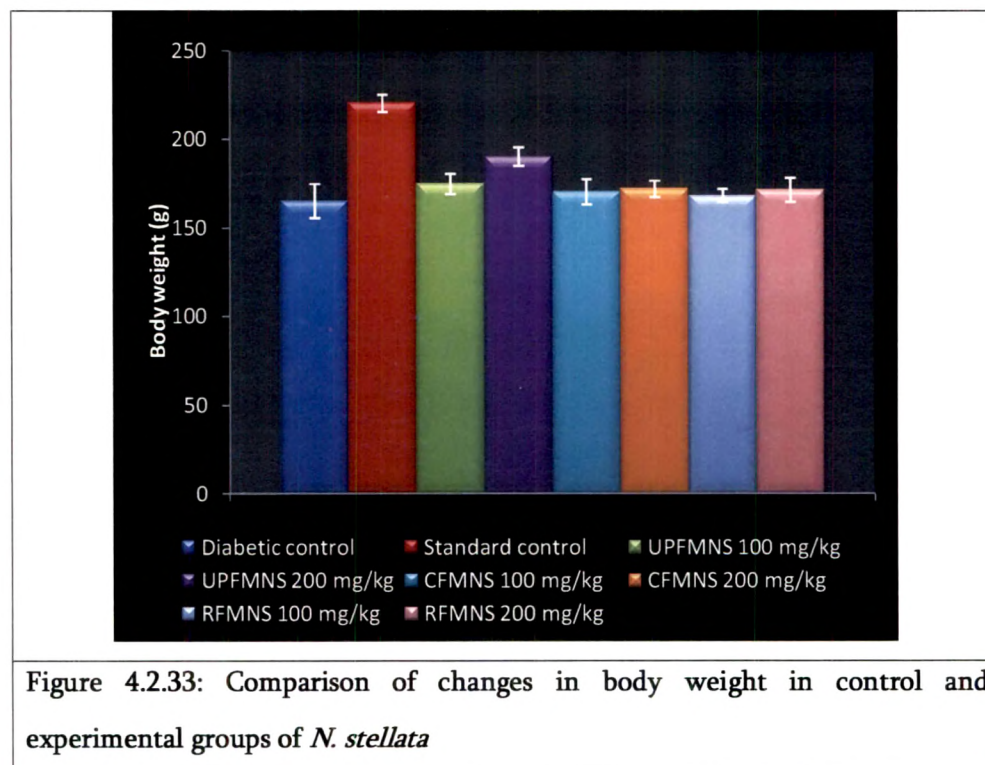


Figure 4.2.33: Comparison of changes in body weight in control and experimental groups of *N. stellata*

STZ-NAD induced diabetes is associated with a characteristic loss of body weight which is due to increased muscle wasting in diabetic state (Swanston-Flatt et al., 1990; Raju et al., 2001). Metformin and UPFMNS 200 mg/kg treated groups showed significant change ($p < 0.01$) in restoring the body weight (Table 4.2.19, Figure 4.2.33). The reversal of weight loss in the UPFMNS treated diabetic rats indicates the reversal of gluconeogenesis and glycogenolysis. However, it did not normalize the body weight completely. The resumption of moderate body weight also strongly suggests that sugar and lipid metabolism in these animals may be improved.

Diabetic control group (Figure 4.2.34) showed shrunken islets of Langerhans displaying degenerative and necrotic changes while acinar structure appeared in disarray. Prominent disruption of the islet cellular architecture was found and acini with large clear vacuoles. Significant reduction in total number of cells per pancreatic islet with marked degranulation was also observed. This provides clear evidence that STZ-NAD treatment destroyed the pancreatic β -cells. The metformin treated group (Figure 4.2.34) showed significant higher number of cells per islet and the cellular architecture was preserved. It showed no vacuoles and degranulation.

UPFMNS 100 mg/kg, CFMNS (100 and 200 mg/kg) treated (Figure 4.2.34) and RFMNS (100 and 200 mg/kg) treated (Figure 4.2.34) showed shrunken islet with disrupted cellular architecture, significant reduction in total number of cells per islet and vacuoles; similar observation as that of diabetic control with no significant change. UPFMNS 200 mg/kg treated groups (Figure 4.2.34) showed relatively intact, larger size islet and reduced vacuoles. Significant increase in number of cells per islet suggests that UPFMNS treated shows signs of regenerated pancreatic islet cells.

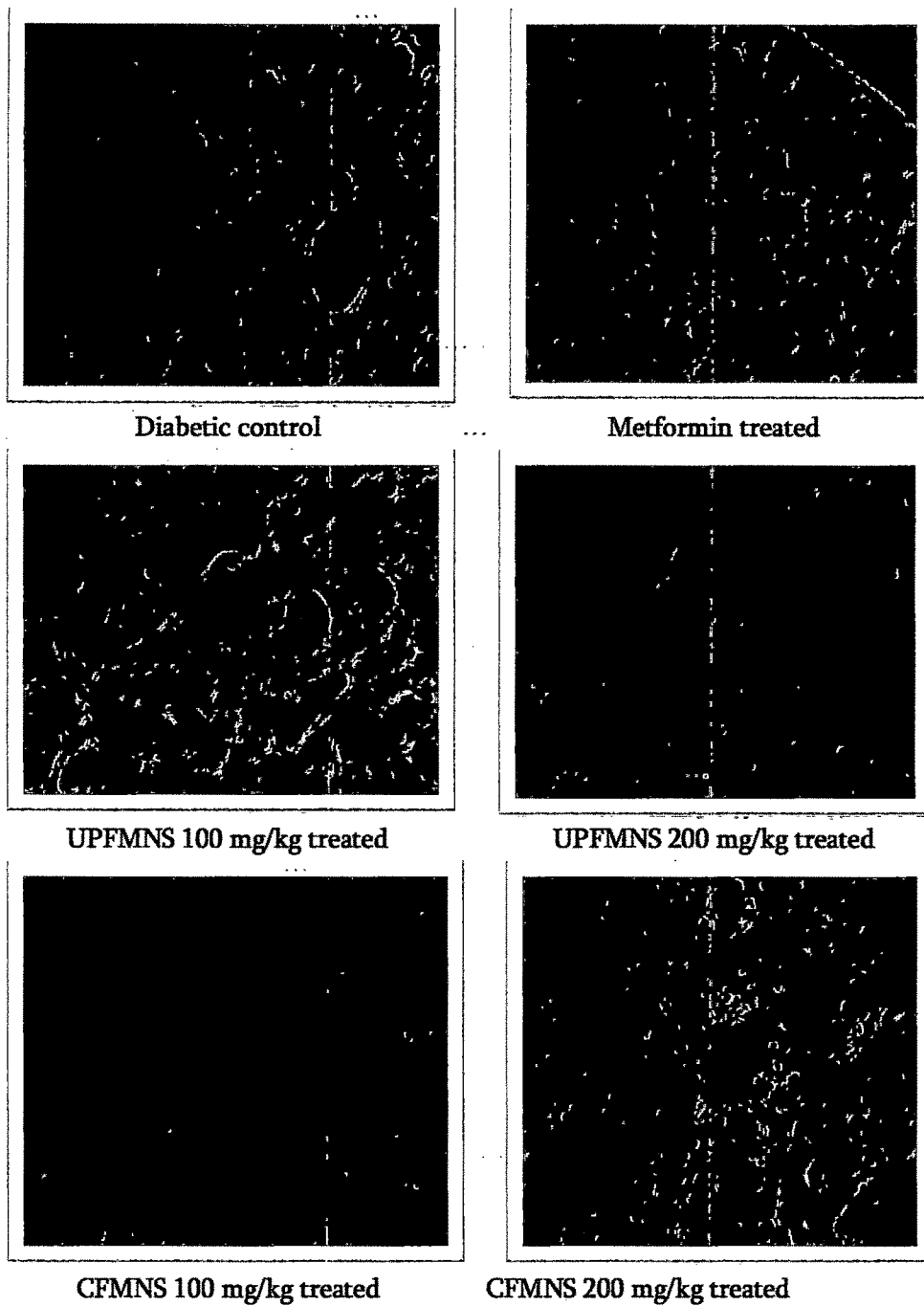


Figure 4.2.34: Histological slides showing changes in the endocrine (islets of Langerhans) and exocrine pancreas (acini) of control and experimental groups of *N. stellata* (Cont.)

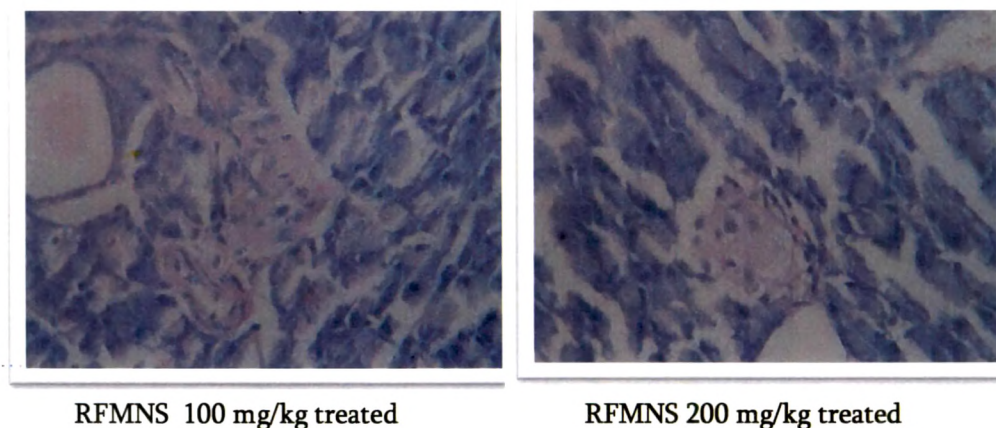


Figure 4.2.34: Histological slides showing changes in the endocrine (islets of Langerhans) and exocrine pancreas (acini) of control and experimental groups of *N. stellata*

The overall results show that CFMNS and RFMNS at both dose levels (100 mg/kg and 200 mg/kg) are completely inactive. UPFMNS has shown nearly comparable effect to that of metformin on all the parameters.

In addition β -sitosterol, β -carotene, lupeol, betulinic acid and oleanolic acid were also identified from UPFMNS. β -sitosterol has been reported for its antihyperglycemic due to insulin releasing effect (Ivorra et al., 1988; Ivorra et al., 1989; Marles and Farnsworth, 1994 ; Marles and Farnsworth, 1995). β -sitosterol lowers hepatic cholesterol level (Ikeda et al., 1985; Fuhrman et al., 1997) and exerts hypocholesterolemic effect (Pollak, 1985; Ling and Jones, 1995; Wang and Ng, 1999). However, it has been stated that 'the ubiquitous occurrence of β -sitosterol, plant sterols in general, and their glucosides in all vegetables makes it highly unlikely that they have any drug related properties and many reports on their medicinal properties are based on *in vitro* or unrealistically high *in vivo* doses which make a therapeutic application of these compounds highly unlikely (Marles and Farnsworth, 1994; Marles and Farnsworth, 1995). In a way this statement is correct, since sitosterol is not drug in the accepted sense, but rather

slow acting essential micronutrients or adaptogens better considered as minor but nevertheless important cell membrane constituents.

Reddy et al., 2009 demonstrated lupeol's antidyslipidemic activity along with an antihyperglycemic effect (Harborne and Baxter, 1983) which revealed the lupeol's potential as a scaffold for developing drugs targeting coronary diseases and diabetes (Reddy et al., 2009). β -carotene being an antioxidant could exhibit antidiabetic activity. Beneficial role of beta-carotene in reducing diabetic complications like glycosylation in alloxan-induced diabetic rats (Aruna et al., 1999) has been reported previously. β -carotene has been reported to significantly decrease blood glucose levels and provide more protection to pancreatic tissues against damage caused by STZ (Attia, 2009). β -carotene is also reported for hypocholesterolemic effect (Wang and Ng, 1999). Dietary supplementation with lycopene brought about a decline in plasma LDL cholesterol level, probably by inhibiting macrophage HMG CoA reductase activity (Fuhrman et al., 1997).

The insulin releasing effect of β -sitosterol, antihyperglycemic effect lupeol and antioxidant activity of β -carotene may have contributed to the observed synergistic antidiabetic of UPFMNS. Hypocholesterolemic and hypolipidemic of β -sitosterol, β -carotene and lupeol explains the altered lipid metabolism contributing to weight gain observed in UPFMNS. The signs of β -cell regeneration in the histopathological study may be due to pancreatic protective effect of β -carotene or due to unidentified compounds of UPFMNS.

In addition to their well-established roles in dietary lipid absorption and cholesterol metabolism, bile acids (BAs) have been shown to activate mitogen-activated protein (Qiao et al., 2003) and nuclear hormone receptors such as farnesoid X receptor R (FXRRa) (Wang et al., 1999). Through activation of these two pathways, BAs can regulate their own metabolism. BAs are also ligands for the G-protein coupled receptor TGR5 (Itoh et al., 2004) and activation of this receptor

by bile acids results in an effect on energy homeostasis. Indeed, the administration of BAs to mice fed with high fat diet increases energy expenditure in brown adipose tissue, preventing obesity and insulin resistance (Watanabe et al., 2006). Betulinic acid and oleanolic acid exhibits TGR5 agonist activity in a selective manner compared to bile acids and also activated FXR, the nuclear bile acid receptor (Genet et al., 2010).

In animal models of hypertension or diabetes, endothelial NO synthase (eNOS) has been found upregulated, however, the upregulated enzyme turned out to be dysfunctional (Hink et al., 2001). Betulinic acid possesses combined properties of eNOS upregulation and NADPH oxidase downregulation (Steinkamp-Fenske et al., 2007). Betulinic acid elevates significantly the plasma hormone levels of insulin and causes greater decrease in plasma amylase activity than the lipase (De Meol et al., 2009). Apart from the hypoglycemic effect of oleanolic acid (Hao et al., 1991), it also increases hepatic glycogen and insulin levels (Liu et al., 1994).

An extract of *Ganoderma lucidum*, exerts its hypoglycemic activity by functioning as a β -blocker, inhibiting the effects of catecholamines, which are known to promote gluconeogenesis and glycogenolysis. The option of UPFMNS being a β -receptor antagonist cannot also be ruled out.

Biguanides produce hypoglycaemia in diabetic animals by an extrapancreatic mechanism and are devoid of significant activity in normal animals (Schweizer et al., 1983). Although biguanides do not require the pancreas for effectiveness, in practice, they appear to augment rather than to create insulin. With the biguanide, metformin, insulin is a prerequisite to convert glucose to glycogen and a patient cannot survive with biguanide alone without some endogenous or exogenous insulin (Kxall, 1970). Therefore, it seemed reasonable to speculate that these extracts may possess a biguanide-like hypoglycaemic activity. From the

results, it may also be postulated that at least more than one hypoglycemic principle with diversified mechanism of actions may be present.

4.2.11 Isolation and characterization of chemical constituents

Nymphayol, a sterol has been reported recently for its partial regeneration of β -cells (Subash Babu et al., 2009). The STZ-NAD model antidiabetic study revealed UPFMNS as a potent candidate. Considering these facts the unsaponified petroleum ether fraction of methanol extract (UPFMNS) was chosen for phytochemical studies.

4.2.11.1 Compound NS I

The fractions obtained by elution with chloroform: ethyl acetate (90:10) yielded 60 mg of white crystalline compound with m.p. 295 °C. The compound showed positive reaction for terpenoids with anisaldehyde sulphuric acid reagent. This compound was designated as NS I.

4.2.11.2 Characterization of NS I

Co-TLC study of NS I with already reported and currently identified steroids/terpenoid compounds from *N. stellata* was carried out. NS I matched the R_f value of betulinic acid. NS I was confirmed as betulinic acid by UV-Vis spectral and IR overlay (Figure 4.2.35).

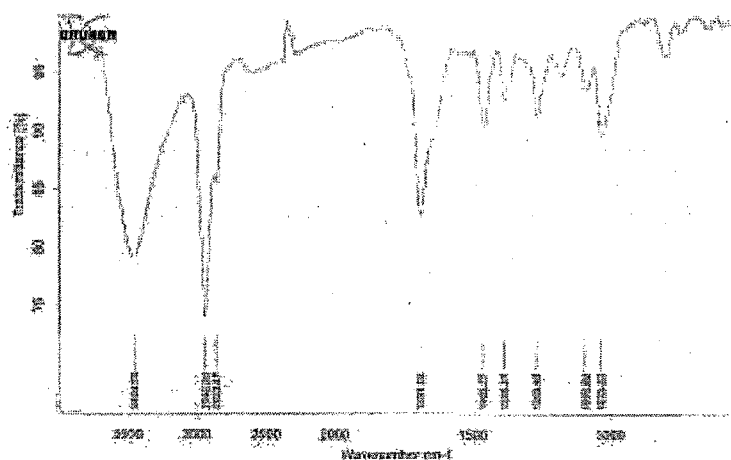


Figure 4.2.35: IR spectrum of NS I

4.2.12 PTP1B inhibition study

Suramin inhibited PTP1B 93.06 %, while UPMNS inhibited 94.44 % (Table 4.2.20, Figure 4.2.36). Betulinic acid and lupeol showed 90.27 and 81.94 % inhibition respectively. Aqueous extract, 50 % methanolic extract and gallic acid exhibited negative inhibition (Figure 4.2.36). Oleanolic acid, methanolic extract and CFMNS inhibited PTP1B by 66.11, 61.11 and 51.11 % respectively. The aqueous extracts negative inhibition may be due to gallic acid. As the polarity of the extracts decreased, the negativity also decreased.

Table 4.2.20: % inhibition of PTP1B by extracts/fractions/compounds of *N. stellata*

Extracts/fractions/isolated or identified compounds	% Inhibition of PTP1B
Suramin (10 μ M)	93.06
Aqueous extract (4000 μ g/ml)	-130.55
50 % methanolic extract (4000 μ g/ml)	-81.94
Methanolic extract (4000 μ g/ml)	61.11
UPMNS (Unsaponified petroleum ether fraction of methanol extract) (4000 μ g/ml)	94.44
CFMNS (Chloroform fraction of methanolic extract) (4000 μ g/ml)	51.11
RFMNS (Residual fraction of methanolic extract) (4000 μ g/ml)	37.22
Oleanolic acid (400 μ g/ml)	66.11
Betulinic acid (400 μ g/ml)	90.27
Gallic acid (400 μ g/ml)	-204.27
β -sitosterol (400 μ g/ml)	50
Lupeol (400 μ g/ml)	81.94
β -carotene (400 μ g/ml)	29.16

Betulinic acid has been reported to be potent inhibitor of PTP1B (Choi et al., 2009). Oleanolic acid has moderate PTP1B inhibition (Li et al., 2005) and lupeol

has been previously reported for PTP1B inhibition (Na et al., 2009). The presence of betulinic acid, lupeol and oleanolic acid may be responsible for the inhibitory activity of UPFMNS. Moreover the % inhibition of UPFMNS is higher than the single compounds suggesting the possibility of synergistic effect. This finding also overlaps with antidiabetic activity exhibited by UPFMNS in STZ-NAD model. The mechanism of antidiabetic activity of UPFMNS can be speculated as PTP1B inhibition.

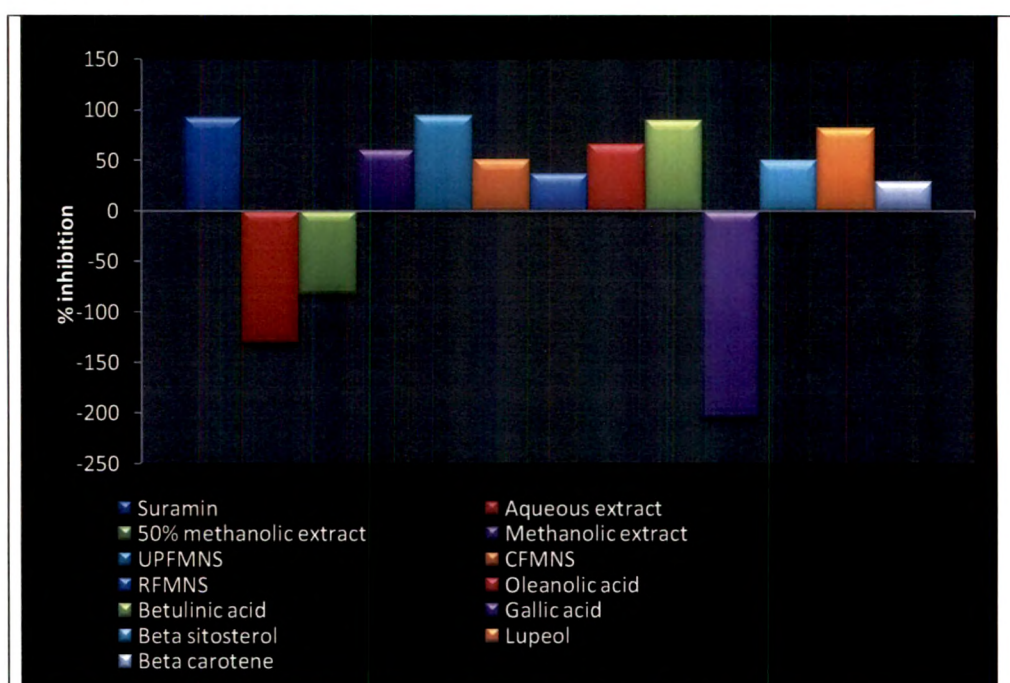


Figure 4.2.36: % inhibition of PTP1B by extracts/fractions/compounds of *N. stellata*

4.2.13 Brine shrimp lethality bioassay

The LC₅₀ values of the brine shrimp lethality bioassay obtained for extracts/fractions or isolated/identified compounds have been presented in Table 4.2.21. LC₅₀ values < 1000 µg/ml are considered significant for crude extracts (Garza et al., 2007). The tested compounds followed the order oleanolic acid>β-carotene>β-sitosterol>betulinic acid in lethality to brine shrimps. Lupeol and gallic acid showed no significant effect till 2000 µg/ml. Although oleanolic acid, β-

carotene, β -sitosterol and betulinic acid are constituents of UPFMNS, it showed no lethality. As the polarity of the extracts increased the lethality also increased, suggesting the presence of polar toxic compound/s.

Table 4.2.21: LC₅₀ values of extracts/fractions/compounds of *N. stellata*

Extracts/fractions/isolated or identified compounds	LC ₅₀ values ($\mu\text{g/ml}$)
Aqueous extract (4000 $\mu\text{g/ml}$)	2760
50 % methanolic extract (4000 $\mu\text{g/ml}$)	3690
Methanolic extract (4000 $\mu\text{g/ml}$)	> 4000
UPFMNS (Unsaponified petroleum ether fraction of methanol extract) (4000 $\mu\text{g/ml}$)	> 4000
CFMNS (Chloroform fraction of methanolic extract) (4000 $\mu\text{g/ml}$)	> 4000
RFMNS (Residual fraction of methanolic extract) (4000 $\mu\text{g/ml}$)	> 4000
Oleanolic acid (400 $\mu\text{g/ml}$)	120
Betulinic acid (400 $\mu\text{g/ml}$)	940
Gallic acid (400 $\mu\text{g/ml}$)	> 2000
β -sitosterol	750
Lupeol	> 2000
β -carotene	520

4.2.14 Anti-platelet aggregation activity

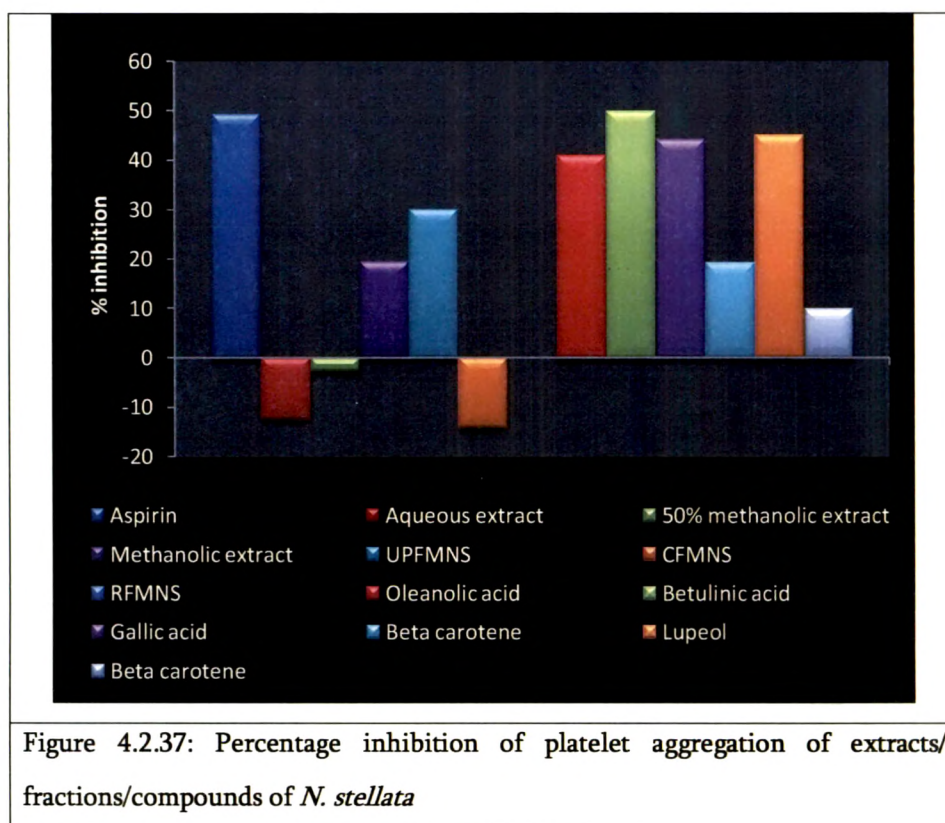
The normal platelet aggregation (viz. Control) was found to be $12.17 \pm 1.14 \Omega$ and the platelet aggregation inhibition by of aspirin (10 μM) was $6.17 \pm 0.95 \Omega$. The standard inhibition range of ADP (10 μM) induced platelet aggregation for aspirin is 6-24 Ω . Aqueous, 50 % methanolic extract, CFMNS and RFMNS showed negative inhibition (Figure 4.2.37), while β -carotene showed no significant change (Table 4.2.22). UPFMNS showed 29.99 % inhibition of platelet aggregation.

Among the compounds studied betulinic acid showed better inhibition than aspirin. Prostaglandin antagonistic activity of betulinic may be the explanation for its anti-platelet activity.

Table 4.2.22: Effects of *N. stellata* extracts/fractions/compounds on ADP induced platelet aggregation

Extracts/fractions/isolated or identified compounds	Change in impedance Mean±SD (Ω)	% Inhibition of platelet aggregation
Control	12.17±1.14	-
Aspirin (10 μM)	6.17±0.95**	49.3
Aqueous extract (4000 μg/ml)	13.7±0.71 ^{ns}	-12.57
50 % methanolic extract (4000 μg/ml)	12.5±0.88 ^{ns}	-2.71
Methanolic extract (4000 μg/ml)	9.8±0.68 *	19.47
UPFMNS (4000 μg/ml)	8.52±0.66 **	29.99
CFMNS (4000 μg/ml)	13.9±0.39 ^{ns}	-14.21
RFMNS (4000 μg/ml)	12.2±0.64 ^{ns}	-0.24
Oleanolic acid (400 μg/ml)	7.2±1.12 **	40.83
Betulinic acid (400 μg/ml)	6.1±0.67 **	49.87
Gallic acid (400 μg/ml)	6.8±0.54**	44.12
β-sitosterol (400 μg/ml)	9.83±1.07 *	19.22
Lupeol (400 μg/ml)	6.7±1.05 **	44.95
β-carotene (400 μg/ml)	10.97±0.40 ^{ns}	9.86

Values are expressed as Mean ± SD; n=3; *-p<0.05; **-p<0.01; ^{ns}-not significant



Gallic acid showed 44.12 % inhibition. P-selectin is an adhesion molecule that is intricately implicated in atherothrombosis by mediating leukocyte-endothelium, leukocyte-platelet, and platelet-platelet interactions (Vestweber and Blanks, 1999; Merten et al., 2000). Gallic acid intervenes in major inflammatory pathobiologies by binding and antagonizing P-selectin (Appeldoorn et al., 2005). Gallic acid may be the reason for the inhibitory activity of methanolic extract. Oleanolic acid and lupeol inhibited platelet inhibition by 40.83 and 44.95 % respectively. Oleanolic has been reported for its anti-platelet aggregation activity (Jin et al., 2004). In spite of betulinic acid, oleanolic acid lupeol and β -sitosterol being constituents of UPFMNS, the platelet aggregation inhibition shown by UPFMNS is moderate. It can be suggested that there is no synergistic effect and the observed result may be due to quantitative difference of these compounds in UPFMNS. Conversely, the lower inhibition rate may be due to the ability of other unidentified compounds to antagonize these compounds or to induce platelet aggregation.

4.2.15 Anti-acetylcholinesterase study

Galanthamine showed highest % inhibition of 87.01 (Figure 4.2.38). Lupeol, oleanolic acid, gallic acid, β -sitosterol and betulinic acid showed 60.88, 44.87, 31.28, 28.53 and 18.92 % acetylcholinesterase inhibition respectively. Among the extracts and fractions tested UPFMNS alone showed higher inhibition of 37.9 % (Table 4.2.23). The inhibition activity of UPFMNS may be to lupeol, oleanolic acid, β -sitosterol and betulinic acid. Acetylcholinesterase inhibition decreased with increase in polarity of the extracts.

Table 4.2.23: % inhibition of acetylcholinesterase by extracts/fractions/compounds of *N. stellata*

Extracts/fractions/isolated or identified compounds	% Inhibition of acetylcholine esterase
Galanthamine (1 μ M)	87.01
Aqueous extract (4000 μ g/ml)	5.38
50 % methanolic extract (4000 μ g/ml)	10.18
Methanolic extract (4000 μ g/ml)	15.83
UPFMNS (4000 μ g/ml)	37.9
CFMNS (4000 μ g/ml)	28.16
RFMNS (4000 μ g/ml)	21.54
Oleanolic acid (400 μ g/ml)	44.87
Betulinic acid (400 μ g/ml)	18.92
Gallic acid (400 μ g/ml)	31.28
β -sitosterol (400 μ g/ml)	28.53
Lupeol (400 μ g/ml)	60.88
β -carotene (400 μ g/ml)	25.30

